OPTIMAL FEEDBACK CONTROL FOR NONLINEAR CONTROL MOMENT GYRO SYSTEMS

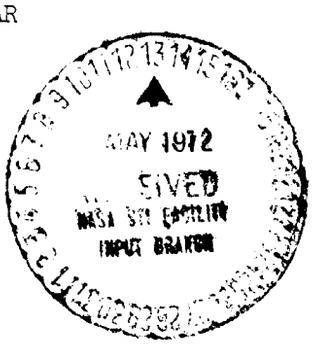

A Thesis

Presented to

the Faculty of the School of Engineering and Applied Science

University of Virginia

In Partial Fulfillment

of the Requirements for the Degree

Master of Aerospace Engineering

(NASA-TM-X-67790) OPTIMAL FEEDBACK CONTROL FOR NONLINEAR CONTROL MOMENT GYRO SYSTEMS Ph.D. Thesis - Virginia Univ. R.G. Kyle (NASA) Jun. 1969 119 p CSCL 09C G3/10

N72-23198

Unclas 26292

by

Robert G. Kyle

June 1969

APPROVAL SHEET

This thesis is submitted in partial fulfillment of

the requirements for the degree of

Master of Aerospace Engineering

Robert G. Kyle

Author

Approved:

John Kenneth Haviland

Advisor: Dr. J. K. Haviland

Peter R. Kurzhals

Co-Advisor: Dr. P. R. Kurzhals

Dean, School of Engineering and
Applied Science

June 1969

ACKNOWLEDGMENTS

The author wishes to thank the National Aeronautics and Space Administration's Langley Research Center in Hampton, Virginia, for permitting this work to be submitted as a thesis. Sincere thanks are also expressed to his advisors, Dr. J. K. Haviland of the University of Virginia, and Dr. P. R. Kurzhals of NASA for their guidance and constructive suggestions which made this thesis possible. Appreciation is also extended to Miss Carolyn Grantham of NASA for her valuable assistance in figure preparation and report editing.

TABLE OF CONTENTS

LIST OF TABLES

LIST OF FIGURES

FIGURE PAGE

FIGURE PAGE

LIST OF SYMBOLS

$\langle E \rangle$	flexible spacecraft disturbance matrix
I	current
$[I]$	spacecraft inertia matrix
$\langle G \rangle$	control torque vector
GAIN	effective gain factor
H	angular momentum, 2000 ft-lb-sec
$\langle H \rangle$	total CMG angular momentum vector
$\langle H_c \rangle$	command momentum vector
HT	normalized angular momentum
$\langle H_i \rangle$	angular momentum vector for ith CMG, i = 1,2,3
h_{ij}	direction cosine components
$\langle h_i \rangle$	unit vector for ith CMG
K	check factor
K_{12}, K_{13}, K_{23}	check factor product components
K_B	back EMF constant
K_G	gear ratio
K_T	stall torque constant
KI	isogonal check factor
K_{LIM}	upper bound on check factor
K_{SL}	control system gain factor
K_i	control system gain, i = 1,2,3,4,5,6
ΔK	delta check factor deadband

$\langle M_C \rangle$	command moment vector
$\langle M_D \rangle$	disturbance moment vector
$\langle M_{CF} \rangle$	filtered command moment vector
P_β	inner gimbal performance factor
P	power consumption
P_G	total gimbal power
P_{Gi}	gimbal electrical power
q_D	modal displacement
R	resistance
s	Laplace transform
T_i	effective gimbal torque command
$[U]$	modal distribution matrix
$[V]$	static compliance matrix
α_i	outer gimbal angle, deg
$\dot{\alpha}_{ic}$	outer gimbal roll-off rate, deg/sec
β_i	inner gimbal angle, deg
β_{iL}	inner gimbal angle roll-off angle, deg
$\dot{\beta}_c$	commanded gimbal rate correction, deg/sec
β_{max}	maximum inner gimbal angle
γ	isogonal angle
γ_F	flexible body attitude
γ_{FD}	flexible dynamic attitude
γ_{FS}	flexible static attitude
ϵ_k	linearization angle

$\pi_{\alpha i}, \pi_{\beta i}$	torque selection factor
$\langle \theta \rangle$	spacecraft attitude vector
$\langle \Omega \rangle$	spacecraft angular rate vector
$\langle \dot{\delta} \rangle$	gimbal rate vector
$[\phi]$	modal participation matrix
ρ_i	filter damping factor
ω_D	modal damping factor
ω_i	filter frequency, rad/sec
ξ	modal damping factor

Subscripts

D	dynamic mode
F	flexible spacecraft
R	rigid spacecraft
S	quasi-static
i	i = 1,2,3 or i = 1,2,3,4,5,6
j	j = 1,2,3
k	k = 1,2,3 or k = 1,2,3,4,5,6
1,2,3	relative to x,y,z axes system
x,y,z	orthogonal axes system
α	outer gimbal angle
β	inner gimbal angle

A dot over a quantity signifies differentiation with respect to time.

ABSTRACT

Momentum feedback schemes, such as the one currently proposed for the Apollo Telescope Mount cluster, provide a relatively simple and effective means of obtaining near-linear control from highly nonlinear control moment gyro (CMG) momentum storage systems. However, these schemes are subject to adverse orientations of the CMG momentum or spin vectors for which spacecraft control capability is lost, although the momentum storage capacity of the CMG system has not yet been fully used or saturated. The adverse CMG orientations occur when all CMG momenta and the desired command momentum are collinear and can be classed as saturation, antisaturation, parallelism, and antiparallelism.

Since the adverse CMG orientations generally occur only for rare combinations of the command momentum and the CMG orientations, a simple correction technique for these conditions appears desirable in order to minimize the onboard control computer requirements. A study was made, leading to development and analysis of a technique allowing the CMG momentum vectors to avoid the adverse orientations and thus to provide optimal control. The technique was formulated in terms of a feedback scheme using a check factor K formed as the product of the dot products of the three CMG momentum unit vectors. These are already available, as direction cosines, in the momentum feedback loop of the control circuit. The parameter K approaches unity for all adverse orientations and is used to initiate a single correction

maneuver to rotate the CMG momenta away from a pending adverse orientation and to reduce K to an acceptable value. A digital computer program for ATM simulations was modified to incorporate this correction maneuver and performance was evaluated in simulated cases. Antiparallelism is the most typical adverse orientation expected and was used as the primary example for the evaluation of the feedback optimization technique. The effectiveness of the technique for other adverse conditions was also examined.

The K-factor correction technique described in this paper permits avoidance of adverse CMG orientations up to saturation and produces control for exit from the adverse orientations in the event that they are arbitrarily acquired.

CHAPTER I

INTRODUCTION

The subject area is optimal feedback control for an advanced control system concept for long-term spacecraft. The control configuration is a momentum storage system using control moment gyros (CMG's). A full-scale CMG unit is shown in Figure 1. A CMG consists of a flywheel spinning at a constant speed and mounted on double gimbals schematically shown in Figure 1(a).

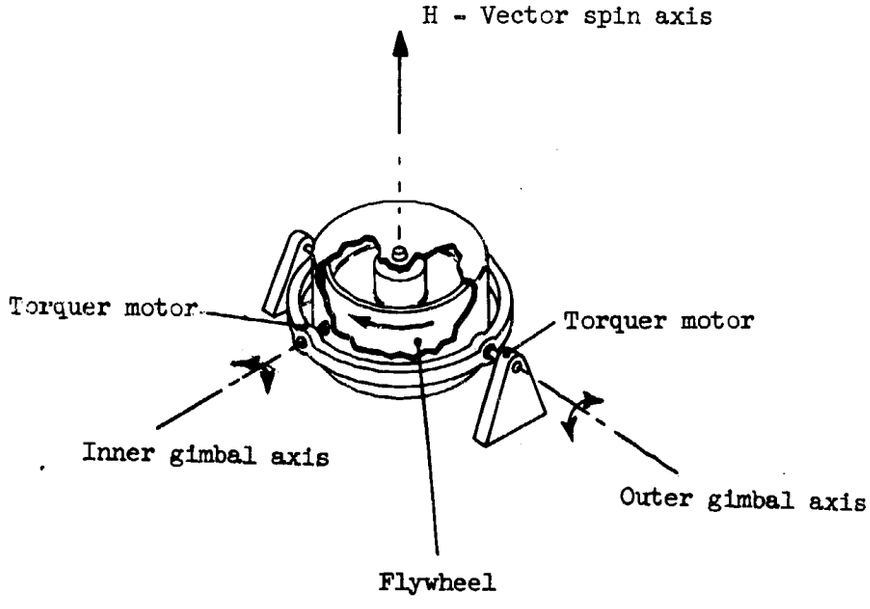

Figure 1(a).- CMG schematic.

These gimbals are alined with a spacecraft axis in their reference position. The outer gimbal cannot move into gimbal lock

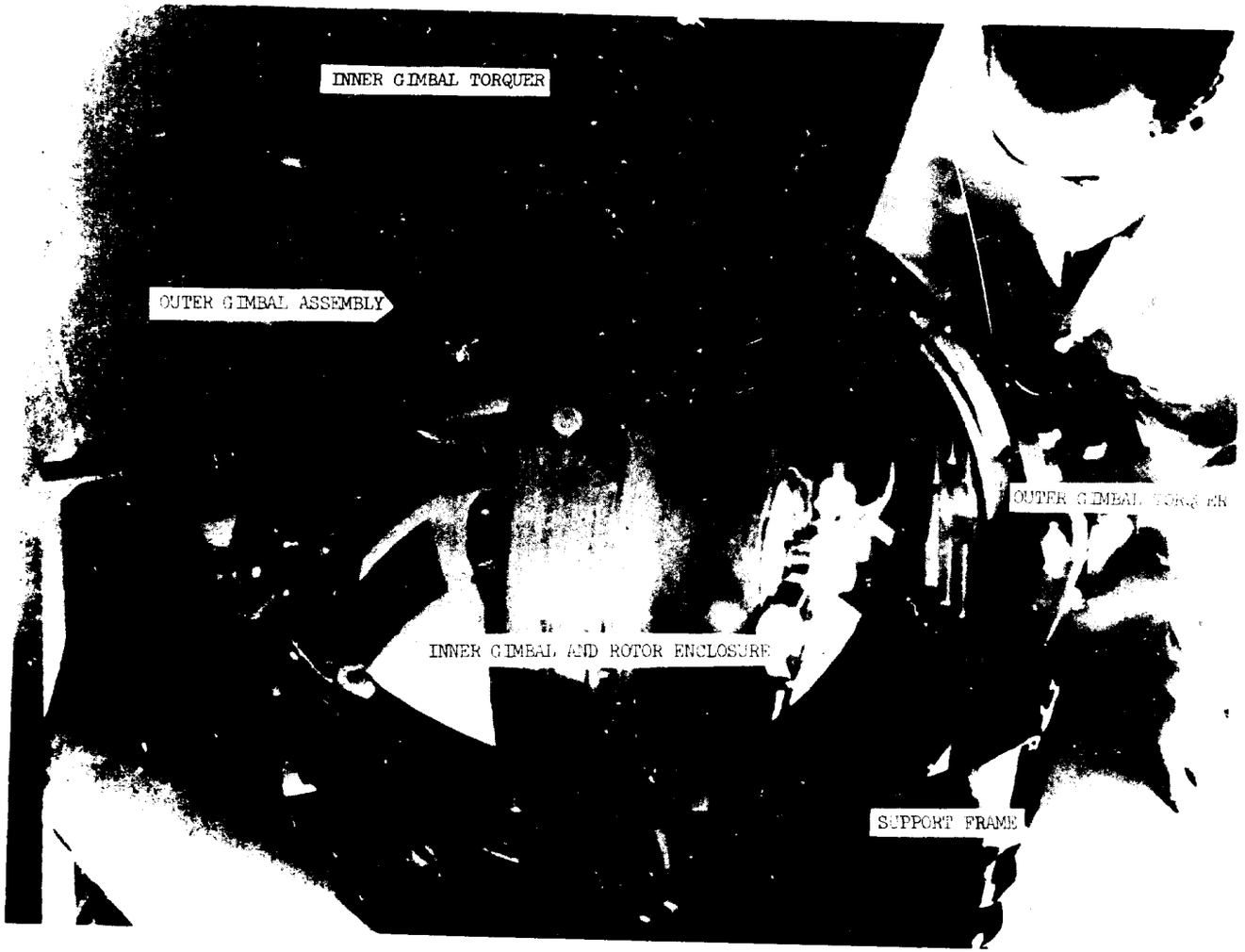

Figure 1.- Control moment gyro (CMG).

and rotates $\pm 180^{\circ}$ from a reference angle to take advantage of the available momentum storage capacity. The inner gimbal can incur gimbal lock at $\pm 90^{\circ}$ and is limited to an angle smaller than this value by means of mechanical stops.

Control torques are introduced by the precession of the constant speed flywheel which is mounted on the gimbals. For example, if a torque is applied to the outer gimbal of the CMG, an equal and opposite torque will act on the spacecraft, and the flywheel rotor will precess about the inner gimbal.

The CMG has been shown to be an effective means of momentum storage for the stabilization of long-term manned spacecraft (Ref. 1). The first manned spacecraft to use CMG's for attitude control is the Apollo Telescope Mount (ATM) cluster configuration comprised of a Saturn S-IVB Workshop and a multiple docking adapter to which is attached the Apollo Command Service Module (CSM), and the Lunar Module - ATM rack which houses a complement of solar pointing experiments (Fig. 2). The control system utilizes three CMG's mounted orthogonally on the exterior of the ATM rack (Fig. 2(a)). Since maneuvers can best be carried out with near-spherical momentum envelopes, all three gyros have been selected to have the same angular momentum of $H = 2000$ ft-lb-sec. The requirement for the CMG control system is to point the ATM cluster to at least 0.1° about all axes while a vernier platform points the experiment package to 2.5 seconds of arc.

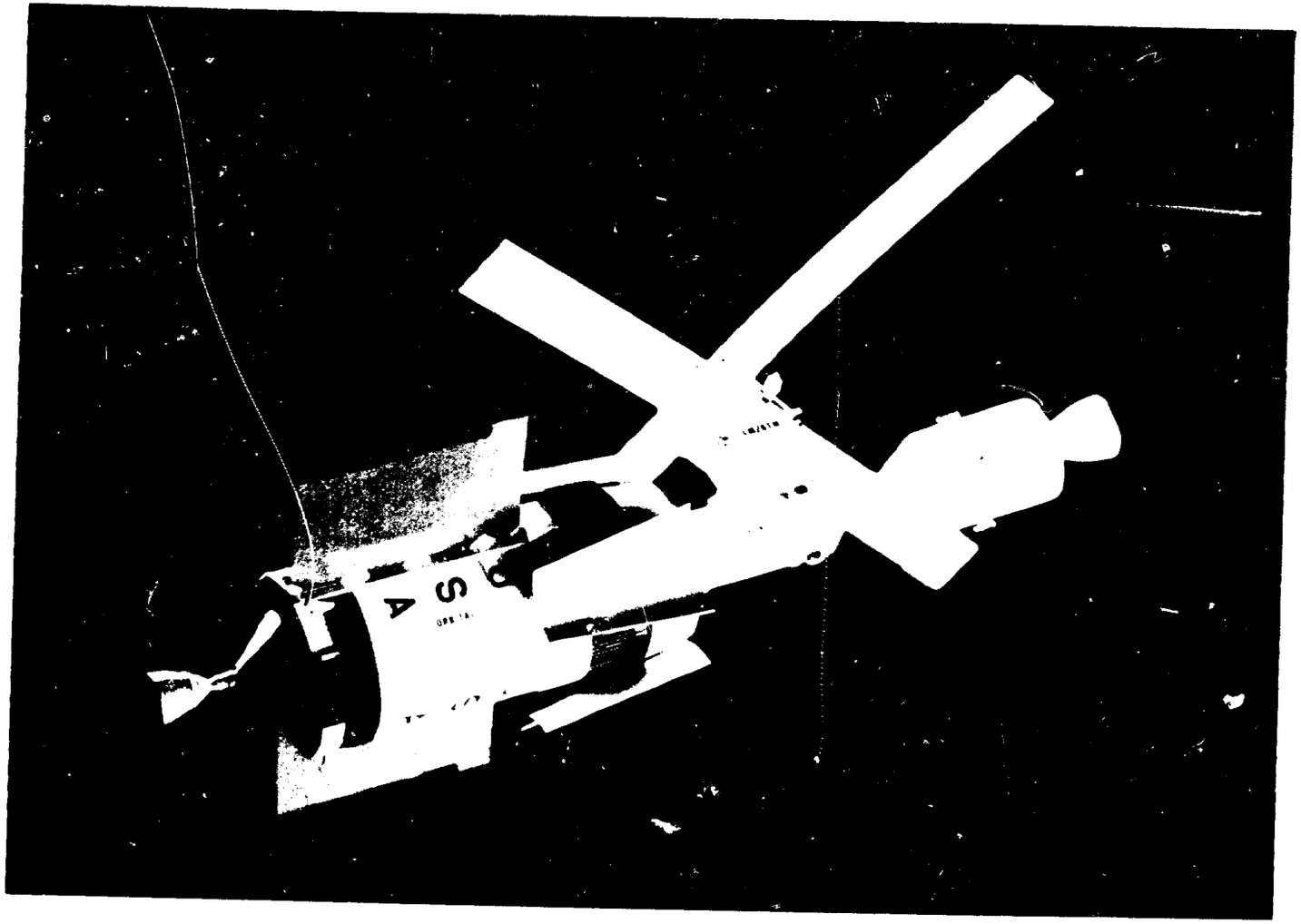

Figure 2.- Apollo telescope mount cluster configuration.

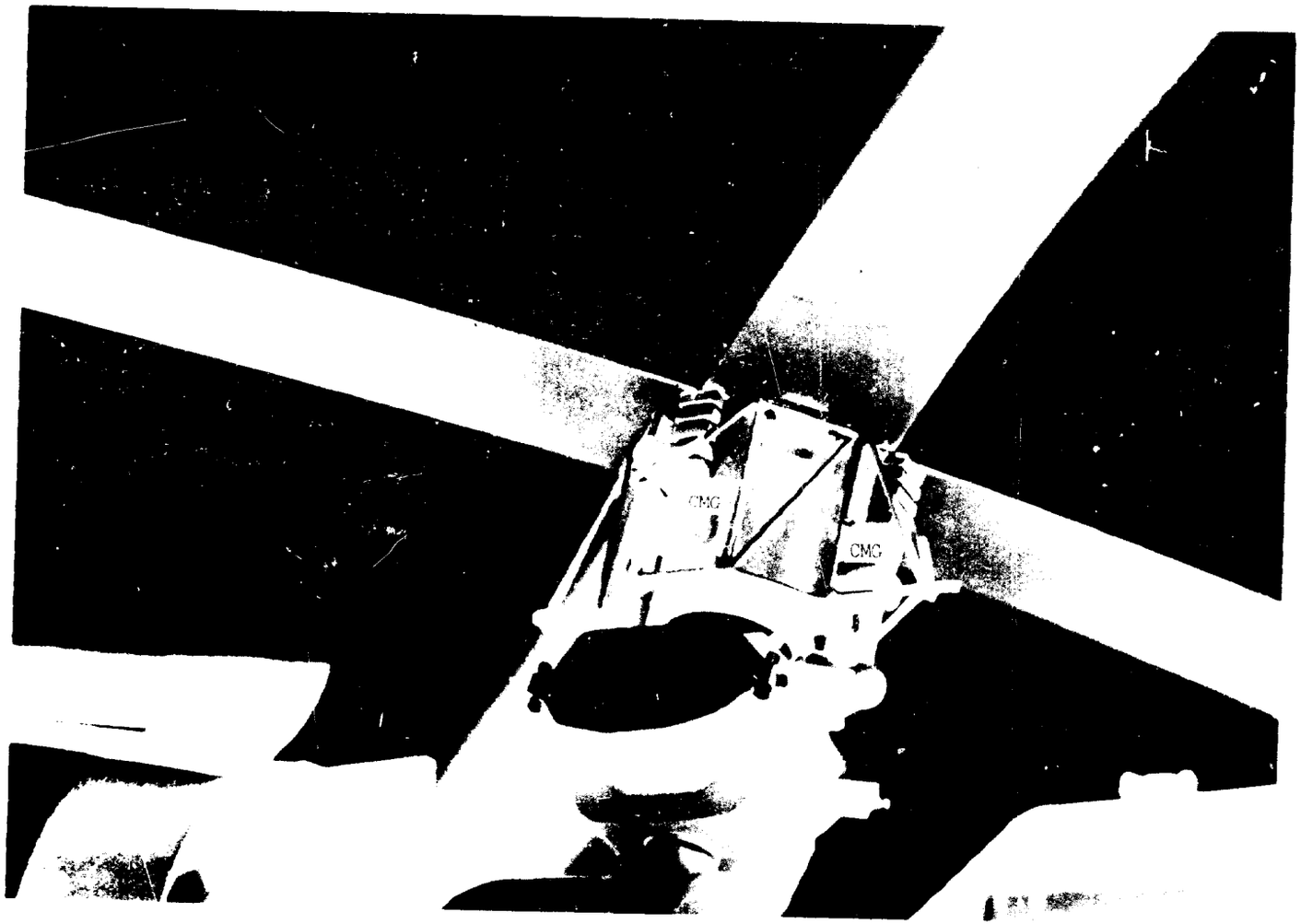

Figure 2(a).- Lunar Module - ATM rack configuration (indicated disks represent CMG's).

The CMG system inherently exhibits nonlinearities in its response and requires angular momentum feedback to establish satisfactory linear control (Appendix A). With the three distinct CMG angular momentum vectors to oppose the commanded momentum, the momentum feedback scheme suffers from variable gain as a function of the relative orientation of the CMG momenta and the commanded momentum and is also subject to adverse CMG system orientations which lead to loss of control and large spacecraft errors. Because of these CMG system control characteristics, techniques are needed for minimizing system gain variation and avoiding adverse CMG orientations. A primary objective is minimization of inner gimbal angles to avoid the selected 80° limit and to reduce gimbal power requirements.

One technique defined as the isogonal correction, employs a distribution law and rotation law for the individual angular momentum vectors (Ref. 2). The desirable distribution is for the individual angular momentum vectors to have equal components along the total control momentum, and thus maintain the angular momentum vectors in an umbrella-like configuration which effectively prohibits the attainment of an adverse orientation. The rotation law is added to minimize the inner gimbal angles and avoid the inner gimbal limits as much as possible. The mechanization of this type of law requires significant additional onboard computer capacity to carryout the additional calculations. The use of this complex procedure and added control computer capability appears undesirable for a flight mission since the adverse CMG orientations generally occur only for rare combinations of the command

momentum and the CMG initial orientations. It was therefore decided that a study of a simpler alternate method of first detecting and then correcting for the approaching adverse orientations would be extremely useful.

The problem areas in the development of this simplified technique included:

1. The determination of a check factor "K" as an indicator of momentum orientation.

2. A deadband technique to keep the check factor within a given range to avoid the adverse orientations in order to keep the spacecraft errors within minimum acceptable levels.

3. A method for varying K to achieve the approximate isogonal correction.

These problem areas constitute the purpose of this research and are examined herein. A performance evaluation with digital computer simulations has been made with the best selected feedback technique to both avoid and exit from the adverse CMG orientations.

CHAPTER II

SPACECRAFT AND CONTROL SYSTEM SIMULATINN

For ATM mission simulations a digital computer solves the spacecraft rigid body and flexible equations of motion. The equations comprising this computer program are from Reference 3 and are included in the Appendices. The contribution of the flexibility to the spacecraft rate and attitude errors is determined from dynamic and quasi-static modal representations of the ATM cluster included in Appendix B. For the present study only biased disturbance torques were applied to the spacecraft. From these disturbances and the resulting spacecraft rate and attitude errors, the computer then solves the control law to command the appropriate gimbal rates to the CMG torque motors which precess the spinning rotors and apply restoring control torques to close the simulation loop. Reference axes for the ATM cluster configuration are defined in Figure 3 where the spacecraft z-axis is taken to be the solar pointing axis, and the x-axis to have the minimum moment of inertia.

The control system for the spacecraft uses a gimbal rate steering matrix and CMG system momentum feedback as presented in Appendix A. The computer program constants used for the ATM simulations are included in Appendix C.

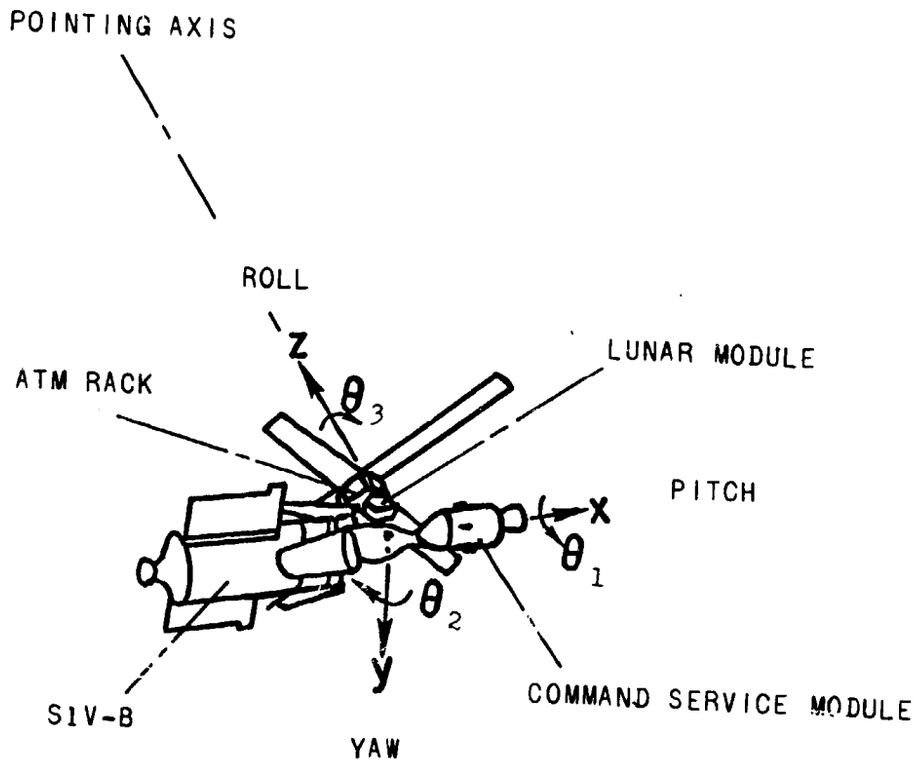

Figure 3.- ATM axes system.

CHAPTER III

ADVERSE CMG ORIENTATIONS

Digital computer simulations with CMG control systems have indicated serious control problem areas associated with particular orientations of the CMG angular momentum or spin vectors that could occur during normal control operations.

The CMG axis placement for the ATM orientation and positive gimbal angle notation for the CMG angular momentum vectors is defined in Figure 4.

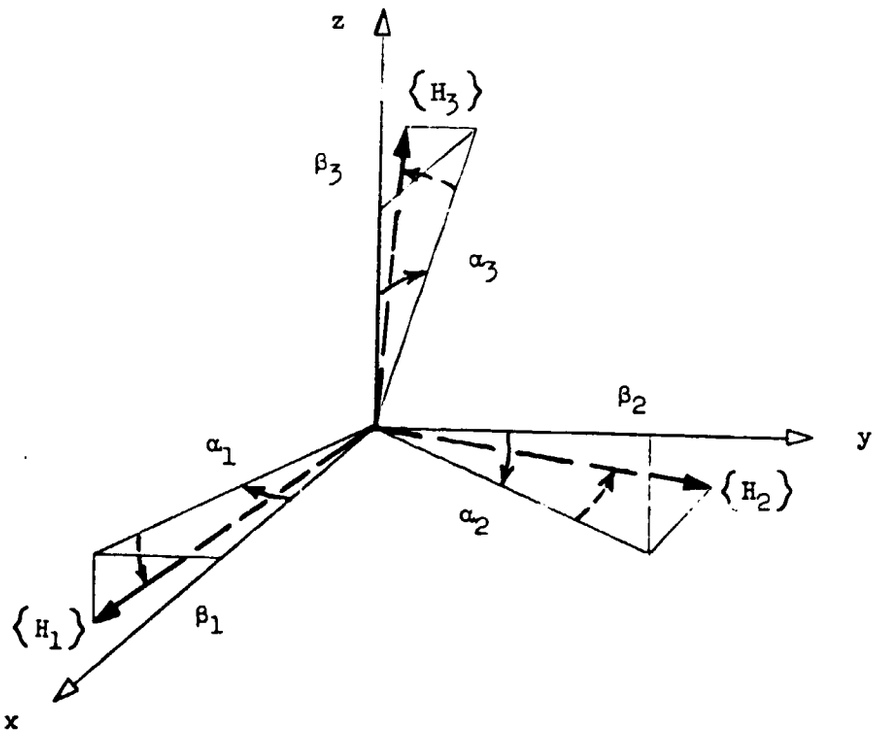

Figure 4.- CMG axes system.

The variables α_i, β_i represent the CMG gimbal angles with the subscript identifying the CMG. The outer gimbal angles are designated by the symbol α and the inner gimbal angles by β. The positive outer gimbal rate $\dot{\alpha}_1$ is about the -z spacecraft axis, $\dot{\alpha}_2$ about the -x spacecraft axis, and $\dot{\alpha}_3$ about the -y axis.

Each of the three CMG units has an angular momentum of

$$H = 2000 \text{ ft-lb-sec}$$

and limits are imposed on the gimbal rates and angles for the ATM system. The CMG inner gimbal angles are limited to $\pm 80^\circ$ as previously mentioned, and the CMG outer gimbal angles are limited to $\pm 175^\circ$ with respect to this zero momentum orientation for which

$$\alpha_1 = 45^\circ \qquad \beta_1 = 0^\circ$$
$$\alpha_2 = 45^\circ \qquad \beta_2 = 0^\circ$$
$$\alpha_3 = 45^\circ \qquad \beta_3 = 0^\circ$$

The CMG gimbal rate magnitudes $\dot{\alpha}_i$, $\dot{\beta}_i$ are restricted to be equal to or less than 3.5 deg/sec by gimbal power limitations.

For the three-gyro system, there are four possible CMG spin-vector orientations which should be avoided during normal operations. Figure 5 indicates the relative placement of the disturbance moment, $\{M_D\}$, and the CMG angular momentum vectors for the undesirable orientations. For these relative placements of the disturbance and control vectors, the CMG control system cannot produce a control torque

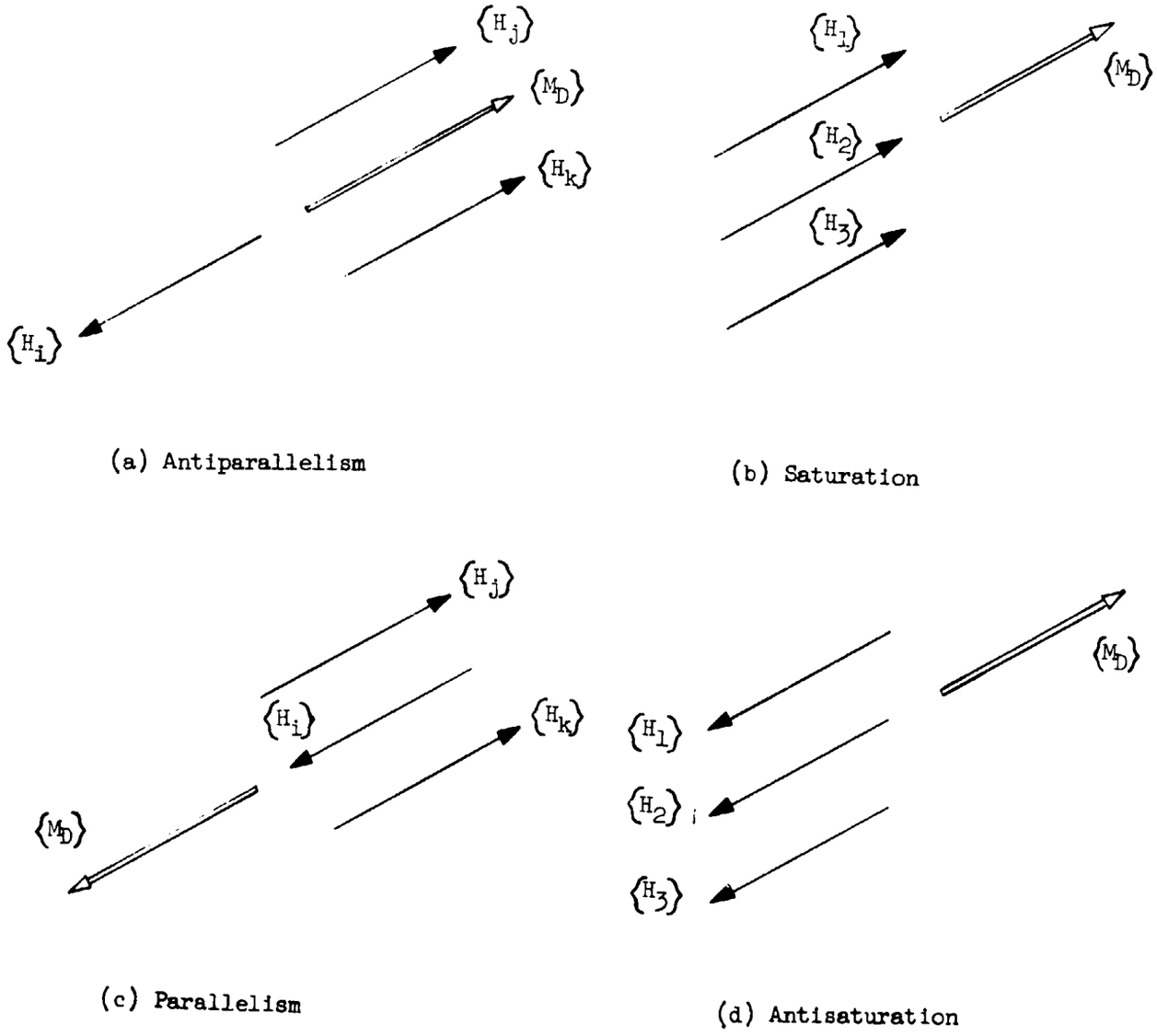

(a) Antiparallelism

(b) Saturation

(c) Parallelism

(d) Antisaturation

Figure 5.- Adverse CMG spin vector - command moment orientations.

to oppose the disturbance torque and excessive spacecraft errors will occur.

For the antiparallel condition bias disturbance torques have driven the CMG spin vectors into a configuration with two H-vectors opposing the third and the disturbance moment, $\langle M_D \rangle$, collinear, but opposed to the third CMG spin vector. For the saturation condition a bias disturbance torque has driven all three CMG H-vectors parallel to each other and alined with and having the same sense as the disturbance moment $\langle M_D \rangle$. The parallel condition is identical with the antiparallel condition in that two H-vectors oppose a third, but the disturbance moment $\langle M_D \rangle$ is now alined with the third CMG spin vector. For the antisaturation condition all three CMG H-vectors are parallel to each other and oppose the disturbance moment. With CMG control lost in any of these adverse orientations, the spacecraft mission is seriously handicapped, and a means of correction for the adverse conditions is needed.

The orientations that predominate during normal operations are the saturation and antiparallel conditions. For the saturation condition all of the control system momentum has been expended and external moments from either reaction jets or spacecraft reorientations, prior to total saturation, are required to change the CMG spin-vector alinements with the bias command moment. In normal earth-orbit operations, the gravity gradient bias moments will eventually saturate the control system, and planned desaturation techniques will be applied during the dark side or night portion of the orbit so as not to interfere

with mission requirements. The antiparallel condition, on the other hand, has used only one-third of the control system momentum, even though effective control is no longer possible.

For these pending adverse orientations, the effective gain of the control system is reduced since the control torque decreases as the adverse orientation is approached. Optimal feedback control can only be obtained by forcing the CMG vectors to maintain favorable orientations relative to the commanded momentum as long as possible. The associated fundamental momentum relations for the CMG system are developed in the following sections.

CMG Momenta

Unit vectors for the individual CMG angular momentum vectors are

$$\frac{\langle H_1 \rangle}{H} = \langle h_1 \rangle$$

$$\frac{\langle H_2 \rangle}{H} = \langle h_2 \rangle \qquad (1)$$

$$\frac{\langle H_3 \rangle}{H} = \langle h_3 \rangle$$

where the vectors $\langle h_1 \rangle$, $\langle h_2 \rangle$, $\langle h_3 \rangle$ comprise the direction cosines for the CMG momenta and become

$$\{h_1\} = \begin{Bmatrix} \cos\beta_1 \cos\alpha_1 \\ -\cos\beta_1 \sin\alpha_1 \\ -\sin\beta_1 \end{Bmatrix} \equiv \begin{Bmatrix} h_{11} \\ h_{12} \\ h_{13} \end{Bmatrix}$$

$$\{h_2\} = \begin{Bmatrix} -\sin\beta_2 \\ \cos\beta_2 \cos\alpha_2 \\ -\cos\beta_2 \sin\alpha_2 \end{Bmatrix} \equiv \begin{Bmatrix} h_{21} \\ h_{22} \\ h_{23} \end{Bmatrix} \qquad (2)$$

$$\{h_3\} = \begin{Bmatrix} -\cos\beta_3 \sin\alpha_3 \\ -\sin\beta_3 \\ \cos\beta_3 \cos\alpha_3 \end{Bmatrix} \equiv \begin{Bmatrix} h_{31} \\ h_{32} \\ h_{33} \end{Bmatrix}$$

The components for the h_{ij} are available directly from the CMG gimbal resolvers.

Normalized Momentum

The total control system angular momentum is

$$\{H\} = \{H_1\} + \{H_2\} + \{H_3\} \qquad (3)$$

or

$$\{H\} = H\left[\{h_1\} + \{h_2\} + \{h_3\}\right] \qquad (4)$$

and a normalized total momentum magnitude is defined as

$$HT = \frac{\left[\langle H\rangle \cdot \langle H\rangle\right]^{1/2}}{3H} \tag{5}$$

or

$$HT = \frac{1}{3}\left[\left(\langle h_1\rangle + \langle h_2\rangle + \langle h_3\rangle\right) \cdot \left(\langle h_1\rangle + \langle h_2\rangle + \langle h_3\rangle\right)\right]^{1/2} \tag{6}$$

with the resulting bounds

$$0 \leq HT \leq 1 \tag{7}$$

For the antiparallel and parallel orientations

$$HT = \frac{1}{3}$$

and for the saturation and antisaturation orientations

$$HT = 1$$

Antiparallel Orientation

To consider a pending antiparallel orientation examine the CMG spin-vector alinements sketched below.

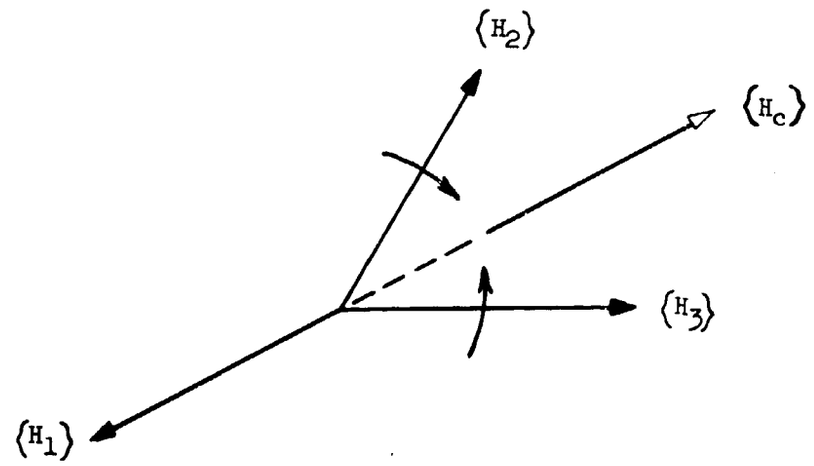

Figure 6.- Spin-vector orientation for pending antiparallel condition.

Two of the CMG spin vectors, here chosen to be $\langle H_2 \rangle$ and $\langle H_3 \rangle$ approach each other, while the third, $\langle H_1 \rangle$ is opposed to the commanded momentum $\langle H_c \rangle$. The antiparallel condition is reached when

$$\begin{aligned} \langle H_1 \rangle \cdot \langle H_2 \rangle &= -H^2 \\ \langle H_1 \rangle \cdot \langle H_3 \rangle &= -H^2 \\ \langle H_2 \rangle \cdot \langle H_3 \rangle &= H^2 \end{aligned} \tag{8}$$

or in terms of the unit vectors when

$$\begin{aligned} \langle h_1 \rangle \cdot \langle h_2 \rangle &= -1 \\ \langle h_1 \rangle \cdot \langle h_3 \rangle &= -1 \\ \langle h_2 \rangle \cdot \langle h_3 \rangle &= 1 \end{aligned} \tag{9}$$

Having developed an expression for the normalized momentum, HT, the next step is the determination of a check factor, K, as a normalized indicator of momentum orientation and relate both normalized quantities to the adverse orientations.

CHAPTER IV

DETECTION OF ADVERSE ORIENTATIONS

To detect an approaching adverse orientation the dot products of the direction cosine vectors are computed as

$$K_{12} \equiv \langle h_1 \rangle \cdot \langle h_2 \rangle = h_{11}h_{21} + h_{12}h_{22} + h_{13}h_{23}$$

$$K_{13} \equiv \langle h_1 \rangle \cdot \langle h_3 \rangle = h_{11}h_{31} + h_{12}h_{32} + h_{13}h_{33} \qquad (10)$$

$$K_{23} \equiv \langle h_2 \rangle \cdot \langle h_3 \rangle = h_{21}h_{31} + h_{22}h_{32} + h_{23}h_{33}$$

and a variable check factor K is defined as

$$K = K_{12}K_{13}K_{23} \qquad (11)$$

From the reasoning leading to equation (11), it is apparent that an adverse condition is pending if

$$K \to 1 \qquad (12)$$

The normalized momentum HT and the check factor K together define the specific adverse orientations and hence establish undesirable control regions.

The relation between the check factor K and the normalized momentum HT for the four adverse conditions is summarized in Table I.

TABLE I.- CHECK FACTOR - NORMALIZED MOMENTUM RELATION FOR ADVERSE CMG ORIENTATIONS

Adverse condition	Check factor, K	Normalized momentum, HT
Antiparallelism	1	1/3
Parallelism	1	1/3
Saturation	1	1
Antisaturation	1	1

Linear Analysis of Impending Adverse Orientations

With a constant disturbance torque bias (characteristic of external torques in an orbit environment) applied to the spacecraft the CMG control system must eventually reach one of the collinear orientations. The objective of the check factor K reduction is to keep the control system away from pending antiparallelism and parallelism at HT = 1/3, for the constant disturbance torque, and allow the system orientation to proceed to saturation at HT = 1 where planned desaturation techniques will be applied. In this way, the full capability of the three double-gimbaled CMG system may be realized prior to any adverse control effects on the spacecraft response.

It was previously indicated that K = 1 for all adverse CMG orientations. The determination of how the total system momentum

varies with the position of the CMG spin vectors, especially for a pending adverse condition, is the necessary first step of analysis since the check factor K has been chosen as an indicator of momentum orientation.

In correcting for a pending antiparallel orientation where the check factor K approaches 1.0, a deadband technique is analyzed and developed to reduce K. This requires the definition of a check factor limit, K_{LIM}, such that when

$$K \geq K_{LIM}$$

the correction maneuver will be initiated. A linear analysis of pending antiparallelism and parallelism was made to determine approximate relations between K_{LIM}, the CMG momenta, and the commanded momentum. Appropriate relations are developed to establish the check factor limit for a given normalized total momentum requirement.

An approximate method may be used to determine the impact of K on the orientation of the CMG unit momentum vectors and on the extent of CMG system saturation. As the saturation or the antiparallel condition is approached, the CMG momenta are driven to approach the commanded momentum in a predictable fashion since the vector sum of the commanded momentum and the CMG system momentum is maintained at zero by the ATM control law.

The permissible resultant CMG momentum vector orientations can be visualized by considering the projections of unit vectors along these momenta onto a plane normal to the commanded momentum vector, as is

done in Figure 7. The commanded momentum vector, which is coming out of the paper, is indicated by a small solid circle in the figure, and the intersections of the CMG momentum unit vectors and the normal plane are denoted by larger circles. Dots and crosses are used to define CMG momenta coming out of or going into the paper, and the projection of these CMG momenta is described by directed, dashed lines. Angles between the various momenta are designated by ϵ_k.

Relations between the saturation ratio and the variable check factor K are developed for the cases of impending saturation and antiparallelism. To simplify the form and application of these equations, it is assumed that the angles ϵ_k between the commanded momentum and the CMG momenta and the angles between the CMG momenta are sufficiently small to yield

$$\left.\begin{aligned} \sin \epsilon_k &\simeq \epsilon_k \\ \cos \epsilon_k &\simeq 1 - \frac{\epsilon_k^2}{2} \end{aligned}\right\} \tag{13}$$

and terms of higher order than ϵ_k^2 are neglected.

Saturation

The general CMG orientation for the case of impending saturation, shown in Figure 7, is characterized by an arbitrary triangle formed by the tips of the CMG momentum vectors and pierced at its geometric center by the tip of the commanded momentum vector. The angles $(\epsilon_4, \epsilon_5, \epsilon_6)$ between the commanded momentum and the CMG momenta are related to the angles $(\epsilon_1, \epsilon_2, \epsilon_3)$ between the CMG momenta by

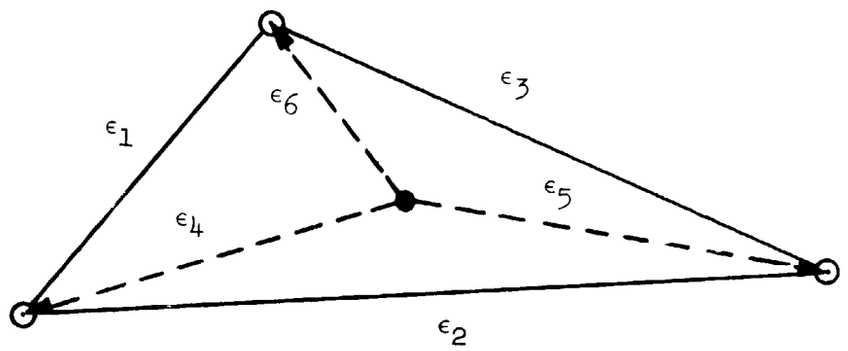

Figure 7.- Impending saturation.

$$\left.\begin{aligned} \epsilon_4^2 &\simeq \frac{1}{9}\left[2\epsilon_1^2 + 2\epsilon_2^2 - \epsilon_3^2\right] \\ \epsilon_5^2 &\simeq \frac{1}{9}\left[2\epsilon_2^2 + 2\epsilon_3^2 - \epsilon_1^2\right] \\ \epsilon_6^2 &\simeq \frac{1}{9}\left[2\epsilon_3^2 + 2\epsilon_1^2 - \epsilon_2^2\right] \end{aligned}\right\} \tag{14}$$

From Figure 7 and equations (6) and (13), the saturation ratio becomes

$$\begin{aligned} HT &\simeq \left[1 - \frac{1}{6}(\epsilon_4^2 + \epsilon_5^2 + \epsilon_6^2)\right] \\ &= \left[1 - \frac{1}{18}(\epsilon_1^2 + \epsilon_2^2 + \epsilon_3^2)\right] \end{aligned} \tag{15}$$

while the variable check factor is

$$K \simeq \left[1 - \frac{1}{2}(\epsilon_1^2 + \epsilon_2^2 + \epsilon_3^2)\right] \tag{16}$$

Equations (15) and (16) give

$$HT \simeq \frac{1}{9}(8 + K) \tag{17}$$

as the approximate relation between the variable check factor and the total CMG system saturation ratio. Figure 8 presents the linear approximation for impending saturation (eq. (17)) plotted on the K versus HT parameter plot for a typical simulation case where anti-parallelism was avoided at K = 1.0 and HT = 1/3 and the control system proceeded to saturation at K = 1.0 and HT = 1.0.

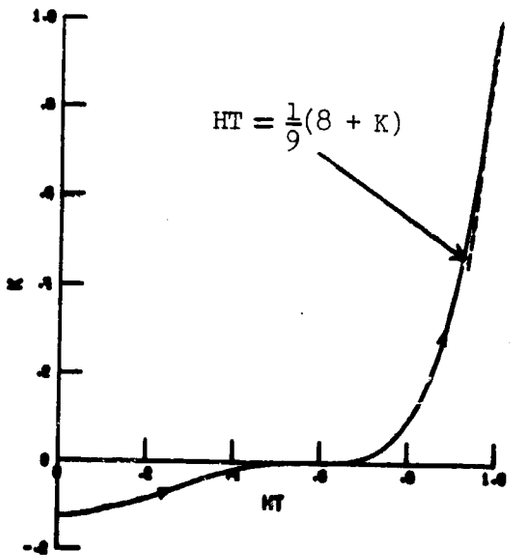

Figure 8.- Linear approximation for saturation.

Antiparallelism

The general CMG orientation for the case of impending antiparallelism, sketched in Figure 9, is characterized by a parallelogram formed by the end of the CMG momentum vectors and the commanded momentum vector. The angle (ϵ_4) between the commanded momentum and the opposing CMG momentum is related to the angles ($\epsilon_1, \epsilon_2, \epsilon_3$) between the CMG momenta by the condition

$$\epsilon_4^2 \simeq \left[2\epsilon_2^2 + 2\epsilon_3^2 - \epsilon_1^2\right] \tag{18}$$

from Figure 9.

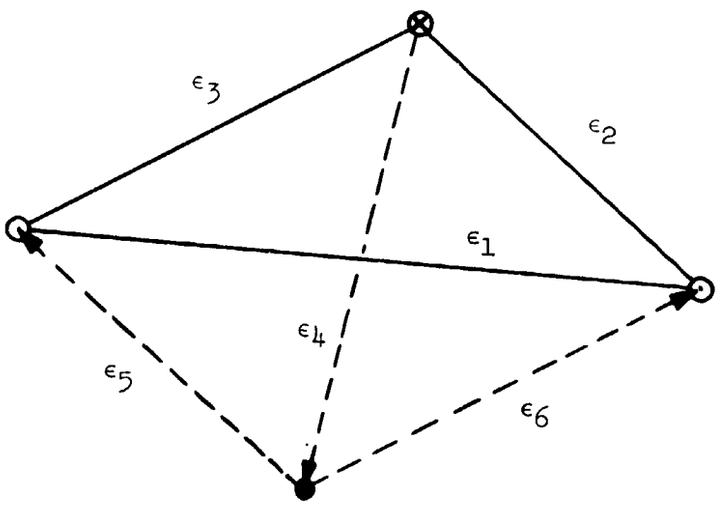

Figure 9.- Impending antiparallelism.

The saturation ratio becomes

$$HT \simeq \frac{1}{3} - \frac{1}{6}(\epsilon_2^2 + \epsilon_3^2 - \epsilon_4^2)$$
$$\simeq \frac{1}{3} - \frac{1}{12}(\epsilon_1^2 - \epsilon_4^2) \tag{19}$$

while the variable check factor is given by

$$K \simeq 1 - \frac{1}{2}(\epsilon_1^2 + \epsilon_2^2 + \epsilon_3^2)$$
$$\simeq 1 - \frac{1}{4}(3\epsilon_1^2 + \epsilon_4^2) \tag{20}$$

Two cases are of interest and correspond to approaches from $HT < 1/3$ (antiparallelism) and from $HT > 1/3$ (parallelism). For the first of these, equation (18) indicates that for $\epsilon_4 > \epsilon_1$ and elimination of ϵ_1 from equations (19) and (20) yields

$$HT \simeq \frac{1}{9}(2 + K) + \frac{\epsilon_4^2}{9} \tag{21}$$

if terms on the order of ϵ_4^2 are neglected in equation (21), then

$$HT \simeq \frac{1}{9}(2 + K) \tag{22}$$

for $HT \leq 1/3$. For this case, Figure 10 presents this linear approximation for impending antiparallelism (eq. (22)) plotted on the K versus HT parameter plot for a typical antiparallel approach case where spacecraft control was lost at $HT = 1/3$. The linear equation

for the antiparallel orientation gives a reasonably good approximation for values of $K > 0.7$ and $HT > 0.3$.

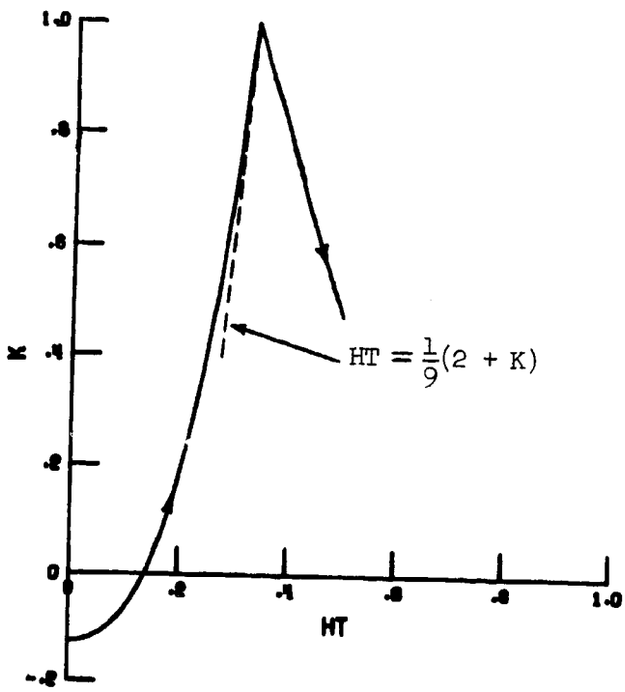

Figure 10.- Linear approximation for antiparallelism.

For the second case, equation (18) gives $\epsilon_4 < \epsilon_1$ and elimination of ϵ_4 from equations (19) and (20) results in

$$HT \simeq \frac{1}{3}(2 - K) - \frac{\epsilon_1^2}{3} \qquad (23)$$

Again, neglecting terms on the order of ϵ_1^2, this reduces to

$$HT \simeq \frac{1}{3}(2 - K) \tag{24}$$

for $HT > 1/3$.

The CMG system response trends characterized by Figures 7 and 9 may be considerably modified by system nonlinearities such as gimbal angle limits and cross coupling which can transform an apparent anti-parallel approach into a normal saturation approach.

Antisaturation and Parallelism

The conditions of antisaturation and parallelism can be reached only through respective saturation and antiparallel approaches, with subsequent change of sign of the disturbance moment after the adverse collinear orientations are acquired. For antisaturation, this yields

$$HT = K \tag{25}$$

and for parallelism

$$HT = \frac{1}{3} K \tag{26}$$

with both HT and K remaining constant.

CHAPTER V

CORRECTION FOR ADVERSE CMG ORIENTATIONS

Correction Maneuver

The basic approach to be studied in reducing K when K_{LIM} is reached is to command an inner gimbal motor actuator to rotate a single CMG spin vector to oppose a pending adverse condition and hence maintain control. The ATM control law automatically compensates for the change in the CMG system momentum due to the inner gimbal rotation, and will thus bring the remaining two CMG momenta out of the adverse orientation while continuing to provide control for the ATM cluster. Since the CMG system momentum is fed directly to the gimbal rate commands, the CMG gimbal torquers automatically compensate for any change in this momentum which is not due to spacecraft momentum requirements (Appendix A). The net result is a rotation of the CMG momentum vectors away from the adverse orientation without the introduction of spacecraft attitude or rate errors.

K-Factor Technique

To correct for an adverse CMG momentum distribution, the gimbal rates can be commanded to move one or more CMG momentum vectors away from the adverse orientation. A deadband on K can serve to implement such a scheme.

The simplest momentum reorientation command would use a single inner gimbal rate (say that for the largest inner gimbal angle, which

can be readily determined by comparison of the available cosine functions for the three inner gimbal angles) and would drive that inner gimbal angle toward its zero value, until an acceptable value of K is reached.

Figure 11 illustrates a possible implementation of such a correction for adverse CMG momentum distributions. The maximum inner gimbal angle and the check parameter K would be continuously or periodically determined. When K exceeds a preselected value, K_{LIM}, the maximum inner gimbal angle is commanded toward its zero value at

$$\dot{\beta}(\beta_{MAX}) = -\dot{\beta}_c \sin(\beta_{MAX}) \tag{27}$$

until K is reduced by ΔK and a more favorable momentum distribution has been established. The correction maneuver is terminated when

$$K \leq K_{LIM} - \Delta K$$

This CMG reorientation also serves to reduce the largest CMG inner gimbal angle, and thus aids in improving the corresponding CMG effective gain. A known torque $H\dot{\beta}_c \sin \beta_{MAX}$ is applied to the spacecraft during the correction. However, this torque is directly compensated for by the CMG system inner loop and can be selected to be sufficiently small to cause negligible spacecraft errors.

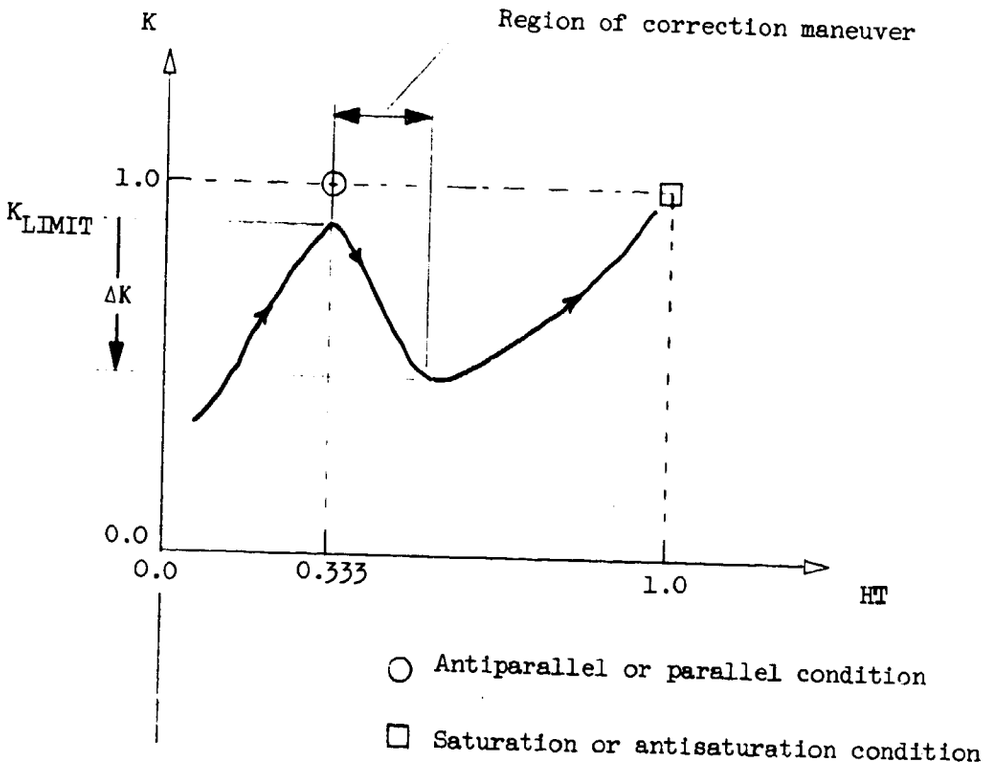

Figure 11.- Constant deadband K-factor correction.

Isogonal Distribution

The most effective control (Ref. 2) with the three available CMG momentum vectors is provided when these control momentum vectors have equal angles between themselves and are grouped in an umbrella configuration about the command momentum as illustrated in Figure 12.

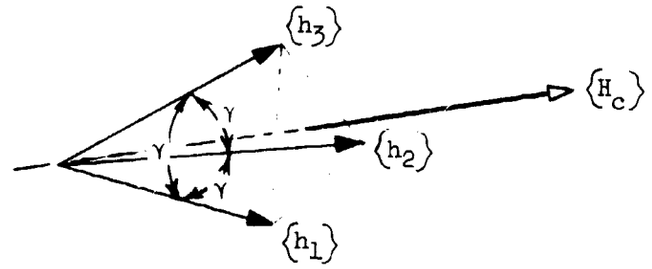

Figure 12.- Isogonal distribution.

The dot products of the unit momentum vectors are

$$\left(\langle h_1\rangle \cdot \langle h_2\rangle\right) = \left(\langle h_1\rangle \cdot \langle h_3\rangle\right) = \left(\langle h_2\rangle \cdot \langle h_3\rangle\right) = \cos\gamma \qquad (28)$$

so that the normalized angular momentum

$$HT^2 = \frac{1}{3} + \frac{2}{9}\left[\left(\langle h_1\rangle \cdot \langle h_2\rangle + \langle h_1\rangle \cdot \langle h_3\rangle + \langle h_2\rangle \cdot \langle h_3\rangle\right)\right] \qquad (29)$$

becomes

$$HT^2 = \frac{1}{3} + \frac{2}{3}\cos\gamma \qquad (30)$$

while the check factor K from equation (11)

$$K = \left(\langle h_1\rangle \cdot \langle h_2\rangle\right)\left(\langle h_1\rangle \cdot \langle h_3\rangle\right)\left(\langle h_2\rangle \cdot \langle h_3\rangle\right) \qquad (31)$$

becomes

$$K = \cos^3\gamma \qquad (32)$$

Eliminating $\cos\gamma$ between equations (30) and (32) yields the relation between the isogonal check factor, KI, and the normalized momentum

$$KI = \frac{1}{8}\left[3HT^2 - 1\right]^3 \tag{33}$$

A plot of KI versus HT is presented in Figure 13.

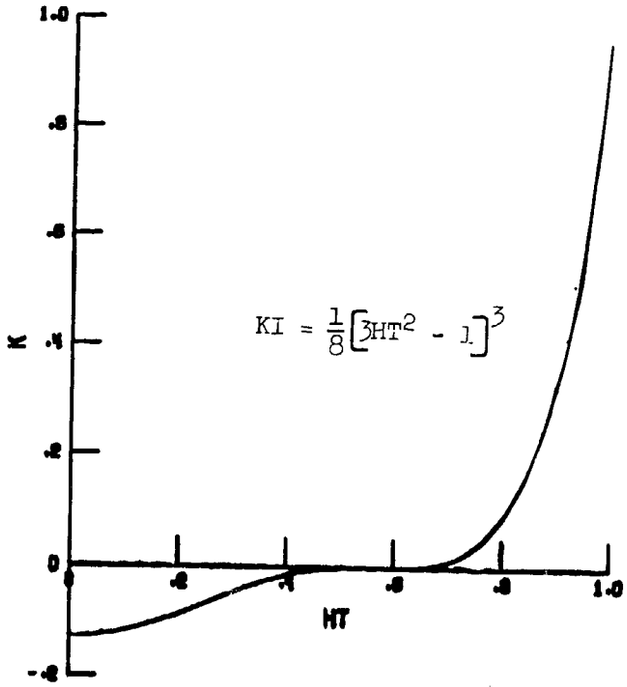

Figure 13.- Variation of the isogonal check factor KI with the normalized momentum.

Extension of K-Factor Correction to Isogonal Case

A simple extension of the K correction technique to yield an isogonal correction appears possible by introducing a variable

deadband for initiation of the largest inner gimbal angle rate command. The isogonal correction satisfies the equation

$$KI = \frac{1}{8}\left[3HT^2 - 1\right]^3 \tag{34}$$

for all values of HT. Since HT^2 is available from the measured CMG system momentum direction cosine vectors, the isogonal value for KI can be directly calculated from this expression.

The resultant value of KI could serve as a lower bound for the K correction, which would now be implemented as shown in Figure 14. A variable deadband defined by a lower limit KI and an upper limit K_{LIM}, where

$$K_{LIM} \equiv KI + \Delta K \tag{35}$$

and ΔK is a preselected constant, is introduced. When K exceeds K_{LIM}, the maximum inner gimbal is commanded at

$$\dot{\beta}_{(\beta_{MAX})} = -\dot{\beta}_c \sin \beta_{MAX} \tag{36}$$

This correction drives β_{MAX} toward zero and continues until K reaches the isogonal value KI.

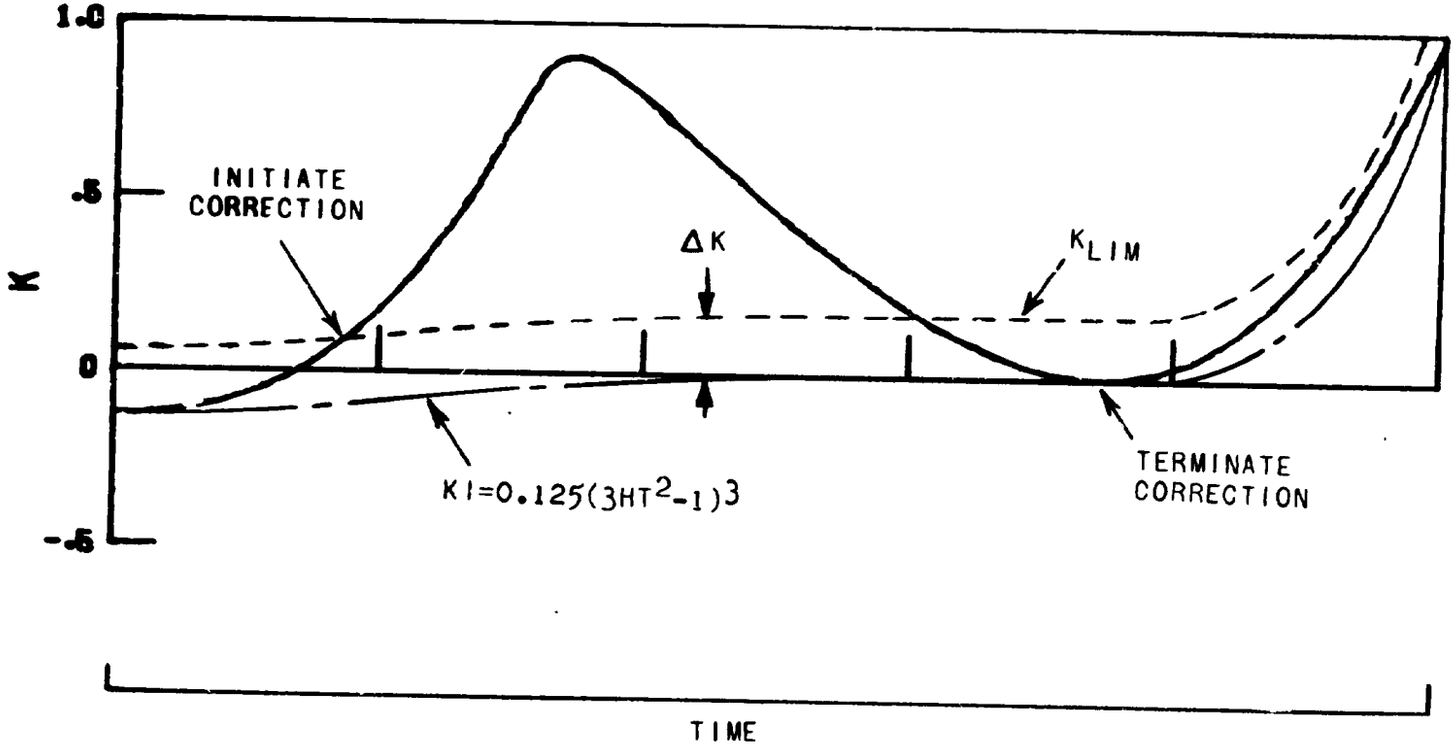

Figure 14.- Variable deadband K-factor correction.

CHAPTER VI

APPLICATION SIMULATIONS TO AVOID ADVERSE ORIENTATIONS

Both the constant and variable deadband versions of the K correction technique have been simulated for the ATM mission. A flexible ATM spacecraft, with seven bending modes incorporated dynamically and the remaining bending modes incorporated quasi-statically, is considered. Bending data and control law parameters and filters are taken as the ATM design values (Appendix C). The CMG servo loops are assumed to be ideal, and yield a CMG transfer function of unity. Example cases are presented here to illustrate the spacecraft and CMG system response for a constant 20 ft-lb disturbance moment representative of a worst case gravity gradient bias disturbance. Zero-momentum and orthogonal initial orientations for the CMG system are considered.

Constant Deadband K-Factor Correction

Figure 15 shows the ATM and CMG system response for a characteristic antiparallel approach starting from a zero-momentum orientation. The applied disturbance torque opposes CMG 1. Rate and attitude errors at the center of the ATM experiment package are given in Figure 15(a). The errors associated with the K correction are small in comparison with the steady-state errors produced by the applied disturbance moment. The GAIN performance factor (Appendix A, eq. (A27)) is

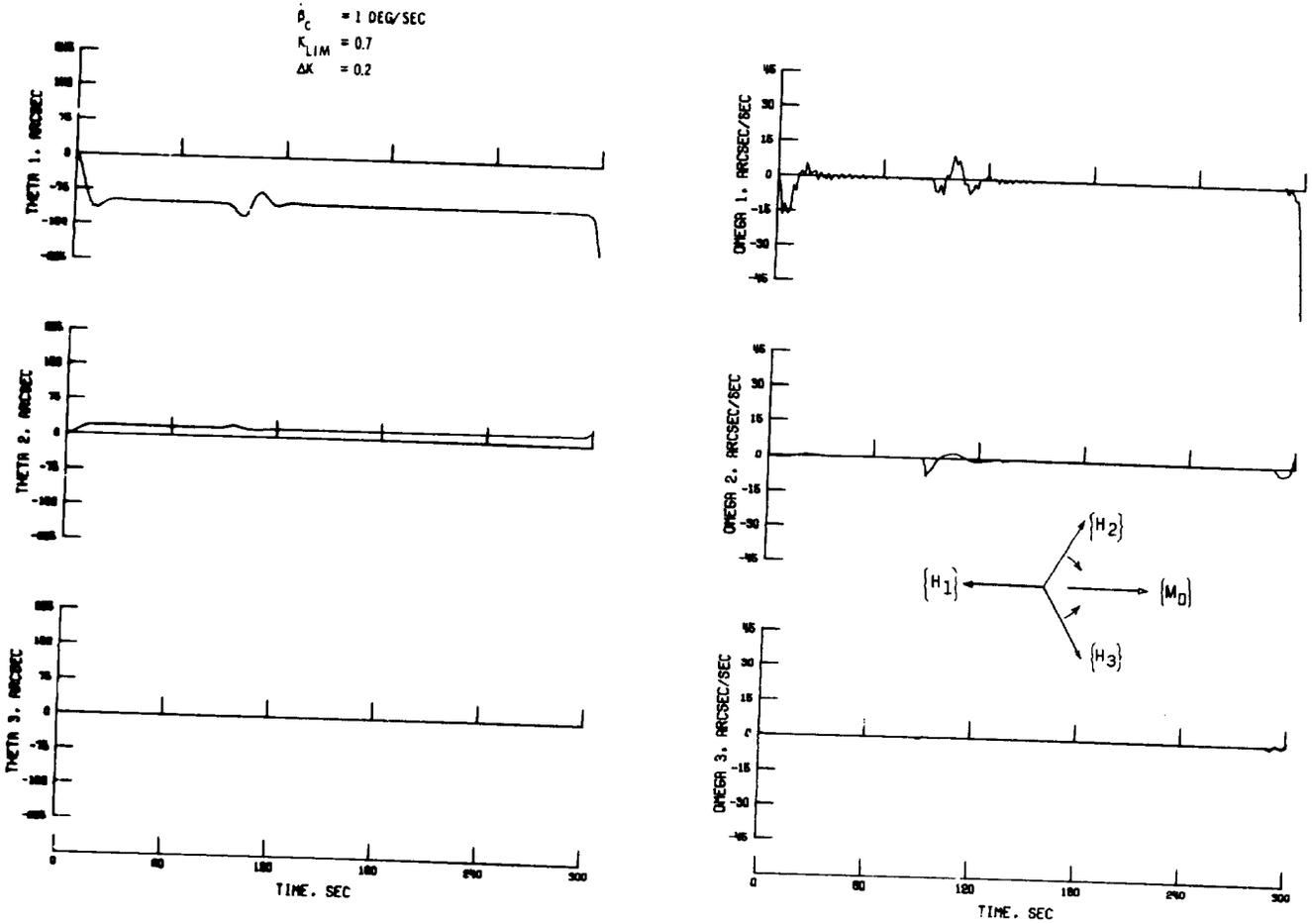

(a) Spacecraft errors.

Figure 15.- Constant deadband antiparallel approach from zero-momentum orientation (20 ft-lb moment opposing CMG 1).

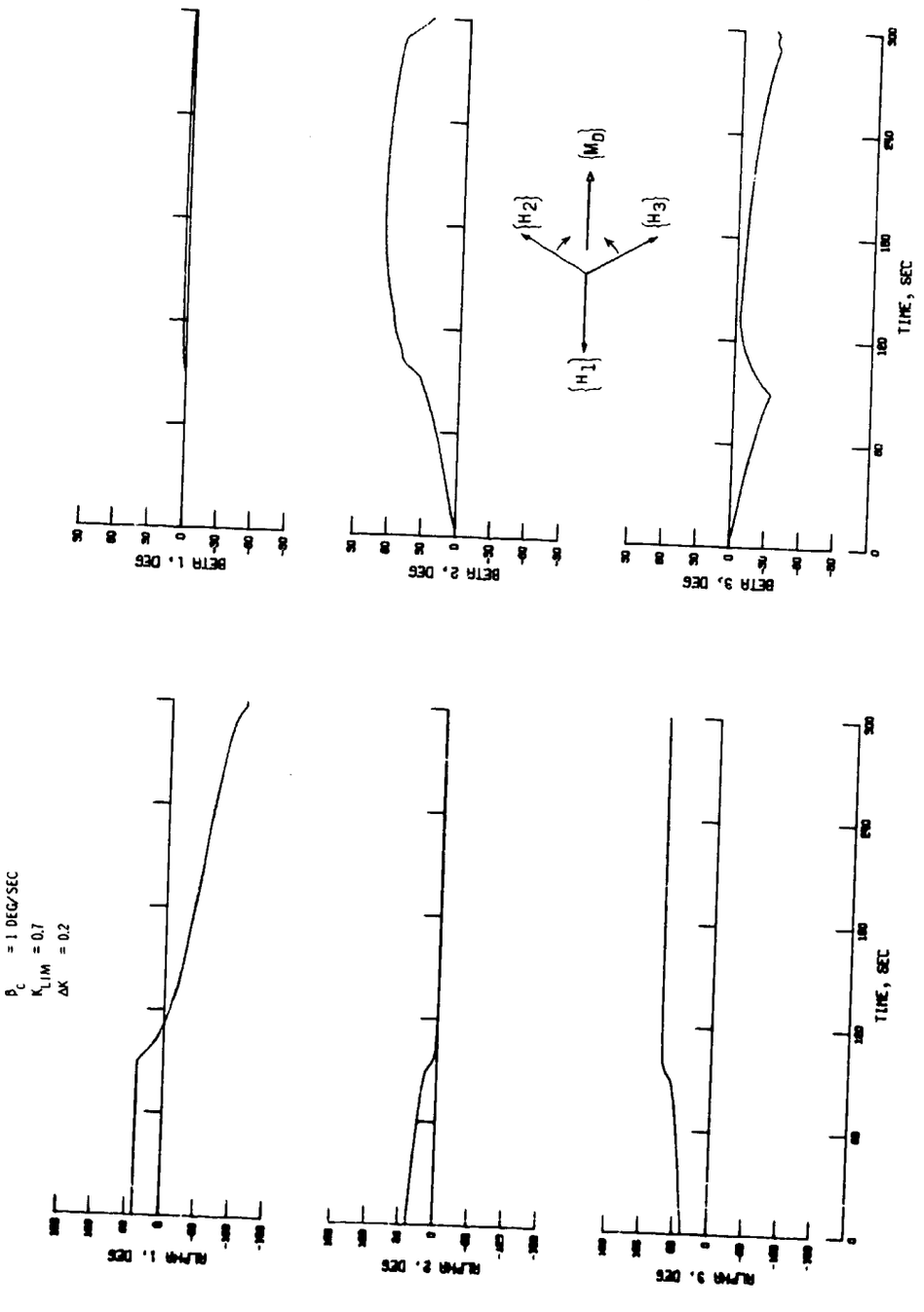

(b) CMG gimbal angles.

Figure 15.- Continued.

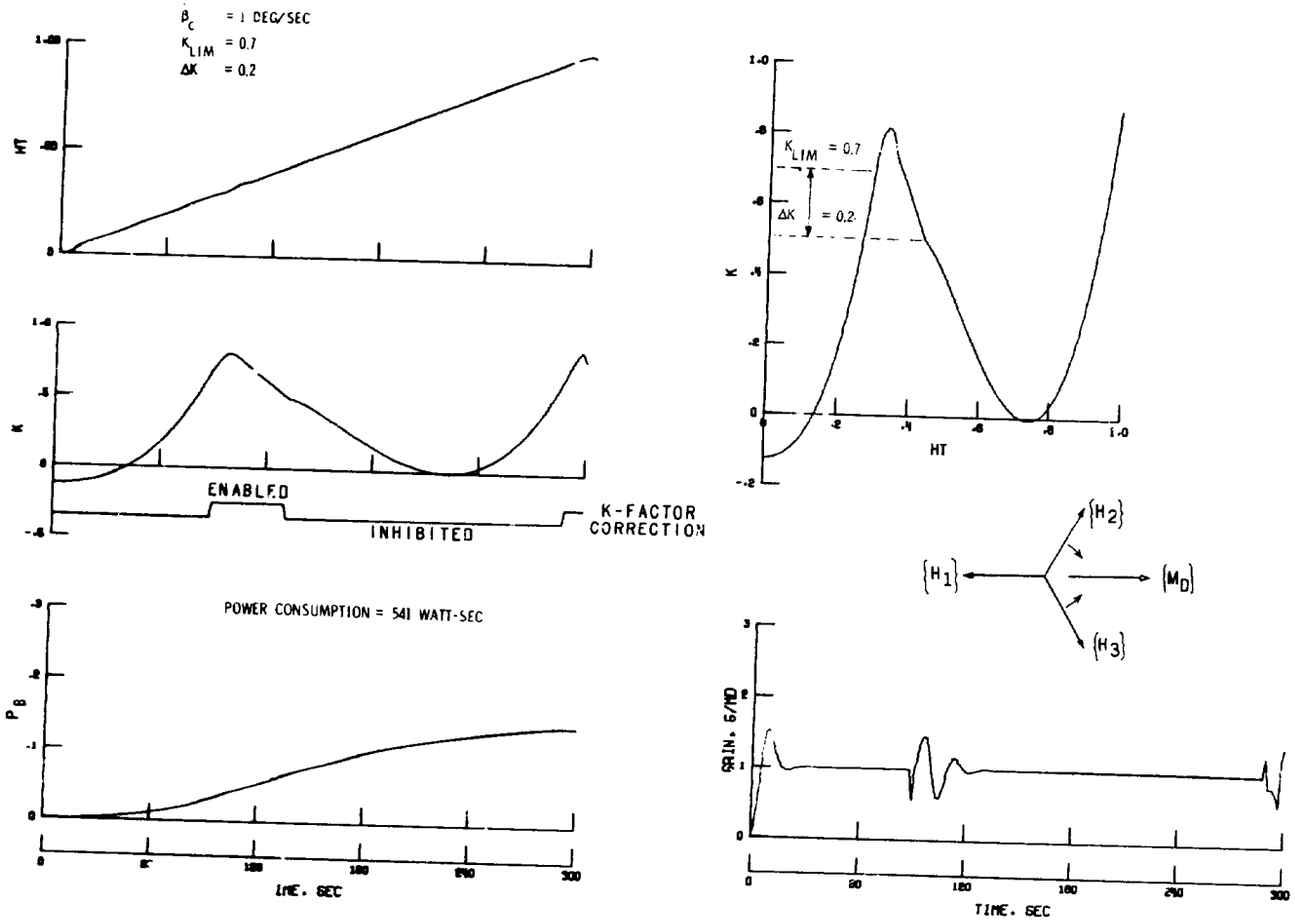

(c) Performance factors.

Figure 15.- Concluded.

defined as the ratio of the control torque magnitude to the disturbance torque magnitude for

$$\text{GAIN} \equiv \frac{G}{M_D} \tag{37}$$

Gimbal angle time histories are presented in Figure 15(b). Note the inner gimbal maneuver of β_3 and the resulting rotation or α_1 of CMG 1 into a favorable position for control in Figure 15(b), and the small GAIN variations during the K correction in Figure 15(c). Additional performance indices for this case are also presented in Figure 15(c). The upper portion of the figure displays the variation of HT and K. It can be seen that HT remains approximately linear with time as expected for the constant applied moment. The correction parameter K increases until the deadband upper limit of $K_{LIM} = 0.7$ is reached and then is driven away from its antiparallel value into a more favorable path to saturation. The lower portion of Figure 15(c) shows inner gimbal and control gain performance parameters. The inner gimbal performance parameter, P_β, is defined by the relation

$$P_\beta = 1 - \frac{1}{3}(\cos \beta_1 + \cos \beta_2 + \cos \beta_3)_{AV} \tag{38}$$

and serves as a measure of the average inner gimbal angle excursion (Appendix A, eq. (A28). Its average value at saturation here is about 0.160 and approximately corresponds to an average inner gimbal angle of 33°. Except for small transient variations initially and during the K correction, the GAIN factor remains at unity up to saturation.

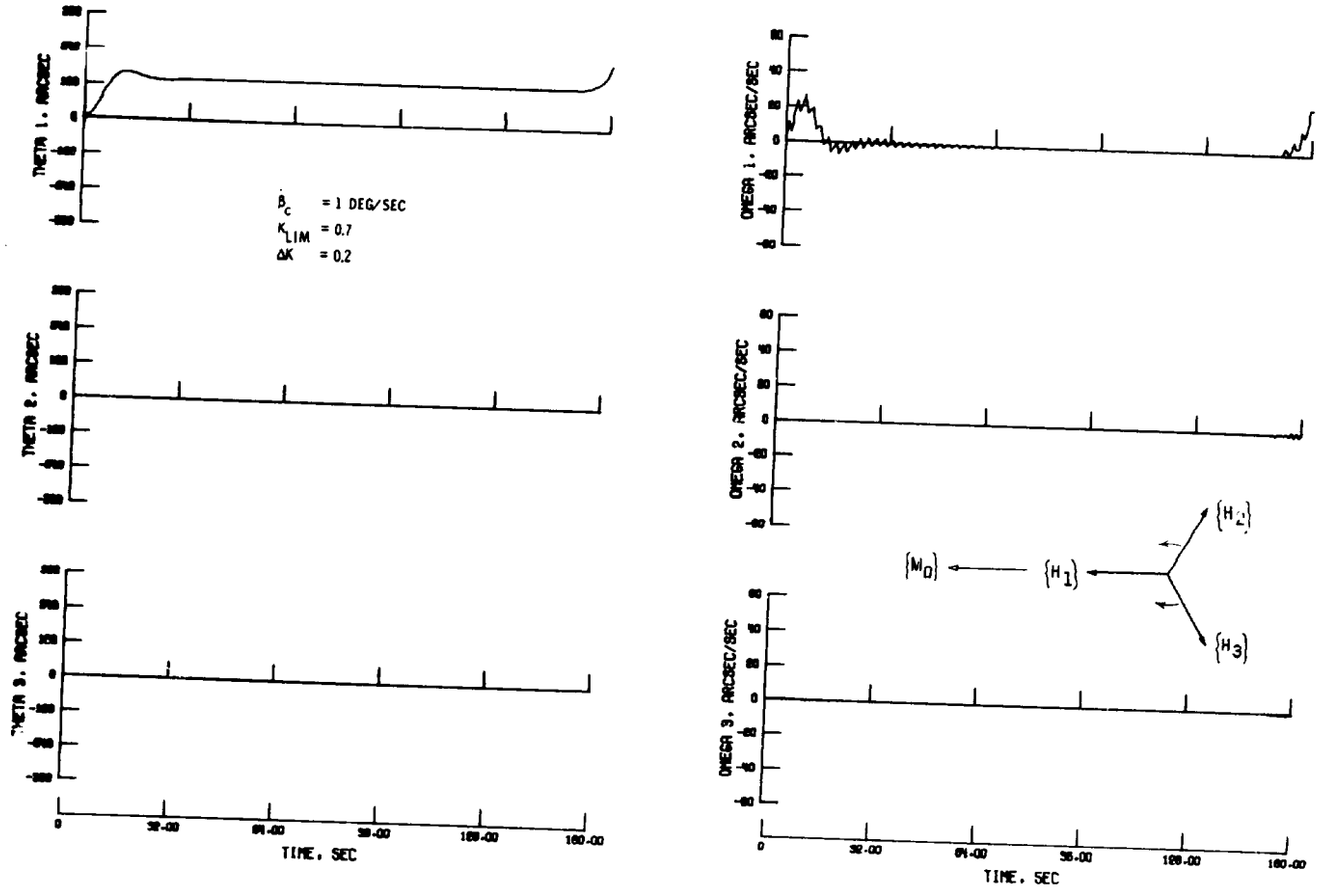

(a) Spacecraft errors.

Figure 16.- Constant deadband saturation approach from orthogonal orientation (20 ft-lb moment along CMG 1).

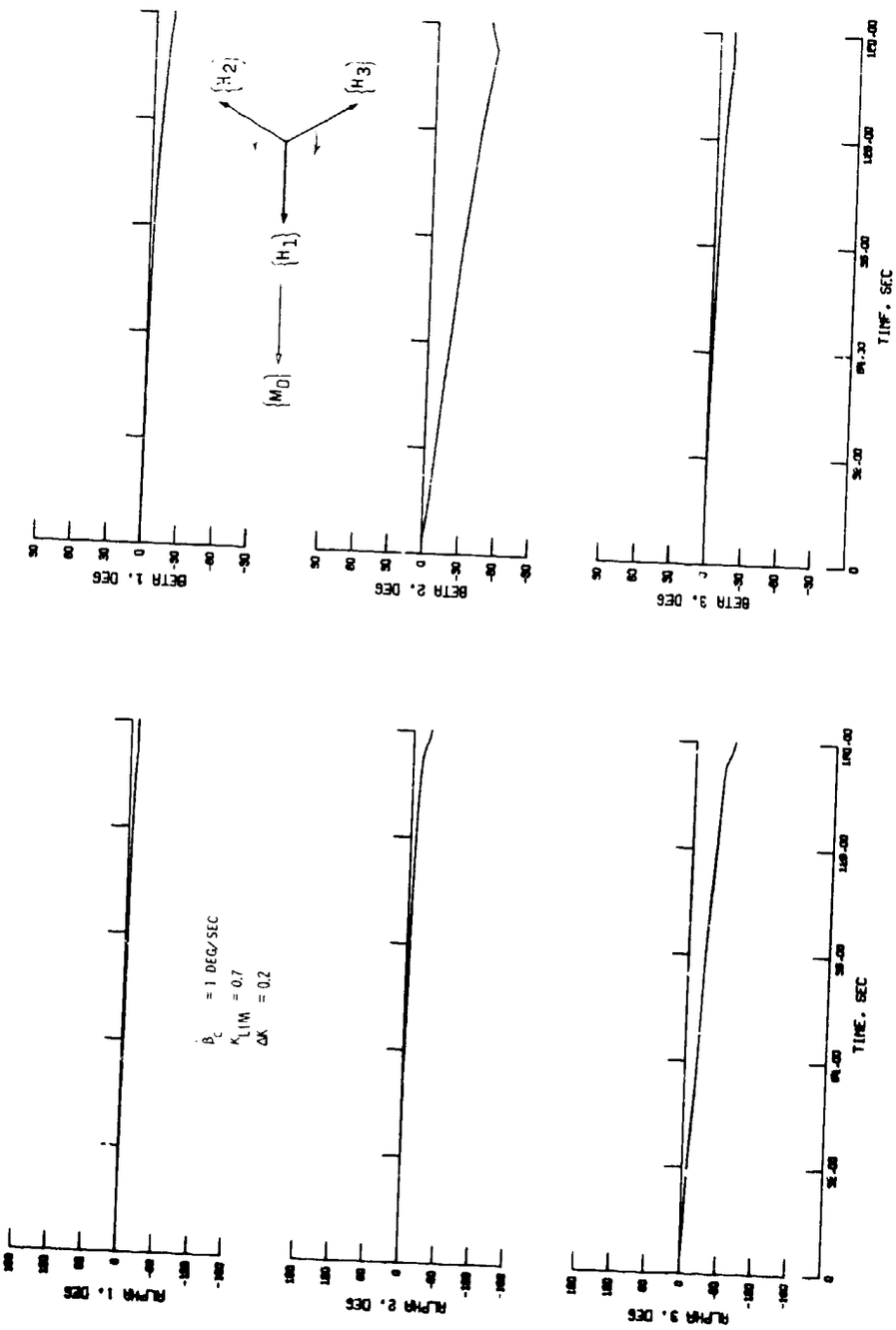

(b) CMG gimbal angles.

Figure 16.- Continued.

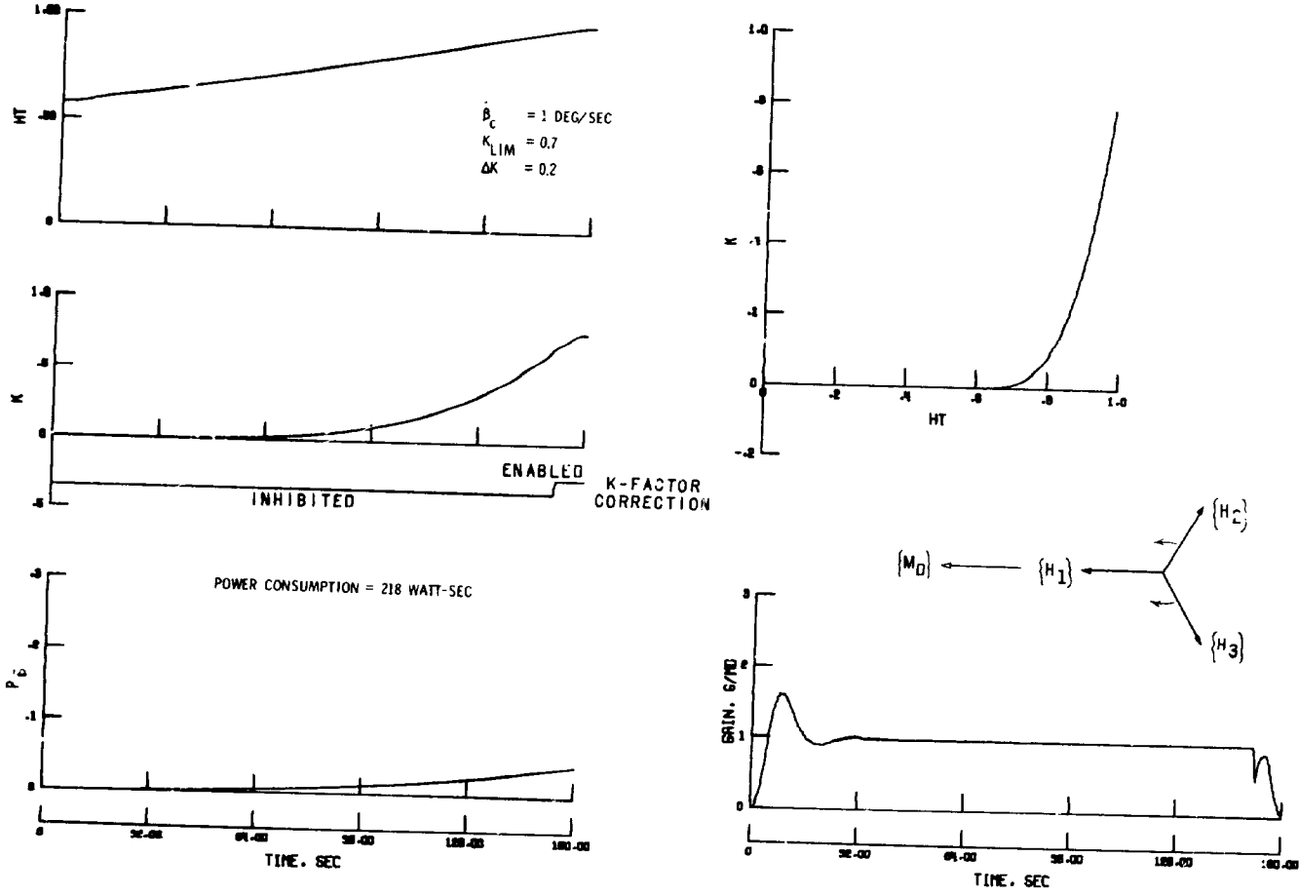

(c) Performance factors.

Figure 16.- Concluded.

Ideal gimbal power consumption for the antiparallel approach is about 541 watt-sec.

Figure 16 illustrates another example for a constant disturbance torque along CMG 1 starting from an orthogonal orientation. The K correction now is not initiated until the CMG system is near saturation and then produces small control torque and spacecraft oscillations until saturation. In the actual ATM mission, desaturation would generally be carried out before the CMG system is fully saturated and all control is lost. Hence, these oscillations near saturation may not occur. Ideal gimbal power for this example is about 218 watt-sec.

Variable Deadband K-Factor Correction

The extension of the K correction technique to incorporate a variable deadband with a lower bound defined by the isogonal value of KI, equation (34), could continuously minimize the CMG system inner gimbal angles and could improve the CMG system effective gain.

Initial antiparallel approach cases for the constant 20 ft-lb disturbance moment were made to determine the effect of parameter variations in the correction technique on the spacecraft response and CMG system performance factors. The correction parameters are $\dot{\beta}_c$, the command gimbal rate for the largest CMG gimbal angle and ΔK which when added to the fixed isogonal value, KI, determines K_{LIM} for initiation of the correction maneuver. For the antiparallel case, the spacecraft response was insensitive to changes in either $\dot{\beta}_c$ or ΔK as shown in Figure 17. The gimbal power requirements, however,

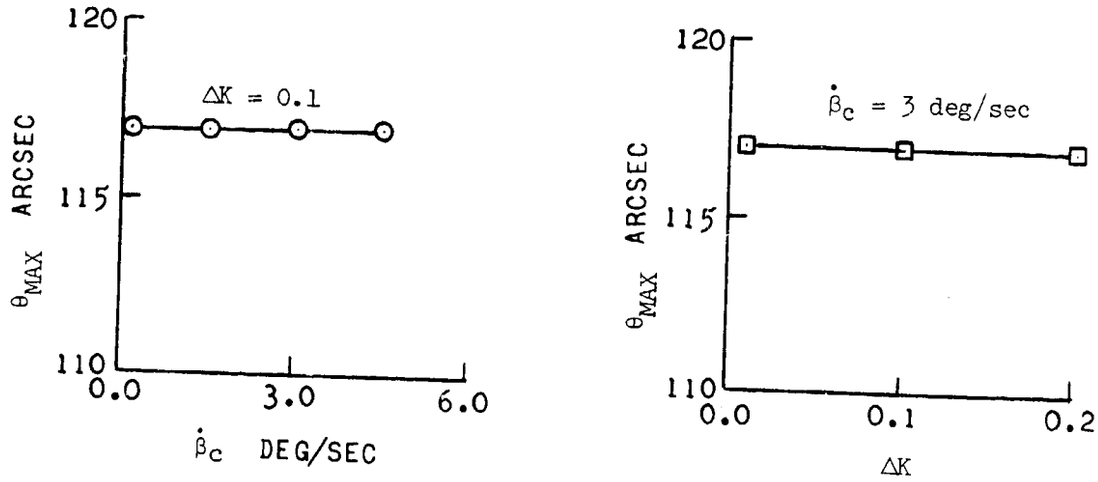

(a) Spacecraft attitude error.

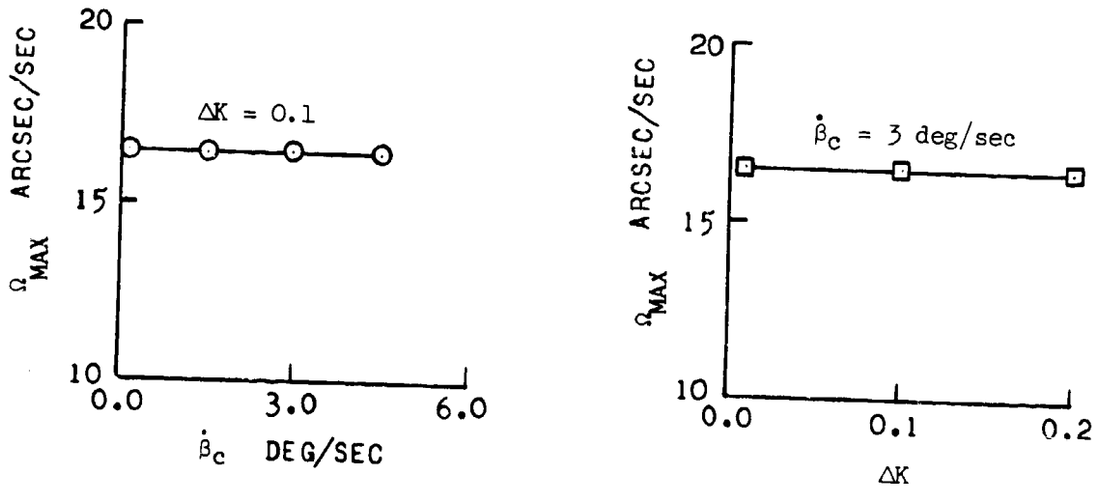

(b) Spacecraft rate error.

Figure 17.- Spacecraft response with the variable deadband correction for variation of $\dot{\beta}_c$ and ΔK.

increased with $\dot{\beta}_c$ for all values of ΔK. Figure 18 illustrates the increasing power requirements and shows that 365 watt-sec of power was required for the characteristic antiparallel case with $\dot{\beta}_c = 3$ deg/sec and $\Delta K = 0.1$.

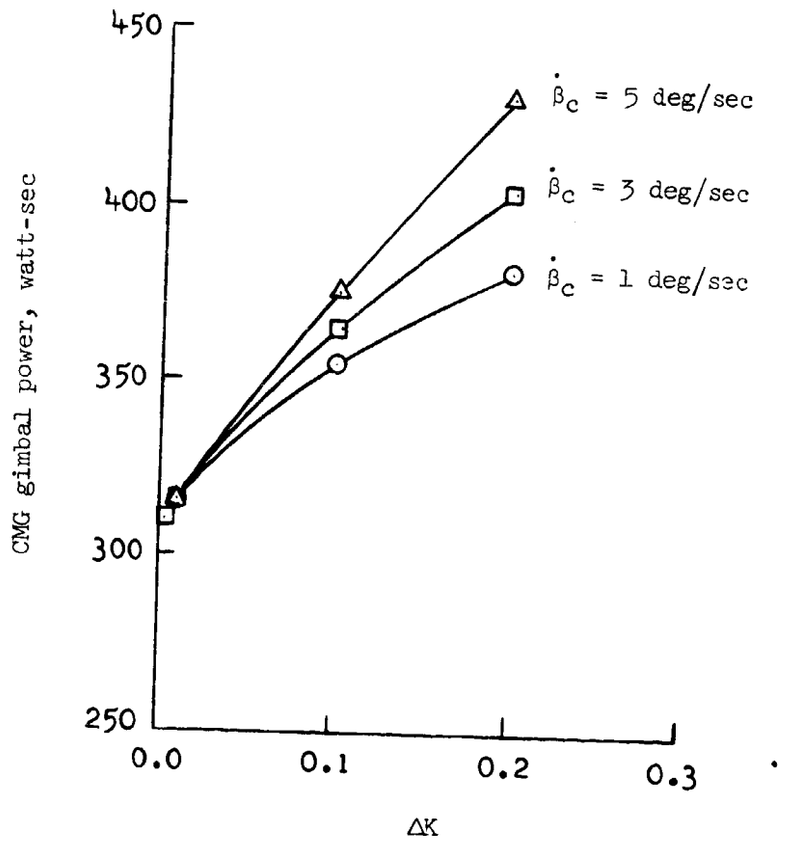

Figure 18.- CMG gimbal power requirements with the variable deadband correction for variation of $\dot{\beta}_c$ and ΔK.

The inner gimbal performance factor was also examined for correction parameter trade offs and is presented in Figure 19.

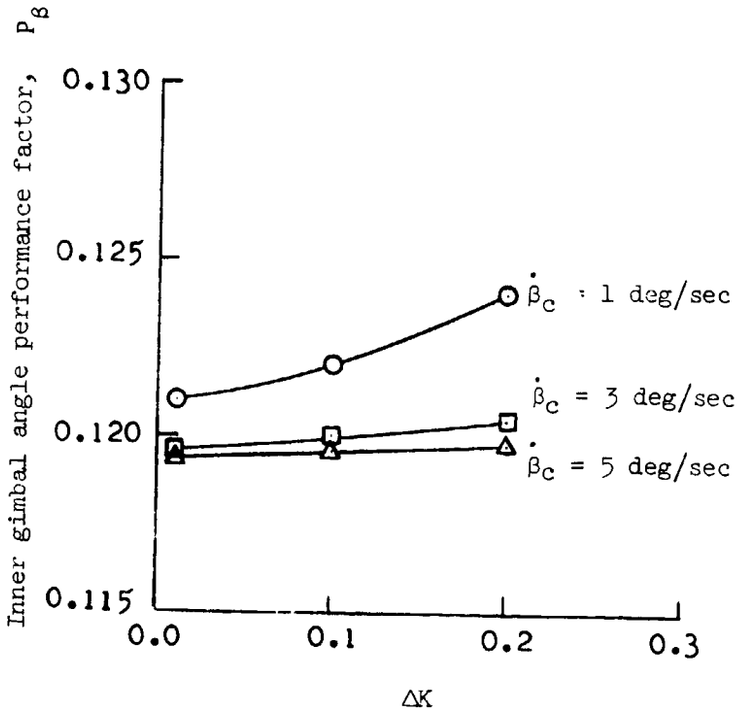

Figure 19.- Inner gimbal angle performance factor for variation of $\dot{\beta}_c$ and ΔK with the variable deadband correction technique.

The data show for increasing command gimbal rate, $\dot{\beta}_c$, the average inner gimbal angle decreased for the antiparallel case. However, no

significant increase in the P_β factor was noted in decreasing the command gimbal rate from 5 deg/sec to 3 deg/sec. This fact, together with the trend of increasing gimbal power requirements with increase in $\dot{\beta}_c$, resulted in selection of an inner gimbal correction rate of $\dot{\beta}_c = 3$ deg/sec as a standard to evaluate the overall performance of the K-factor correction technique. For the delta check factor deadband, a nominal value of $\Delta K = 0.1$ was selected and used with $\dot{\beta}_c = 3$ deg/sec for the following examples of the variable deadband scheme.

Figure 20 again presents an antiparallel approach from the zero-momentum CMG orientation; and Figure 23 illustrates the response for a constant moment applied along the minimum inertia axis starting from an orthogonal CMG orientation. From Figures 15(c) and 20(c), it can be seen that the use of the variable deadband K-factor correction for the antiparallel approach improves the inner gimbal performance of the CMG system and significantly reduces gimbal power requirements. The ideal gimbal power consumption is now 365 watt-sec for the antiparallel approach. In addition, the variable K correction now no longer introduces excessive control torque oscillations near saturation.

Figures 21 and 22 present the performance of this variable deadband scheme for the disturbance moment opposing CMG 2 and CMG 3, respectively. Both cases required the same ideal gimbal power requirement of 365 watt-sec with the same average inner gimbal angle excursion of 28° as was the case for the disturbance moment opposing CMG 1. To permit the comparison of the K correction and the isogonal correction,

the antiparallel approach example was simulated with the isogonal correction. The results are shown in Figures 24, 25, and 26, and should be compared with Figures 20, 21, and 22 for the disturbance moment opposing CMG 1, 2, and 3, respectively. The spacecraft response is similar for the two cases, but the ideal gimbal power required by the CMG system increased by a factor of 2 for the isogonal corrections to approximately 795 watt-sec, while the inner gimbal angle performance index is reduced from 28° to 21°. Note that the control system maintains an identical K versus HT distribution of momentum in addition to an identical average inner gimbal motion for all three isogonal cases.

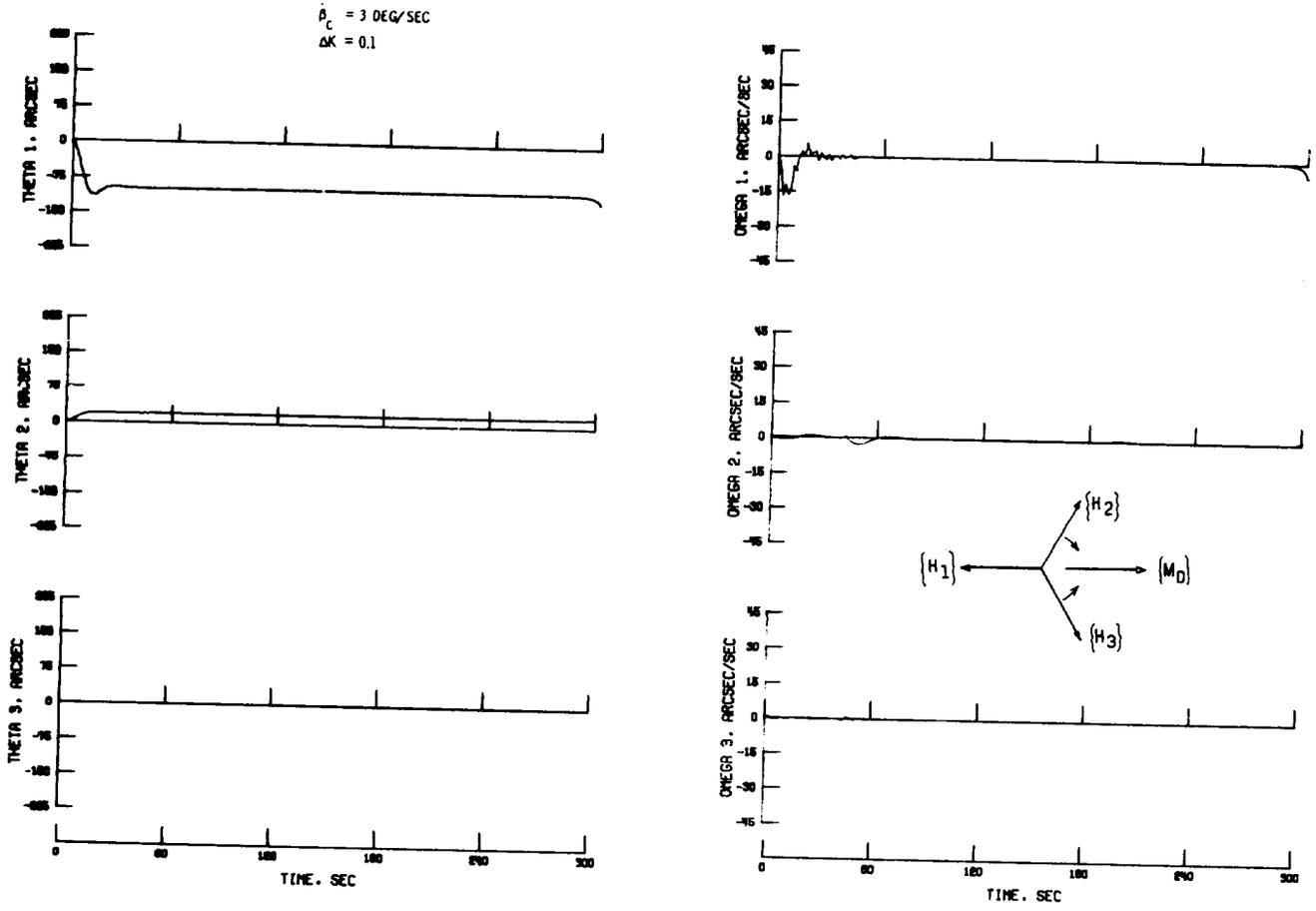

(a) Spacecraft errors.

Figure 20.- Variable deadband antiparallel approach from zero-momentum orientation (20 ft-lb moment opposing CMG 1).

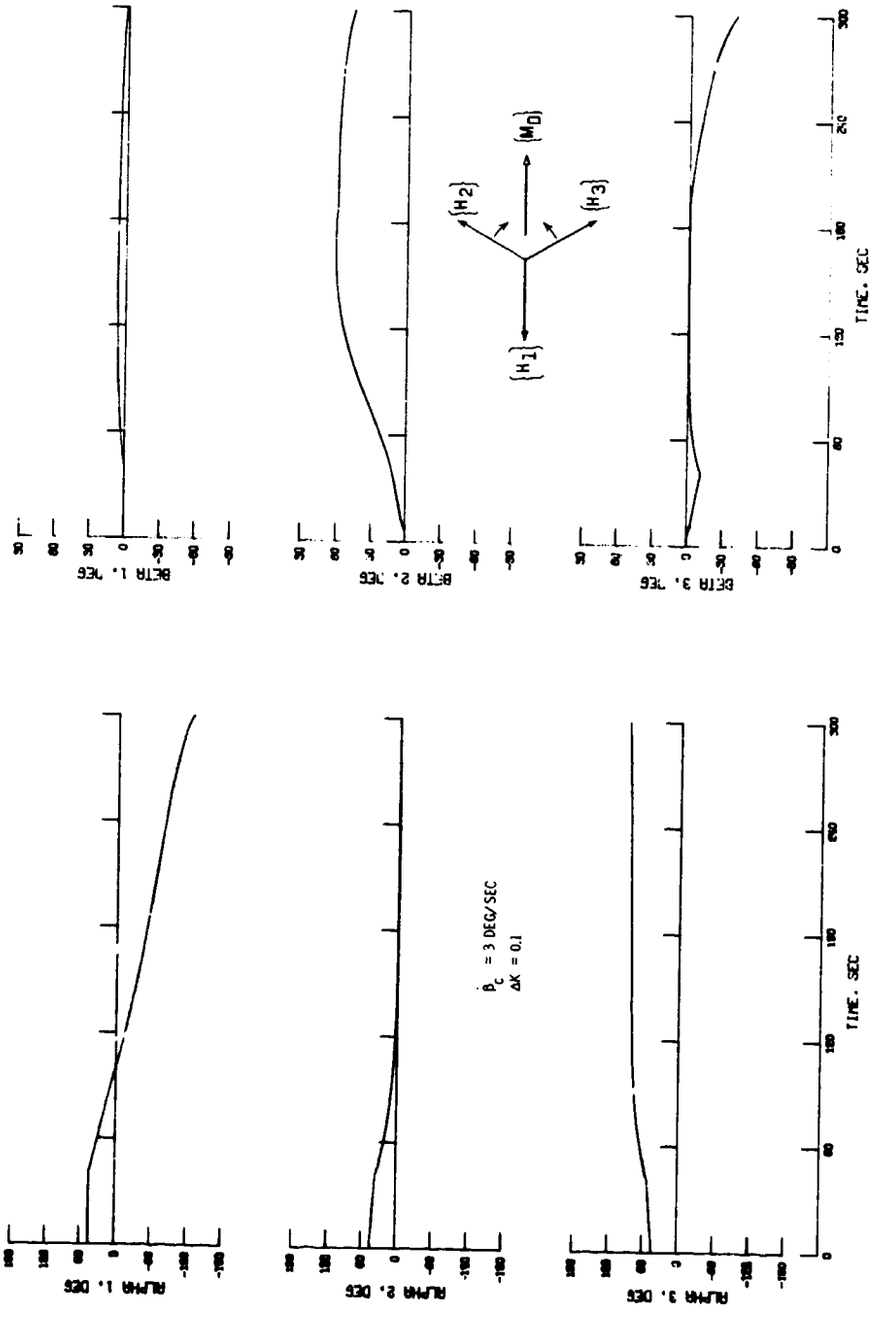

(b) CMG gimbal angles.

Figure 20.- Continued.

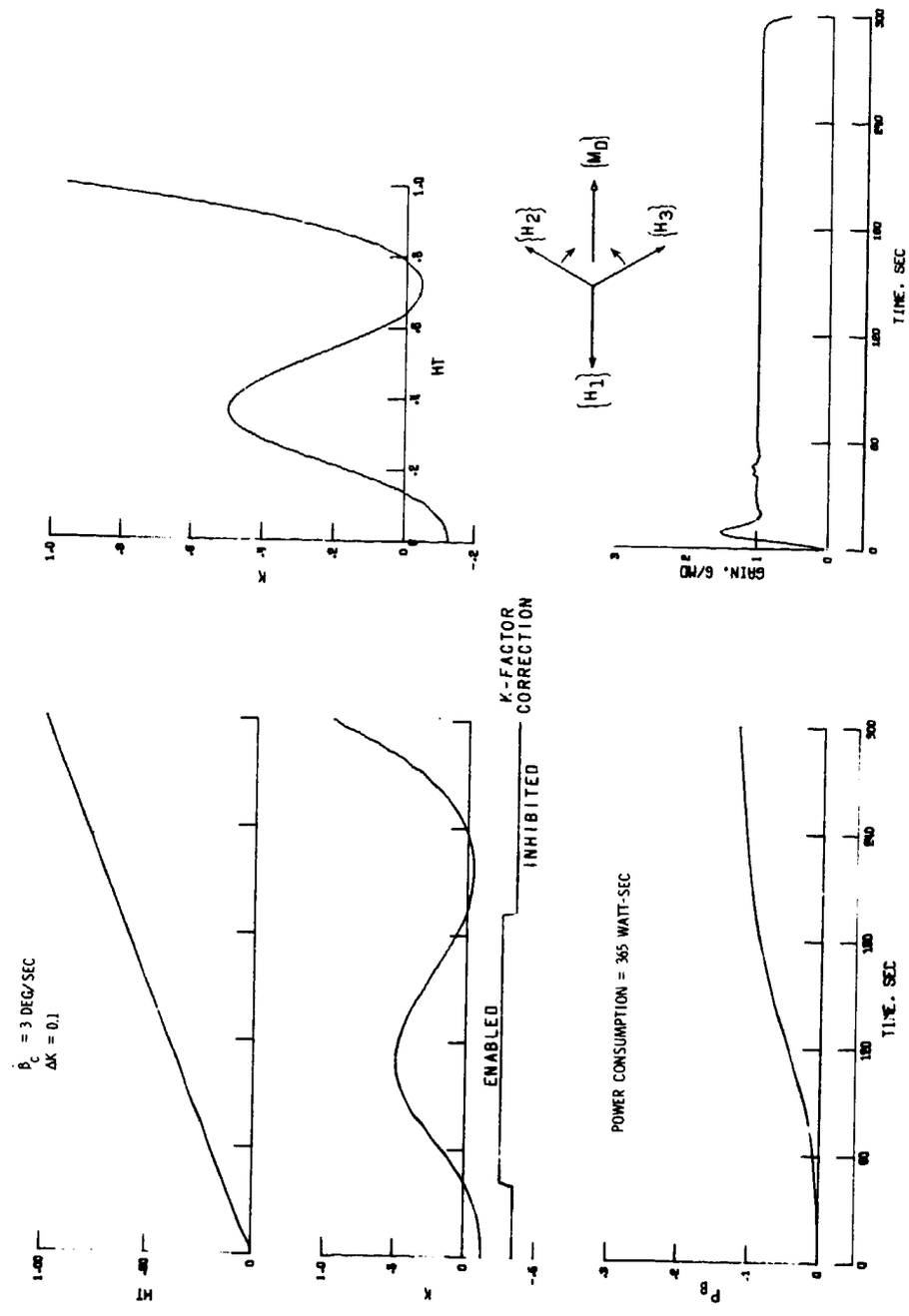

(c) Performance factors.

Figure 20.- Concluded.

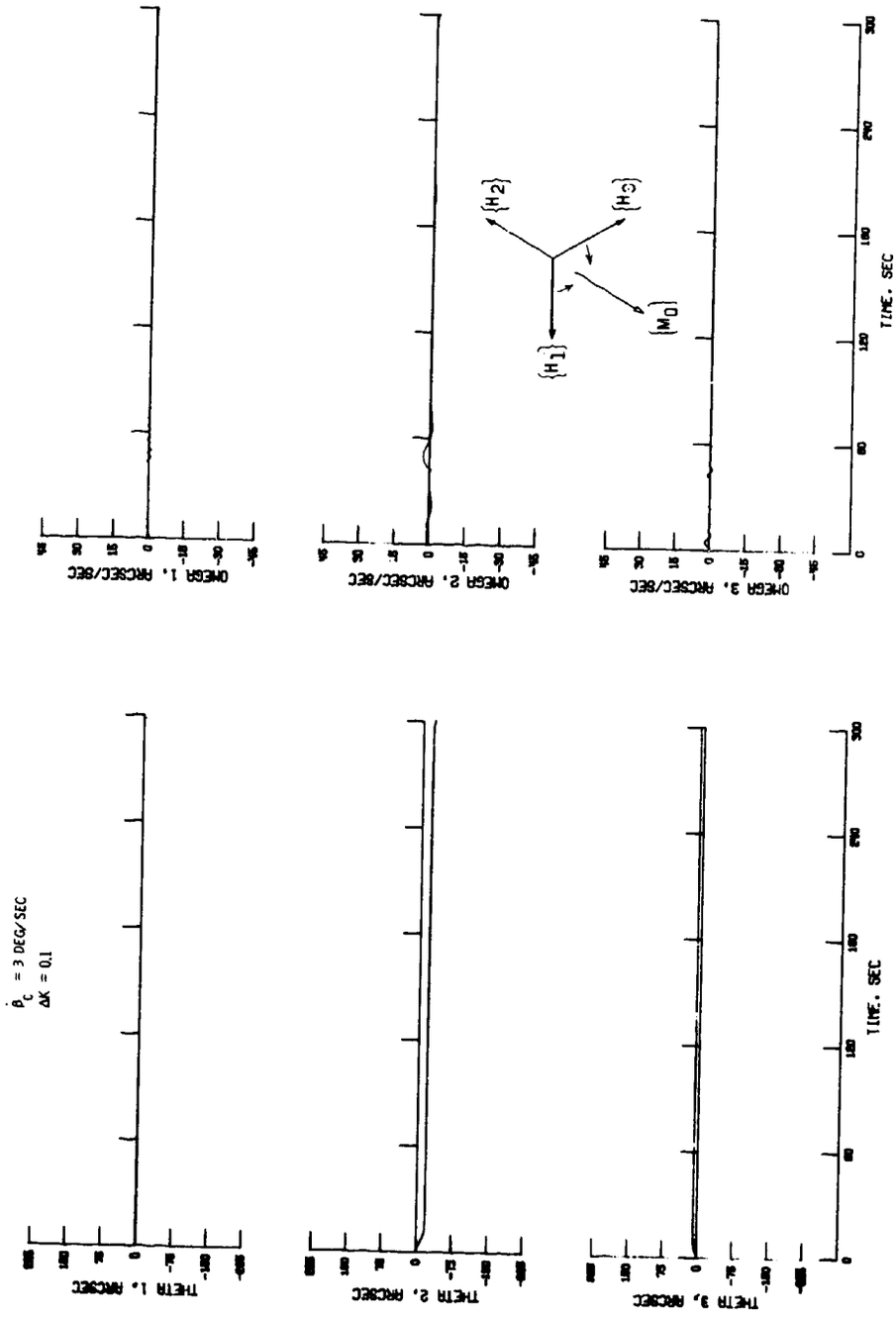

(a) Spacecraft errors.

Figure 21.- Variable deadband antiparallel approach from zero-momentum orientation (20 ft-lb moment opposing CMG 2).

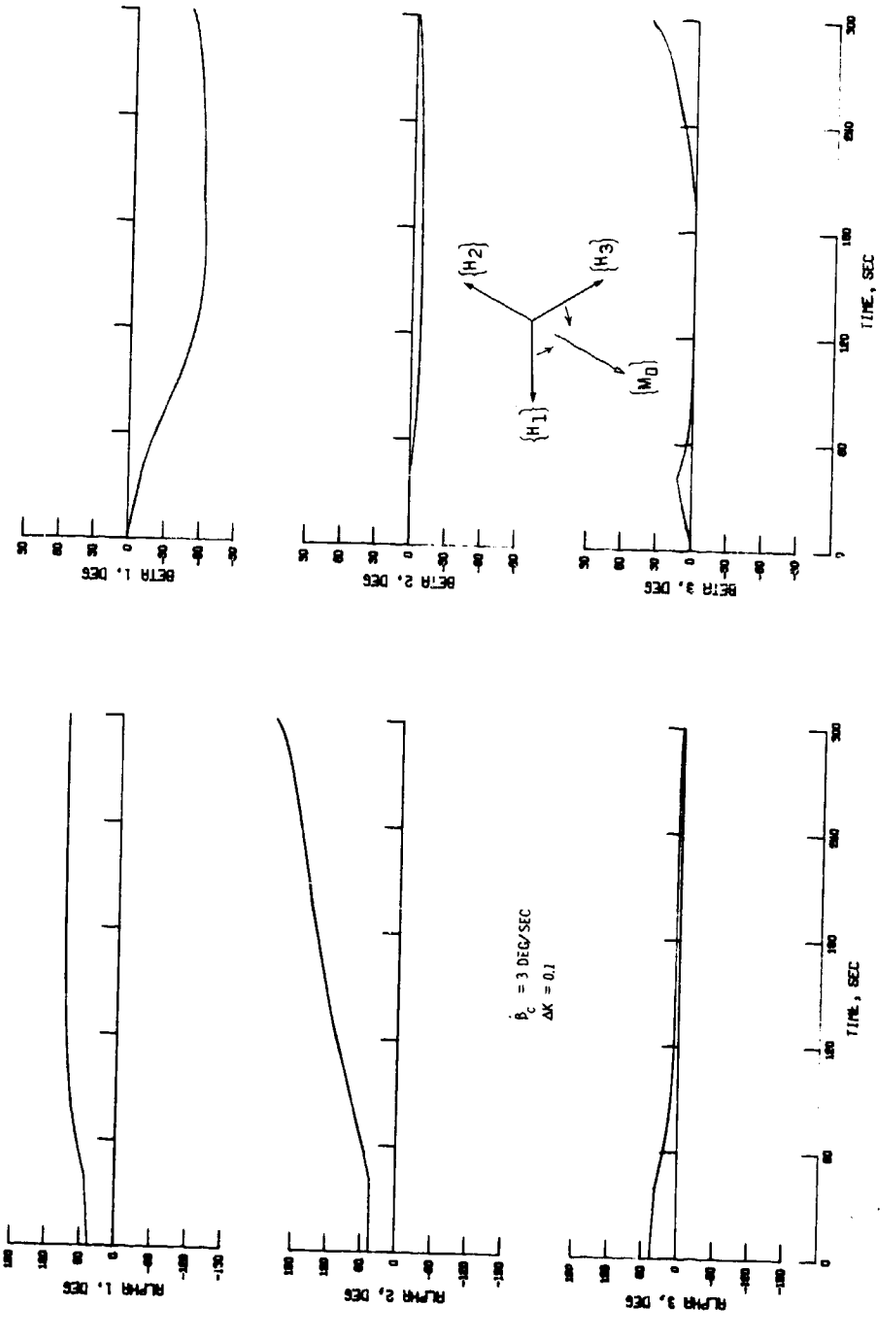

(b) CMG gimbal angles.

Figure 21.- Continued.

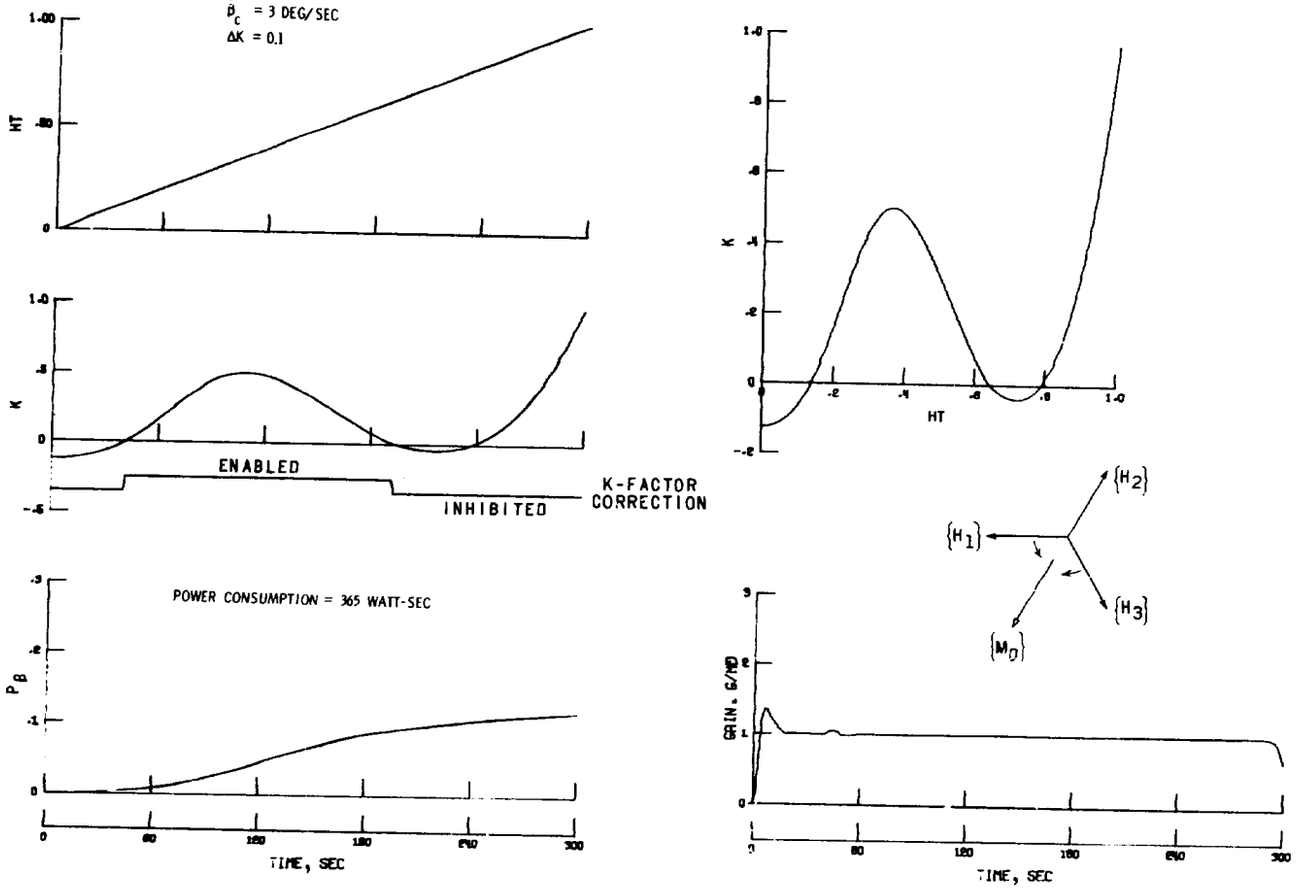

(c) Performance factors.

Figure 21 .- Concluded.

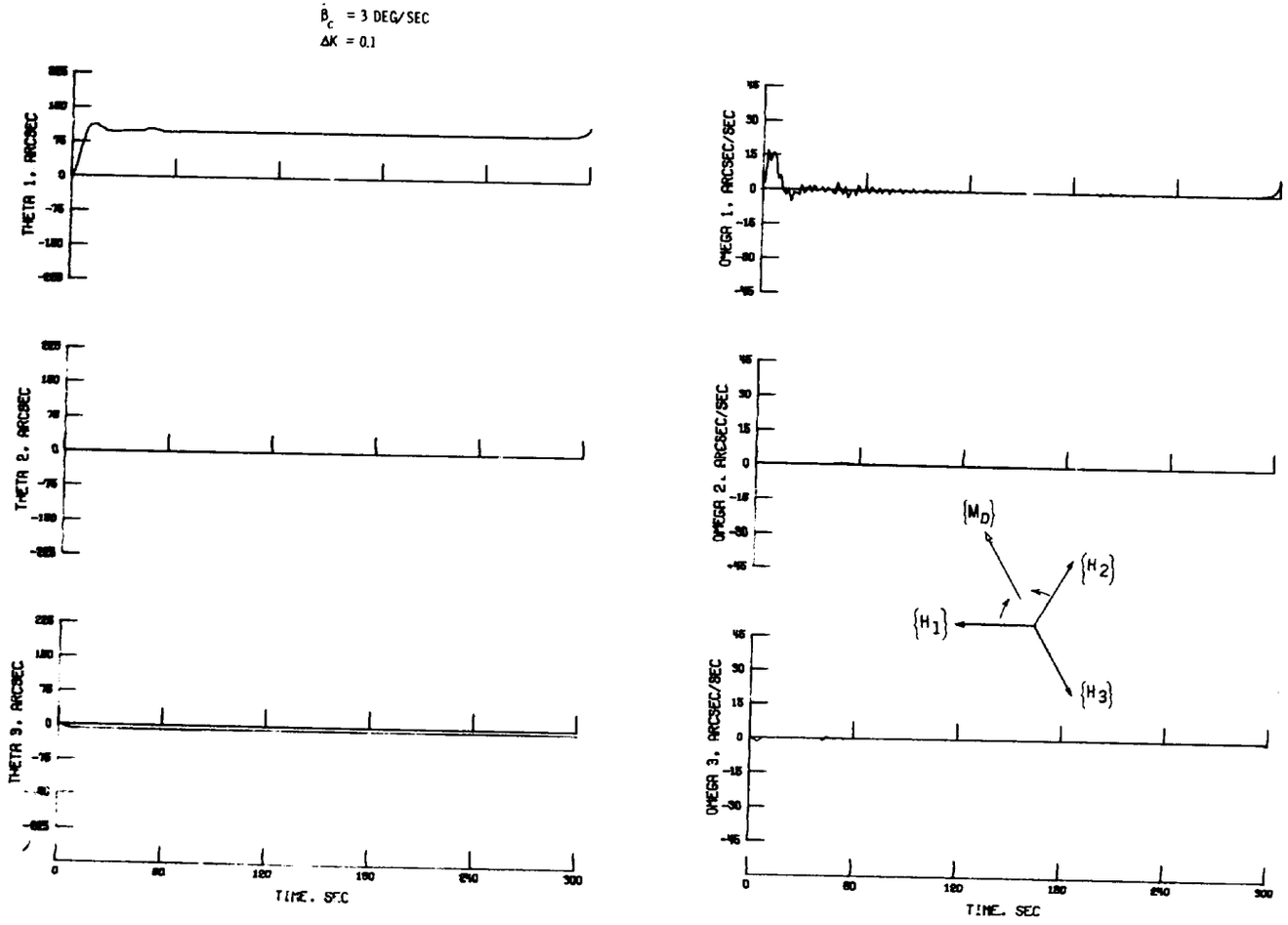

(a) Spacecraft errors.

Figure 22.- Variable deadband antiparallel approach from zero-momentum orientation (20 ft-lb moment opposing CMG 3).

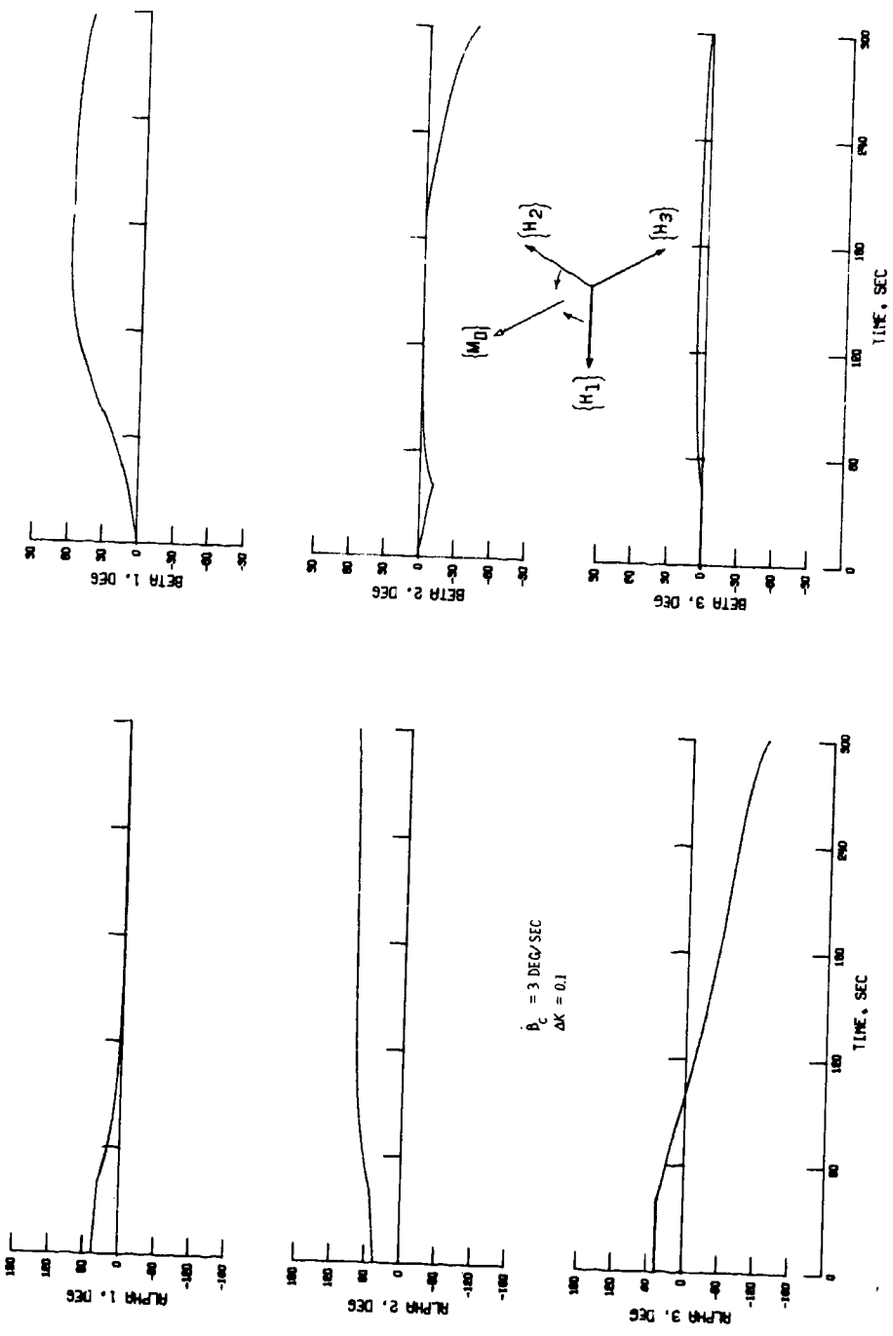

(b) CMG gimbal angles.

Figure 22.- Continued.

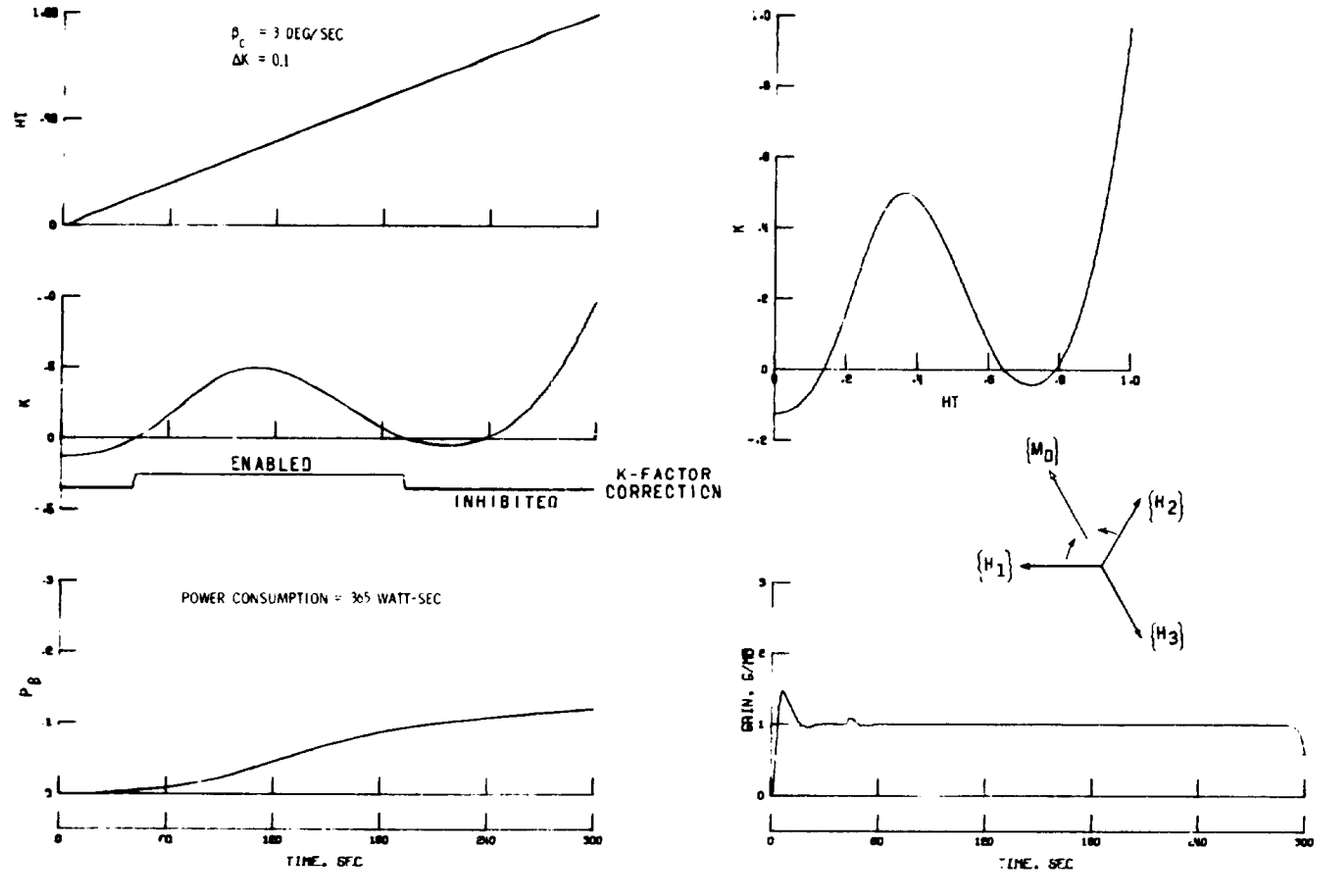

(c) Performance factors.

Figure 22 .- Concluded.

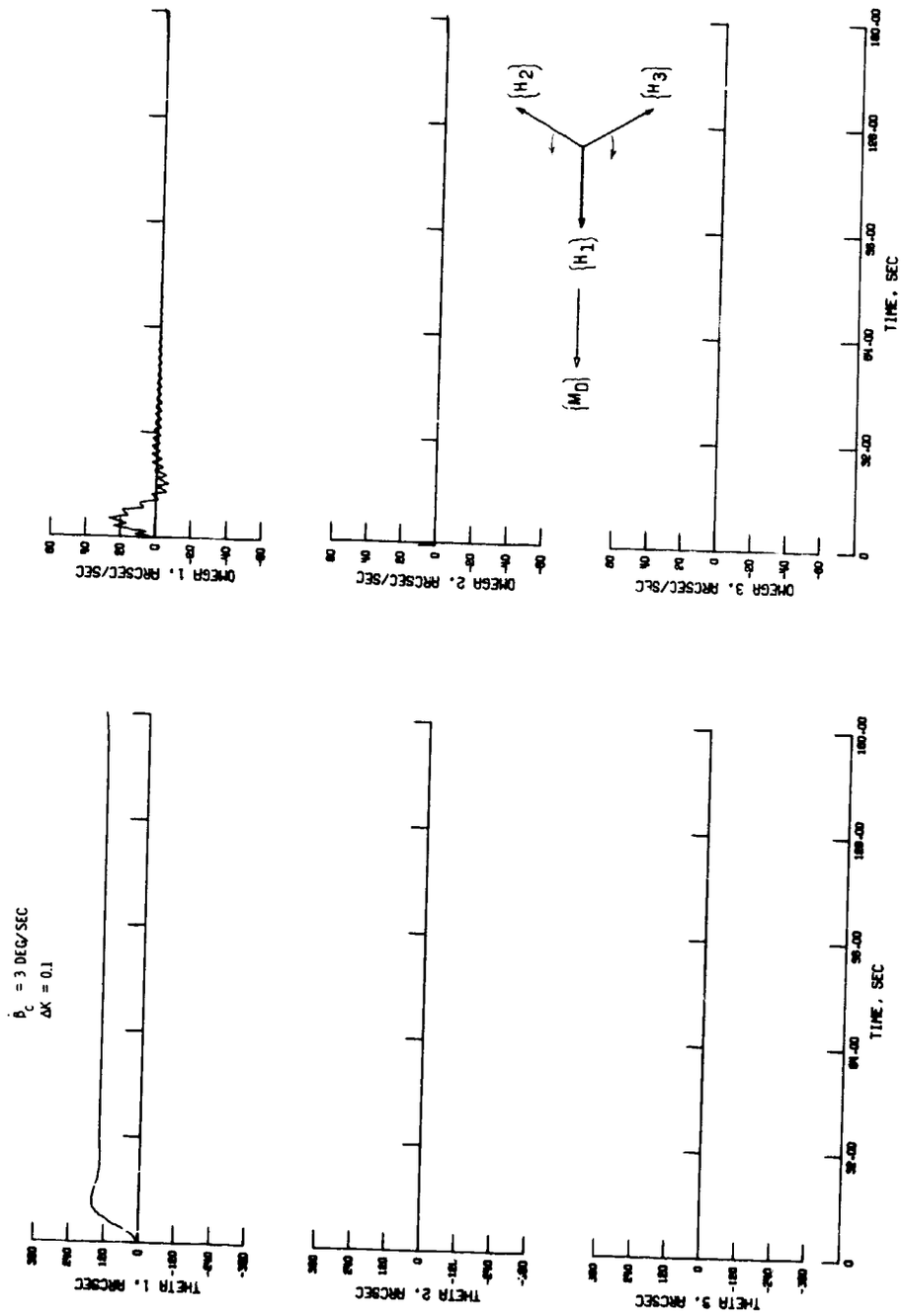

(a) Spacecraft errors.

Figure 23.- Variable deadband saturation approach from orthogonal orientation (20 ft-lb moment along CMG 1).

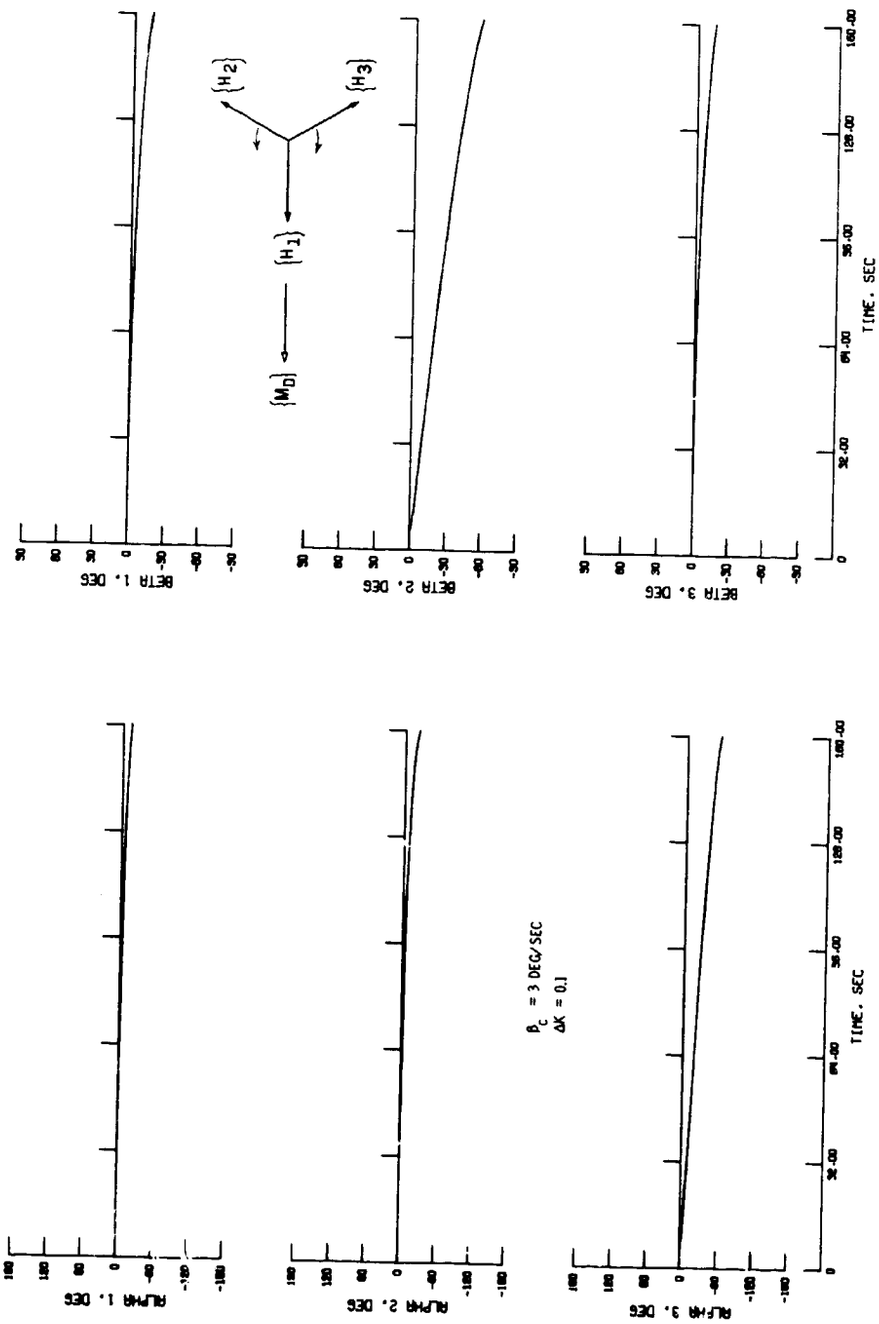

(b) CMG gimbal angles.

Figure 23.- Continued.

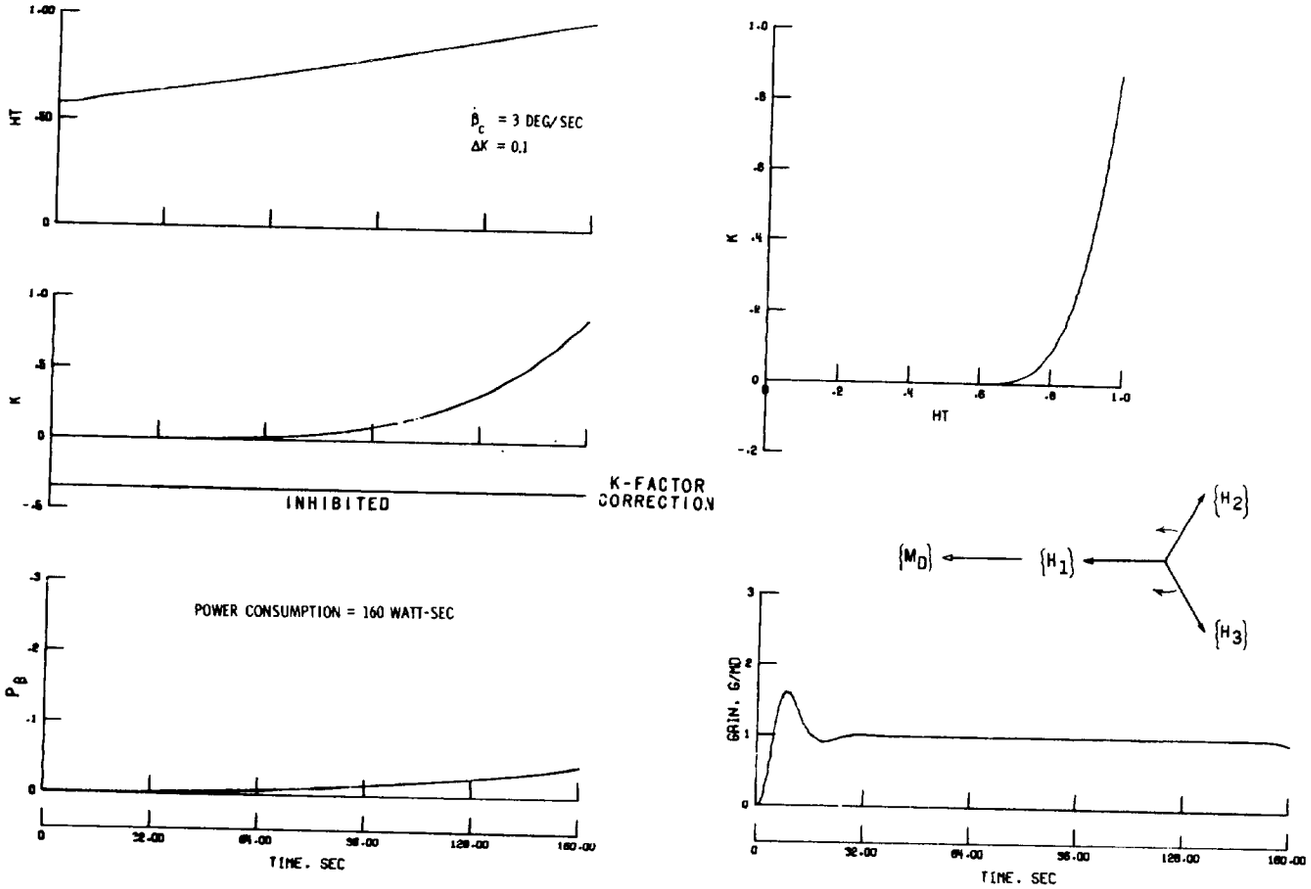

(c) Performance factors.

Figure 23.- Concluded.

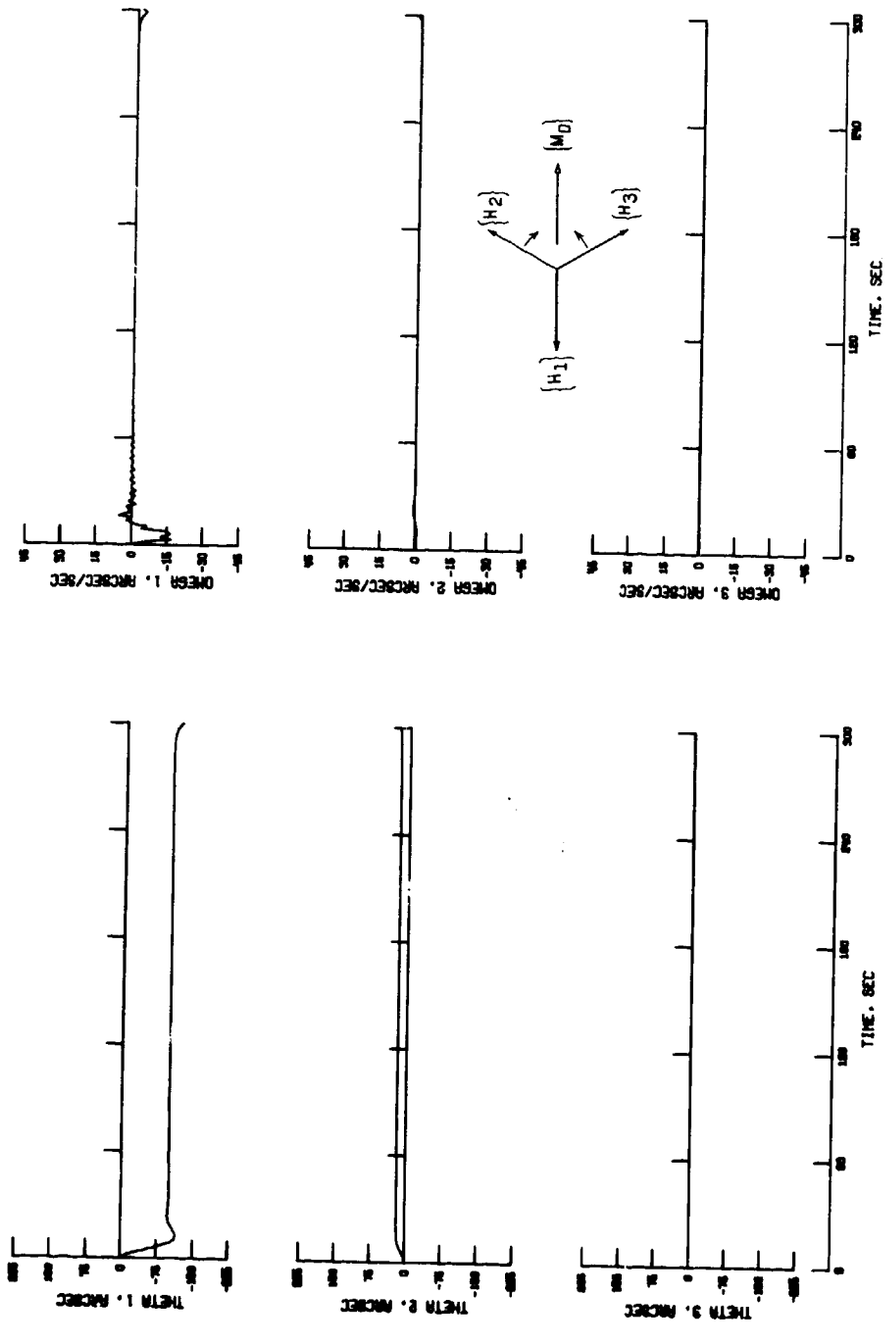

(a) Spacecraft errors.

Figure 24.- Isogonal antiparallel approach from zero-momentum orientation (20 ft-lb moment opposing CMG 1).

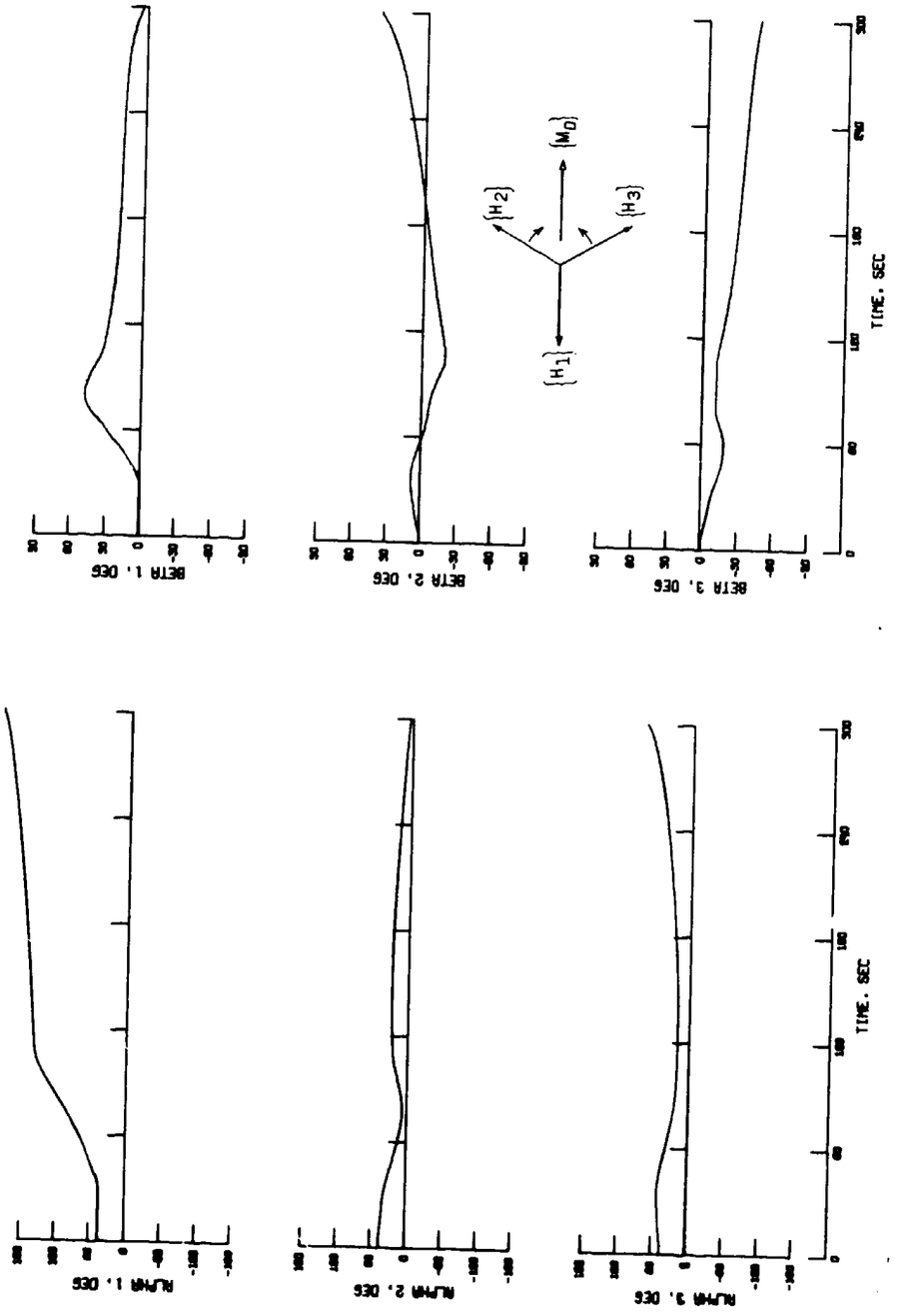

(b) CMG gimbal angles.

Figure 24.- Continued.

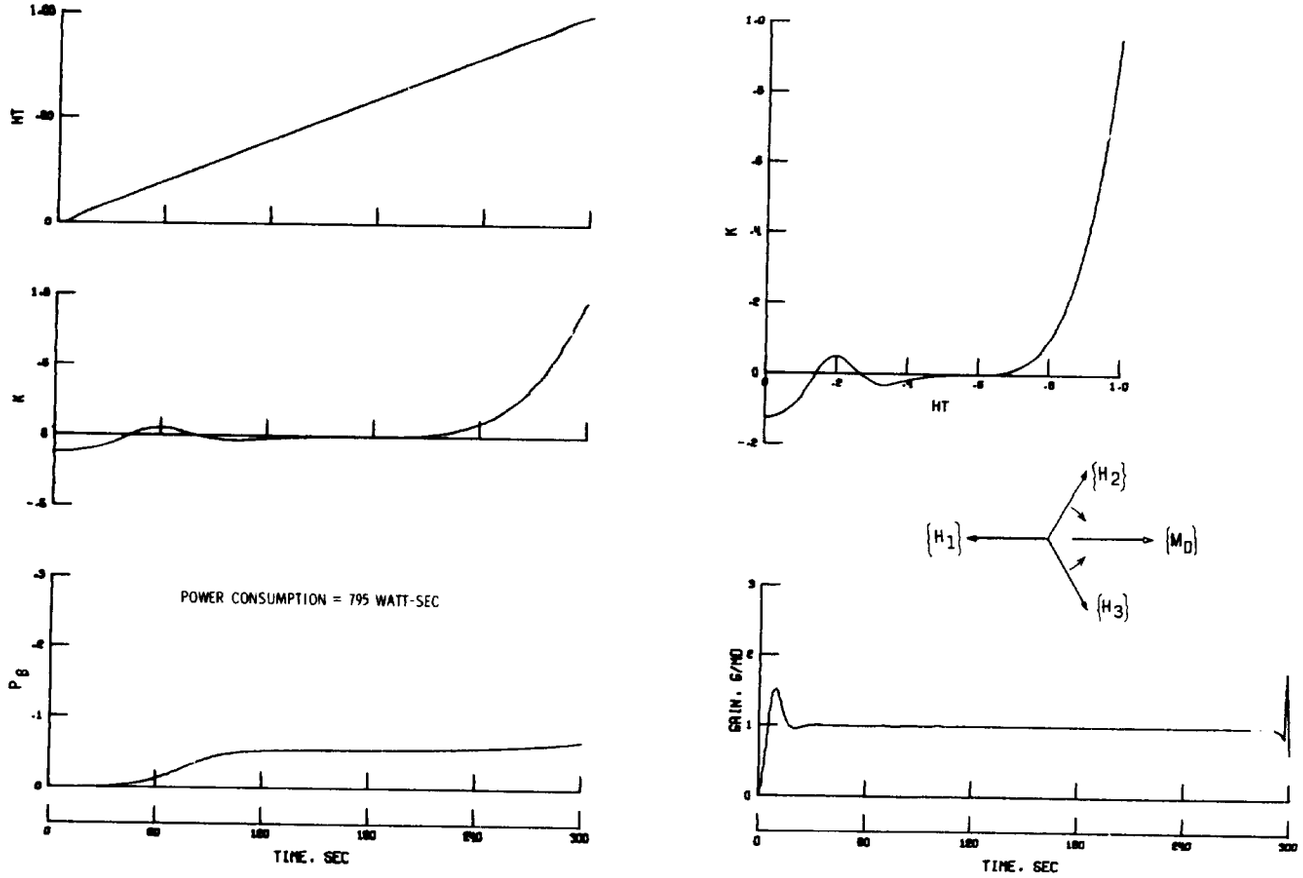

(c) Performance factors.

Figure 24.- Concluded.

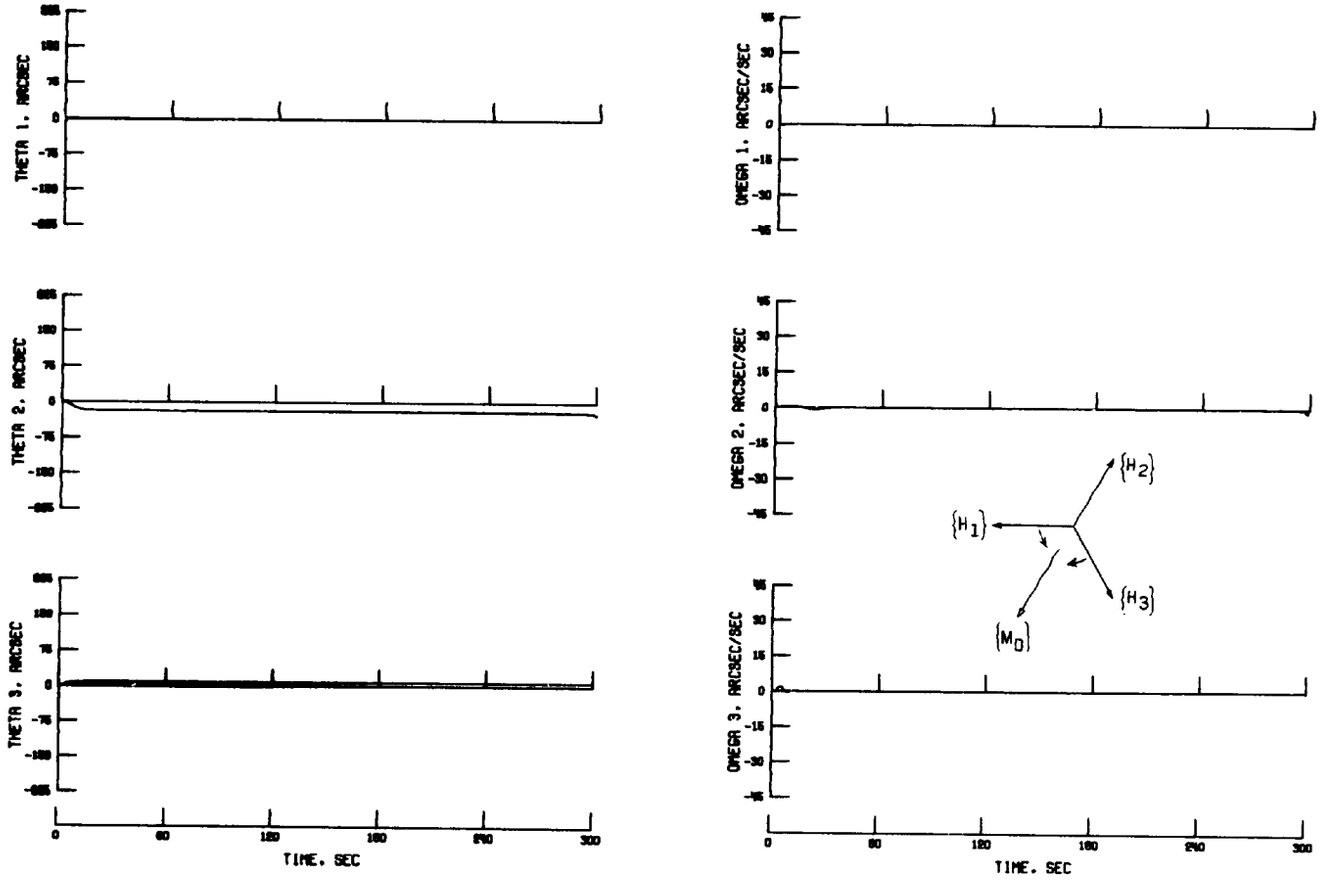

(a) Spacecraft errors.

Figure 25.- Isogonal antiparallel approach from zero-momentum orientation (20 ft-lb moment opposing CMG 2).

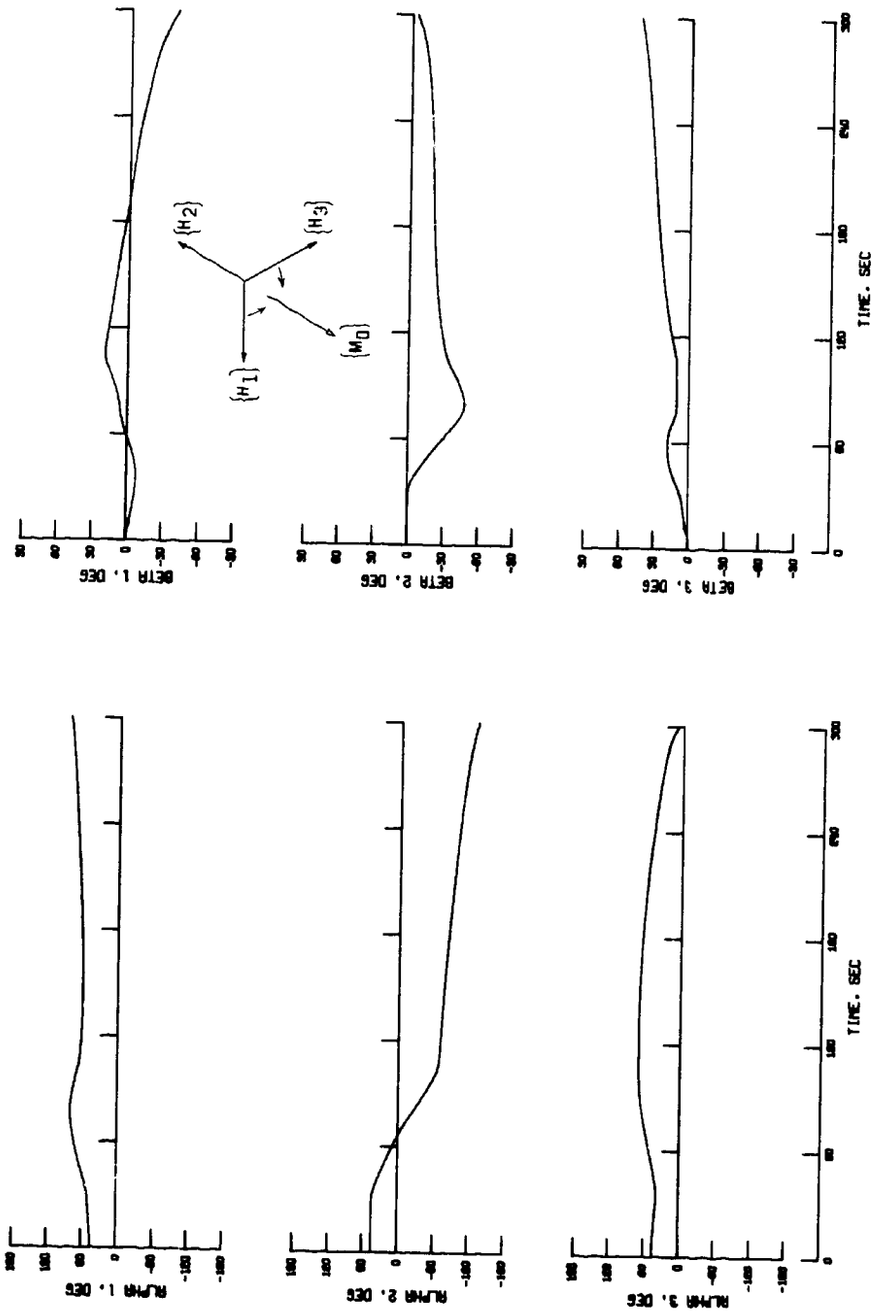

(b) CMG gimbal angles.

Figure 25.- Continued.

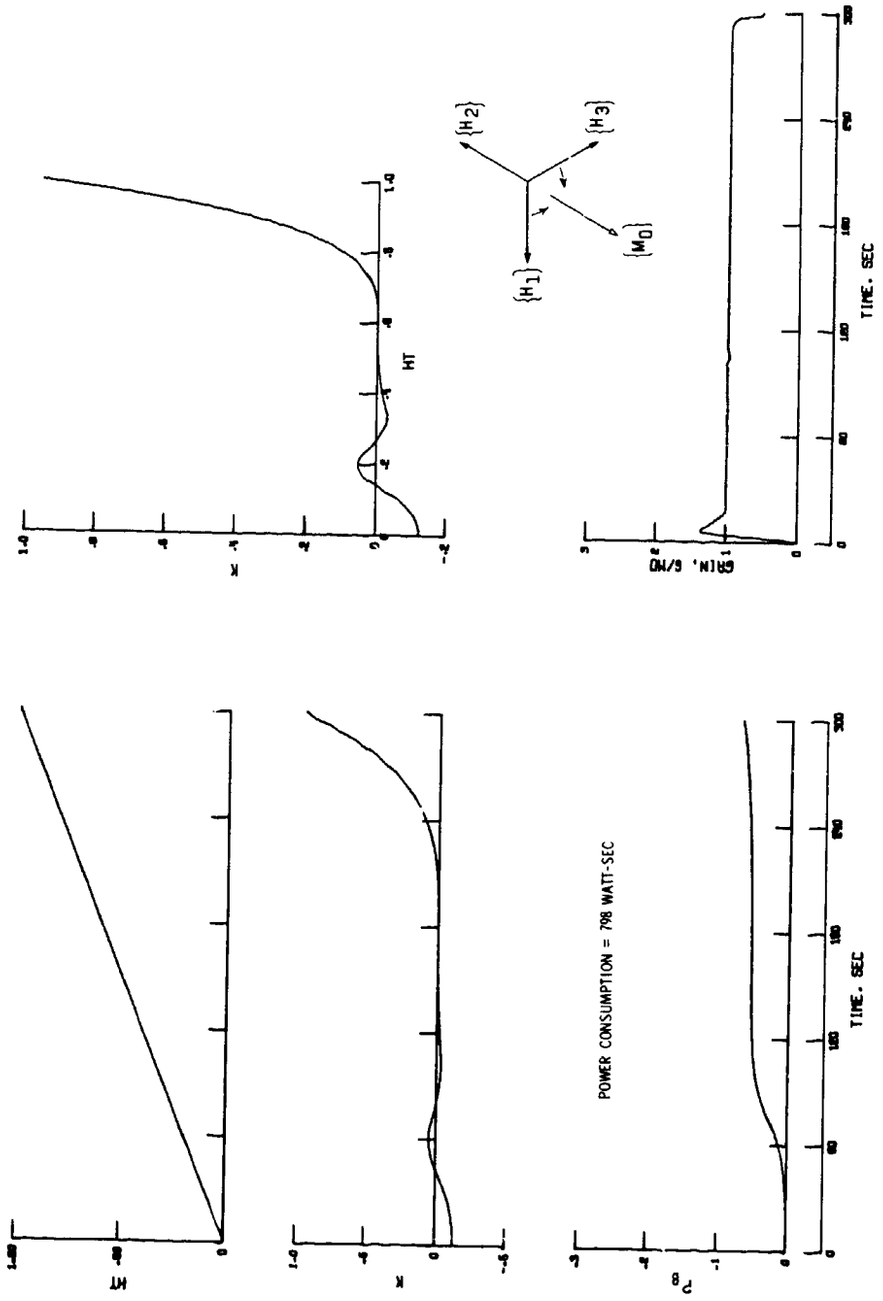

(c) Performance factors.

Figure 25.- Concluded.

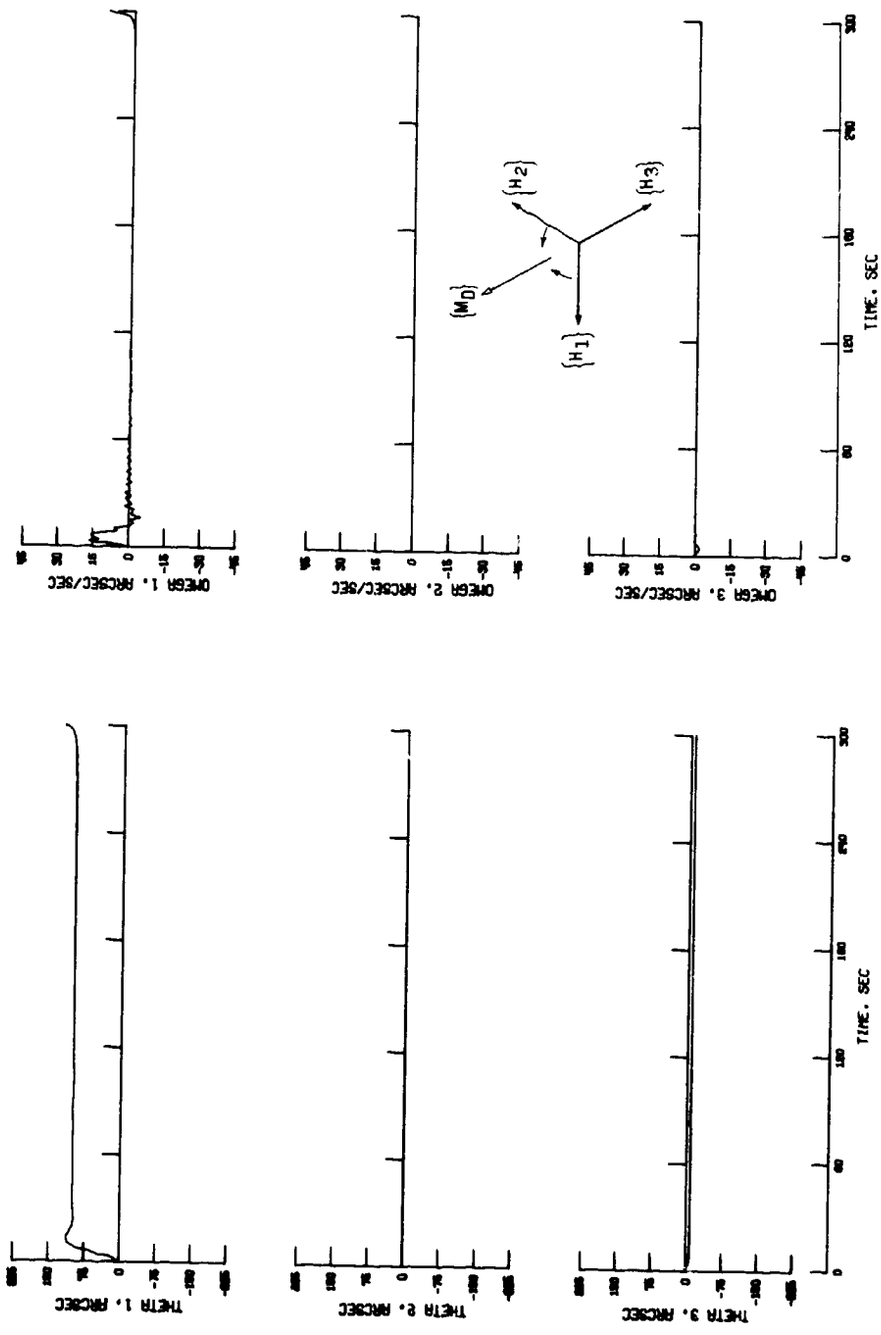

(a) Spacecraft errors.

Figure 26.- Isogonal antiparallel approach from zero-momentum orientation (20 ft-lb moment opposing CMG 3).

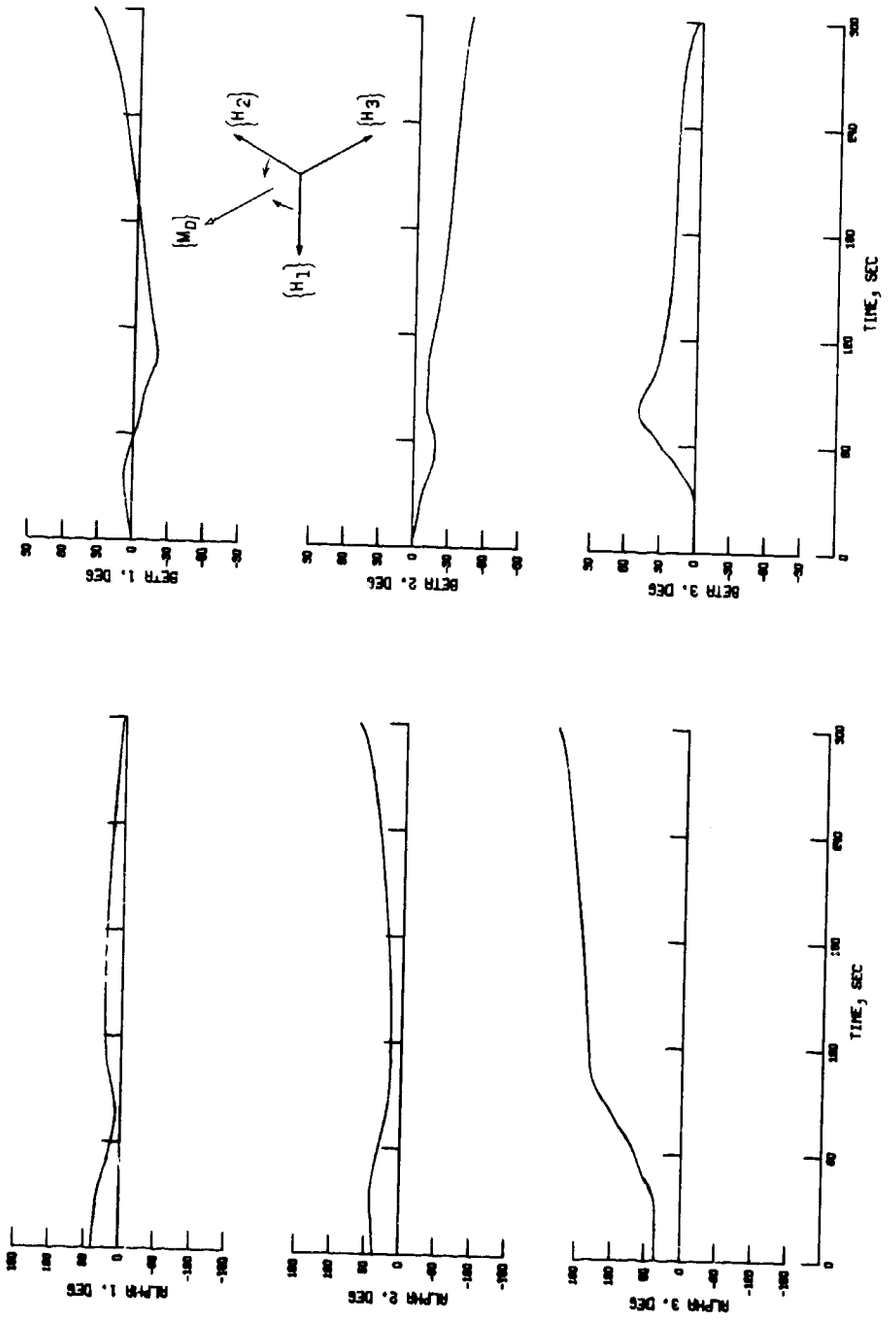

(b) CMG gimbal angles.

Figure 26.- Continued.

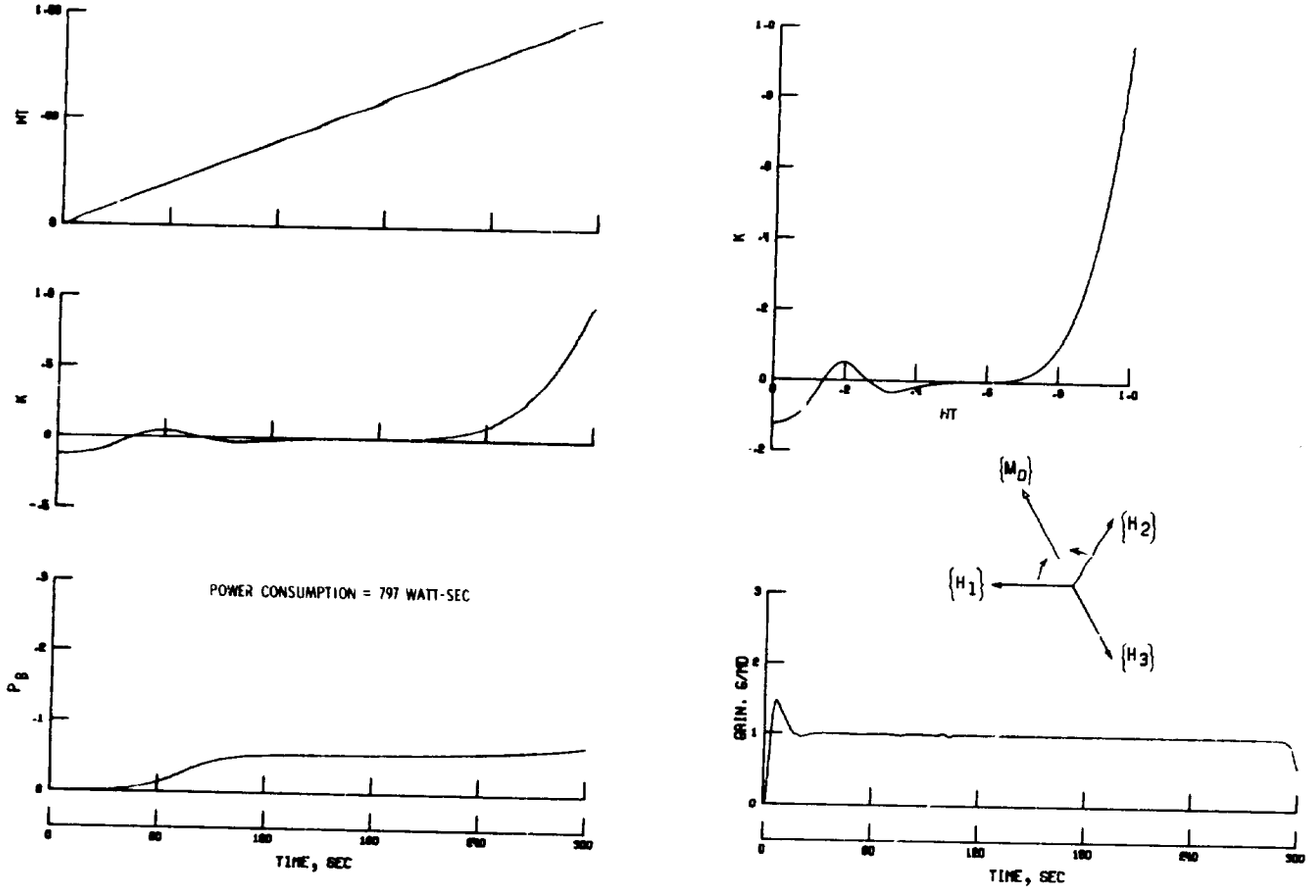

(c) Performance factors.

Figure 26.- Concluded.

CHAPTER VII

APPLICATION SIMULATIONS TO EXIT FROM ADVERSE ORIENTATIONS

Avoidance of the CMG adverse orientations is the primary requirement for optimal control with the CMG control system. In addition, however, an effective technique to avoid those undesirable CMG momentum orientations should also bring the system out of an adverse orientation if such an orientation is arbitrarily acquired. To examine the effectiveness of both the isogonal and simplified logic techniques in countering loss of control when the CMG system is placed in an adverse orientation, the cases of antiparallelism and antisaturation were considered. Initial gimbal angles and the command moment of 20 ft-lb were selected for these adverse orientations, and then the performance of the two different techniques were evaluated in bringing the control system out of these orientations.

Exit From Antiparallel Orientation

With the control system positioned in an antiparallel orientation, it was determined that the K-factor technique could successfully bring the system out of this adverse orientation and permit continued system operation. As Figure 27(a) indicates, the spacecraft initial error is about 670 arc sec for the standard case of $\Delta K = 0.1$ and $\dot{\beta}_c = 3.0$ deg/sec. Ideal power consumption up to saturation was 486 watt-sec for this case and the average inner gimbal angle was 34°. For the K-factor technique, variation of ΔK, or $\dot{\beta}_c$ did not appreciably

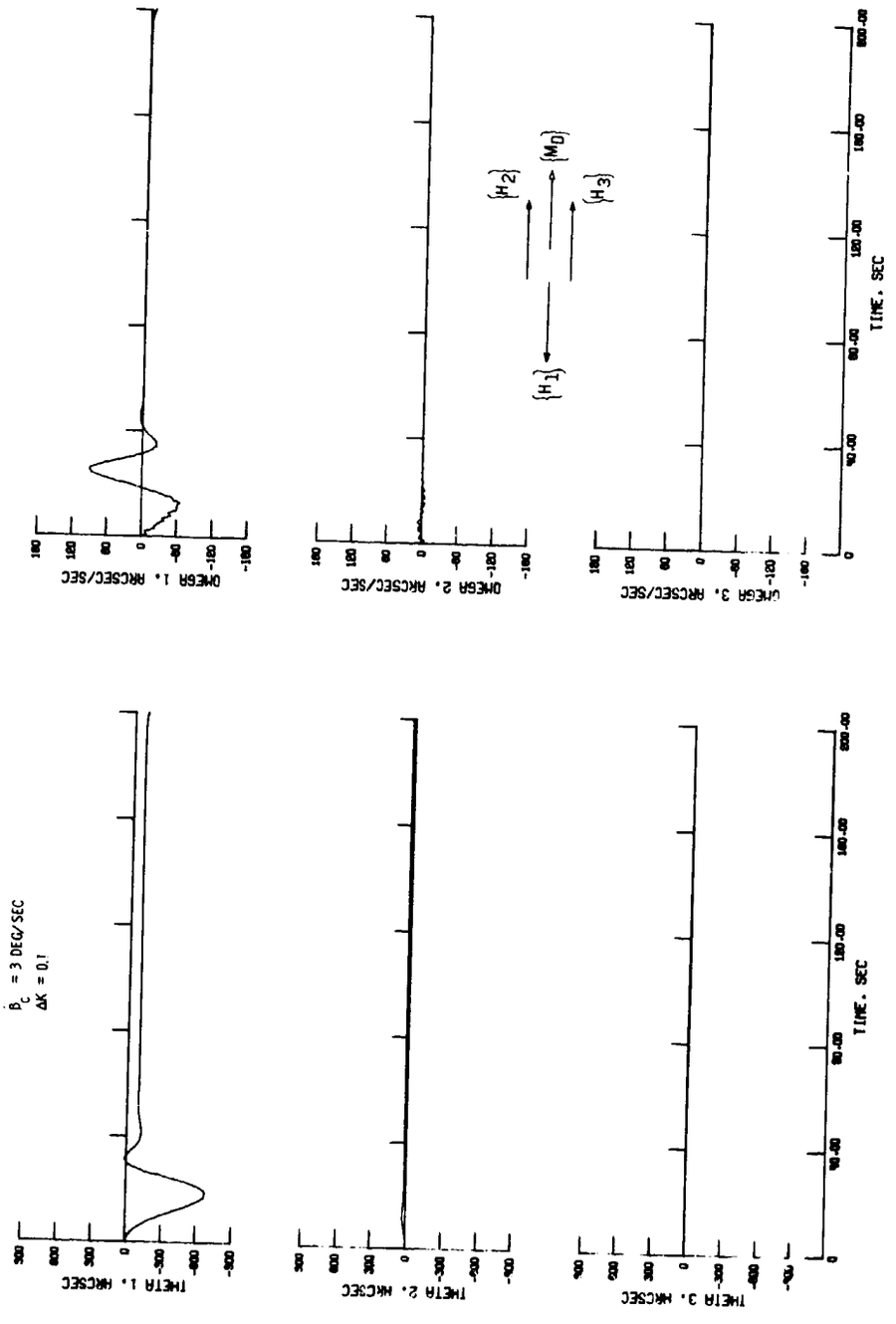

(a) Spacecraft errors.

Figure 27.- Variable deadband exit from antiparallel orientation

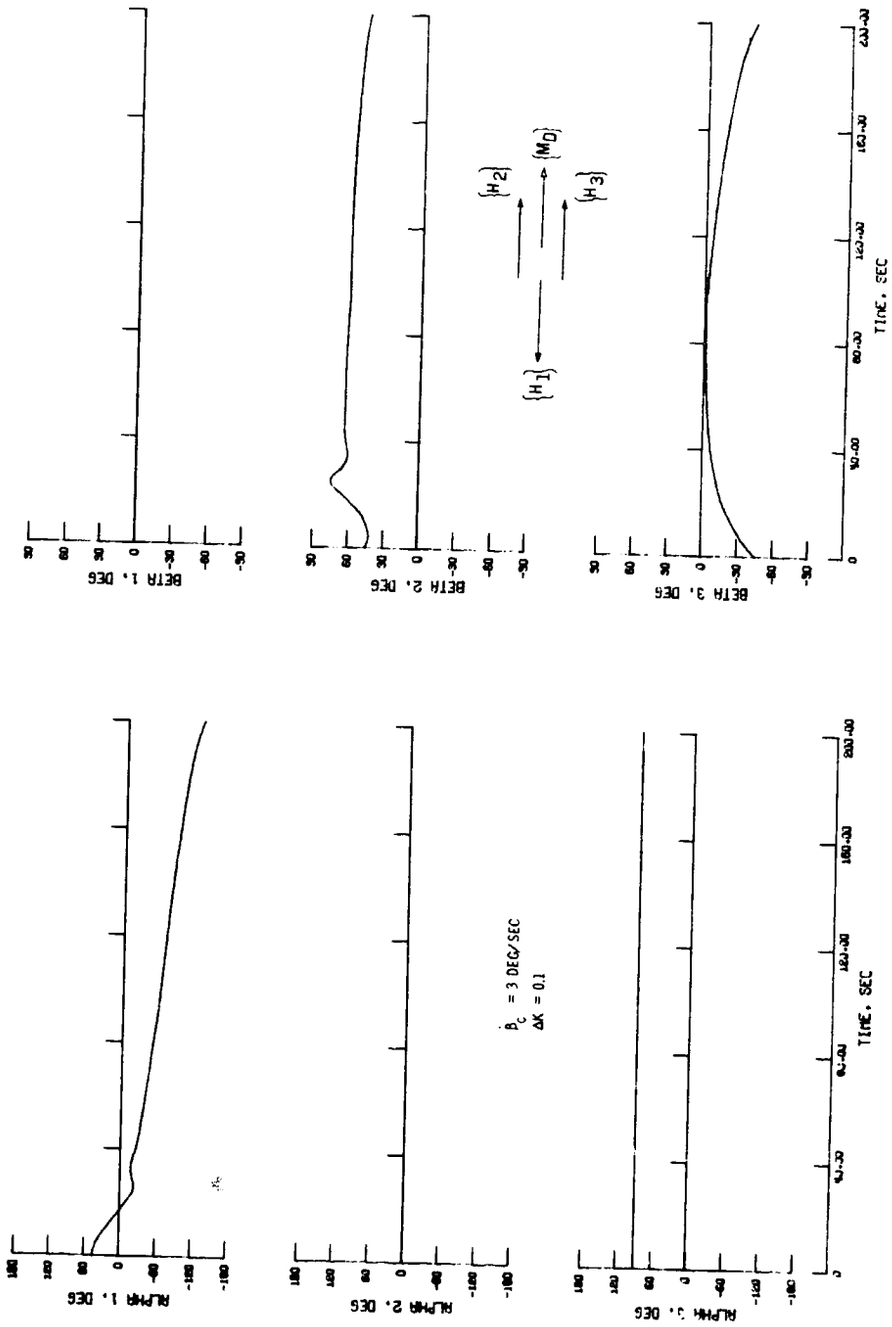

(b) CMG gimbal angles.

Figure 27.- Continued.

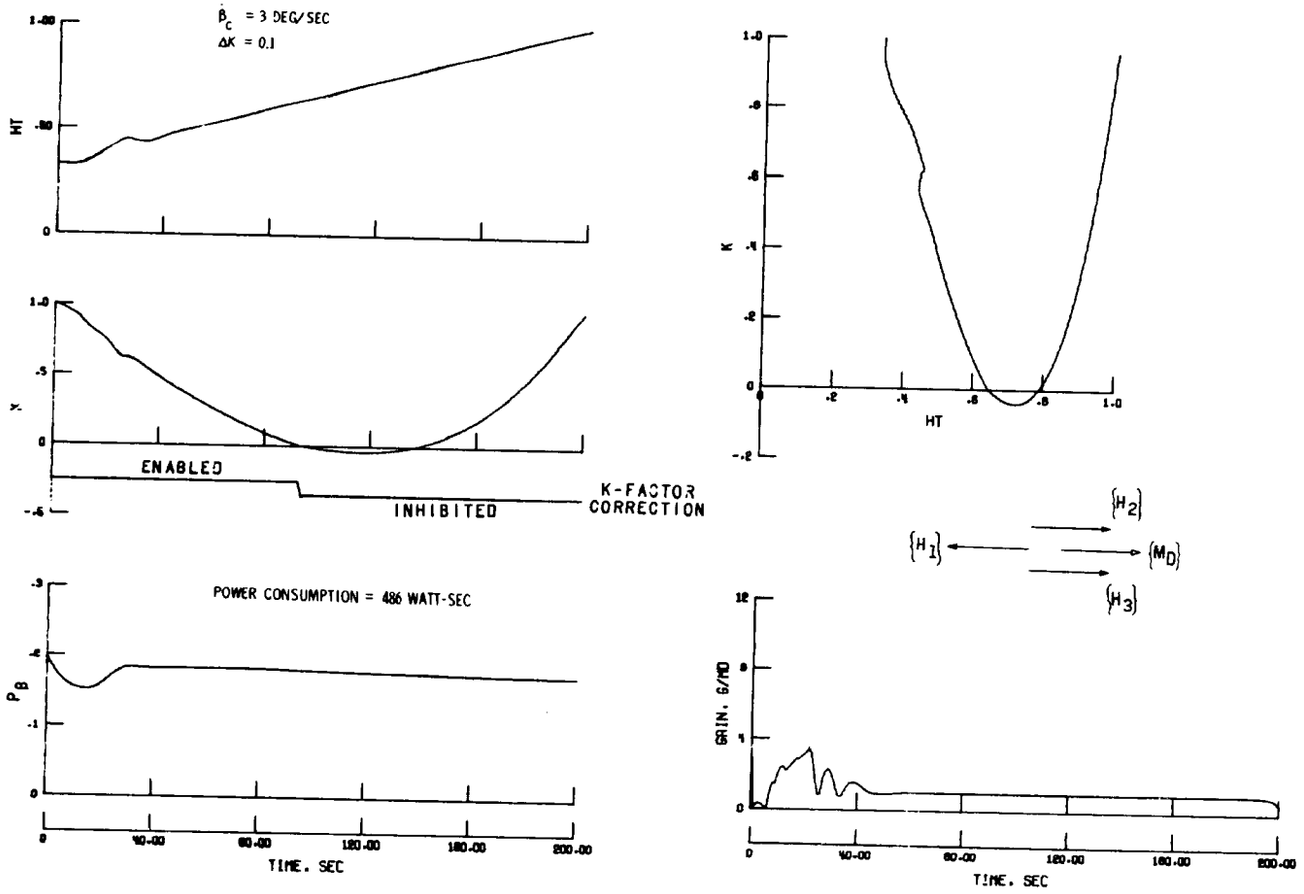

(c) Performance factors.

Figure 27.- Concluded.

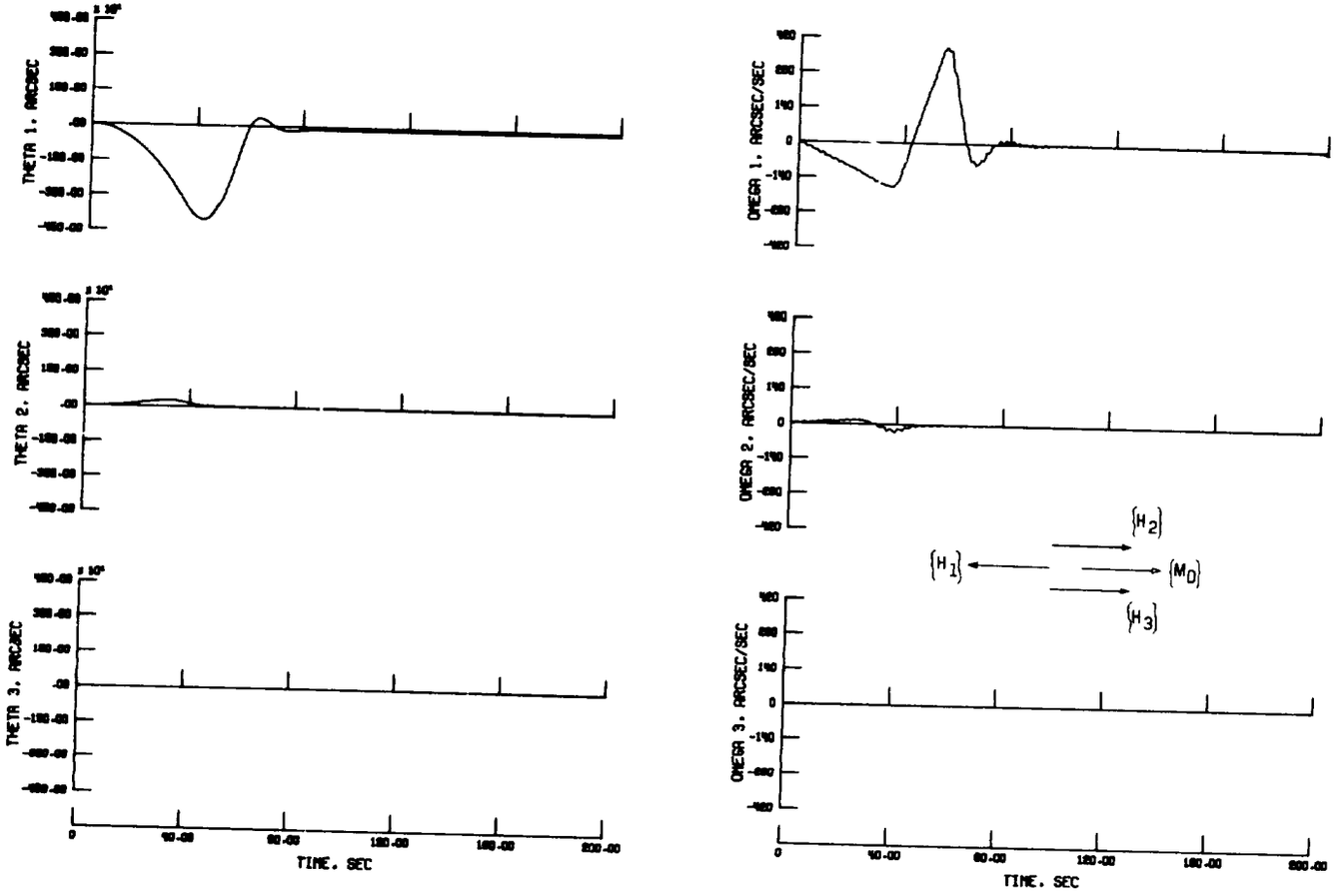

(a) Spacecraft errors.

Figure 28.- Isogonal exit from antiparallel orientation.

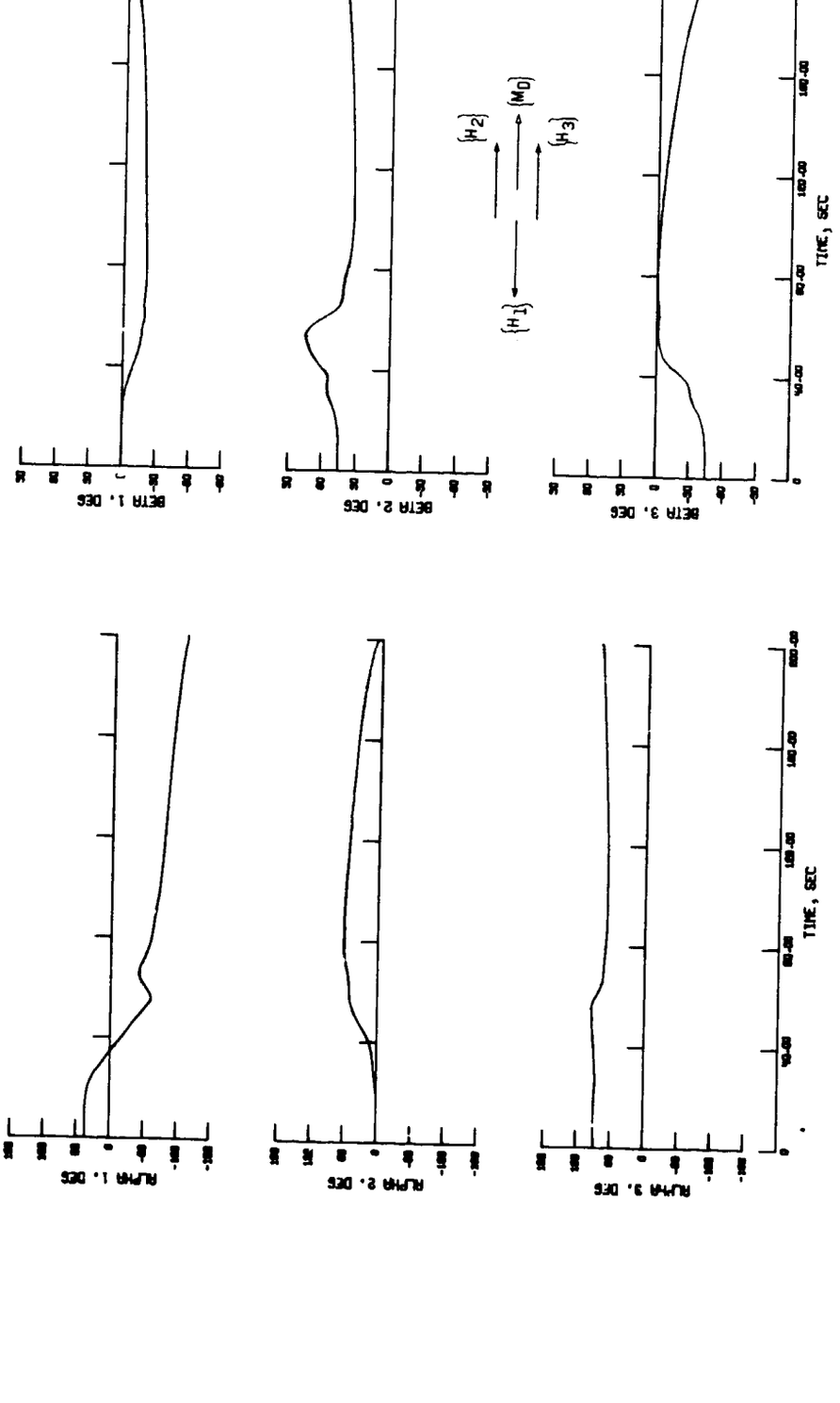

(b) CMG gimbal angles.

Figure 28.- Continued.

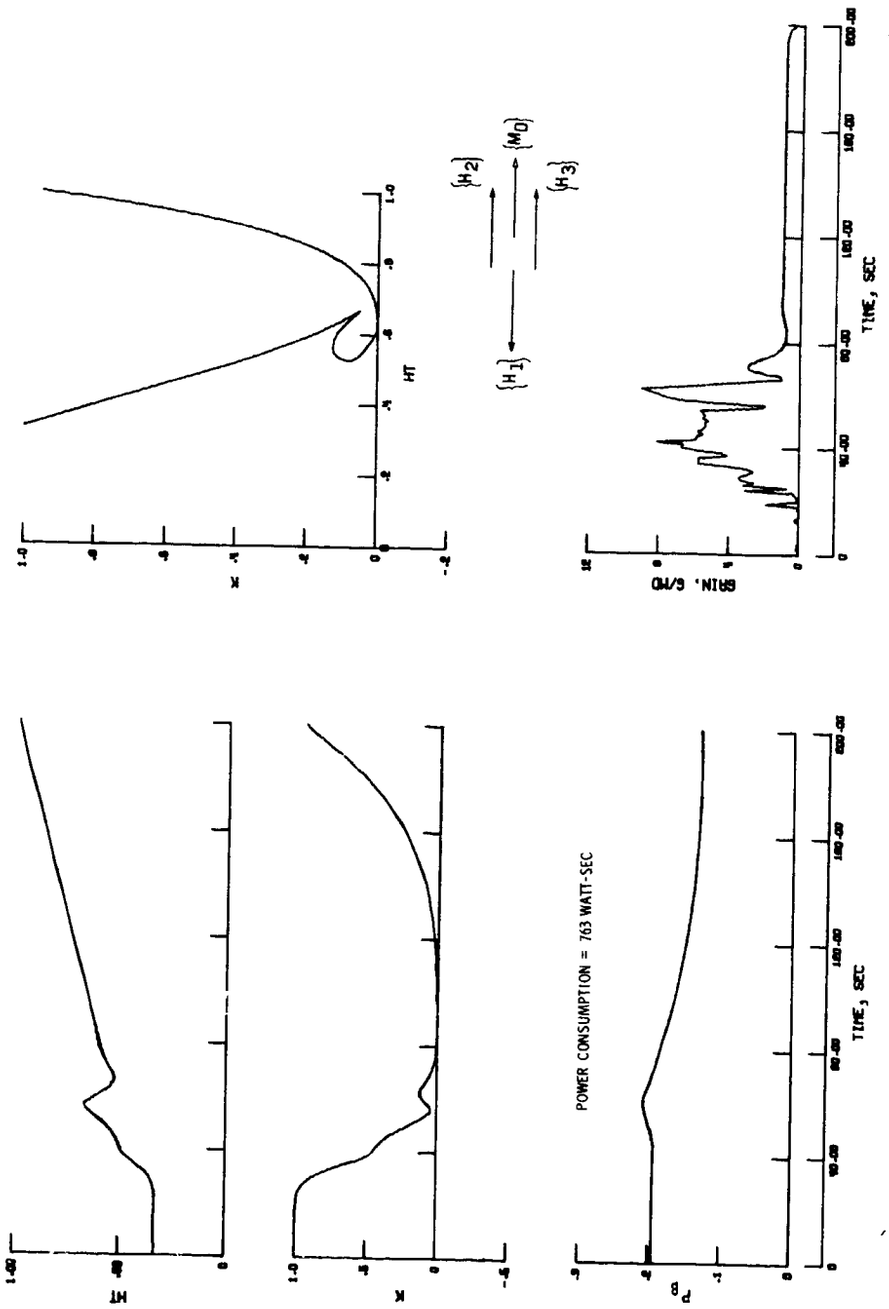

(c) Performance factors.

Figure 28.- Concluded.

affect the spacecraft response or gimbal power requirements for exit from the antiparallel orientation.

The isogonal exit from the antiparallel orientation, presented in Figure 28, resulted in an initial spacecraft error of approximately 4000 arc sec with large GAIN factor variations. In addition, the total gimbal power requirement was approximately 763 watt-sec, and the average inner gimbal angle of 31° was smaller than for the K-factor cases.

Exit From Antisaturation Orientation

To place the control system in the antisaturation condition, the initial conditions for the CMG control system were chosen from the final gimbal angle positions given in Figure 16, and the sign of the command momentum was changed to M_x = -20 ft-lb.

Figure 29 presents data for recovery from the antisaturation orientation for the case of $\dot{\beta}_c$ = 3 deg/sec and ΔK = 0.1. The initial transient response results in an x-axis error of approximately 480 arc sec with a GAIN factor of 4.9 before damping to a steady-state level of 140 arc sec. Under the continuous application of the bias moment, the control system again approaches saturation in about 400 sec with a total power consumption of 510 watt-sec. For this K-factor case, the resulting average inner gimbal angle was 31°.

Figure 30 presents data for the isogonal correction and indicates the spacecraft response and system performance is essentially the same as for the previous K-factor case. The isogonal correction provides

for a smoother transition to eventual saturation resulting in a total power requirement of 422 watt-sec with an average inner gimbal angle of 28°.

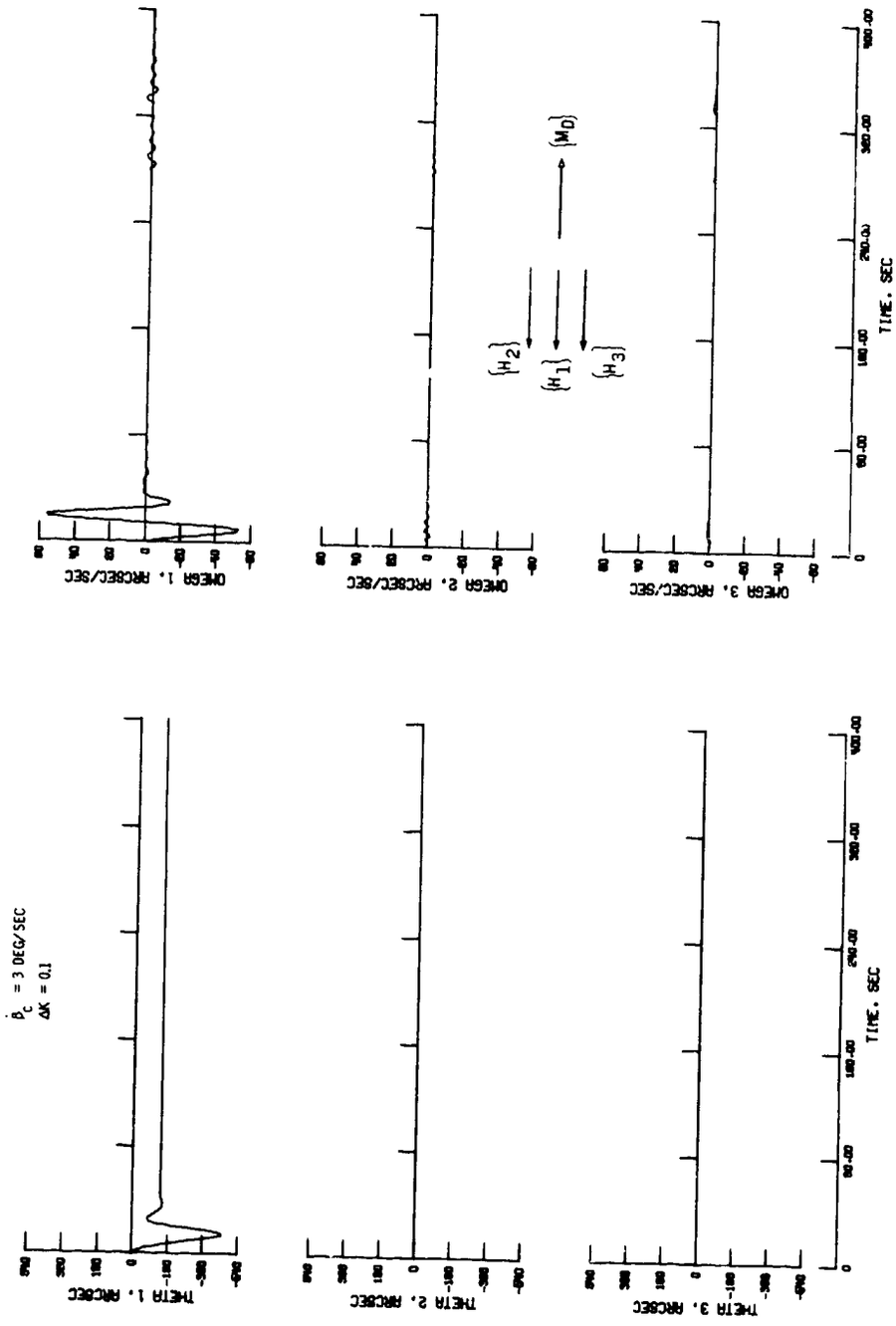

(a) Spacecraft errors.

Figure 29.- Variable deadband exit from antisaturation orientation.

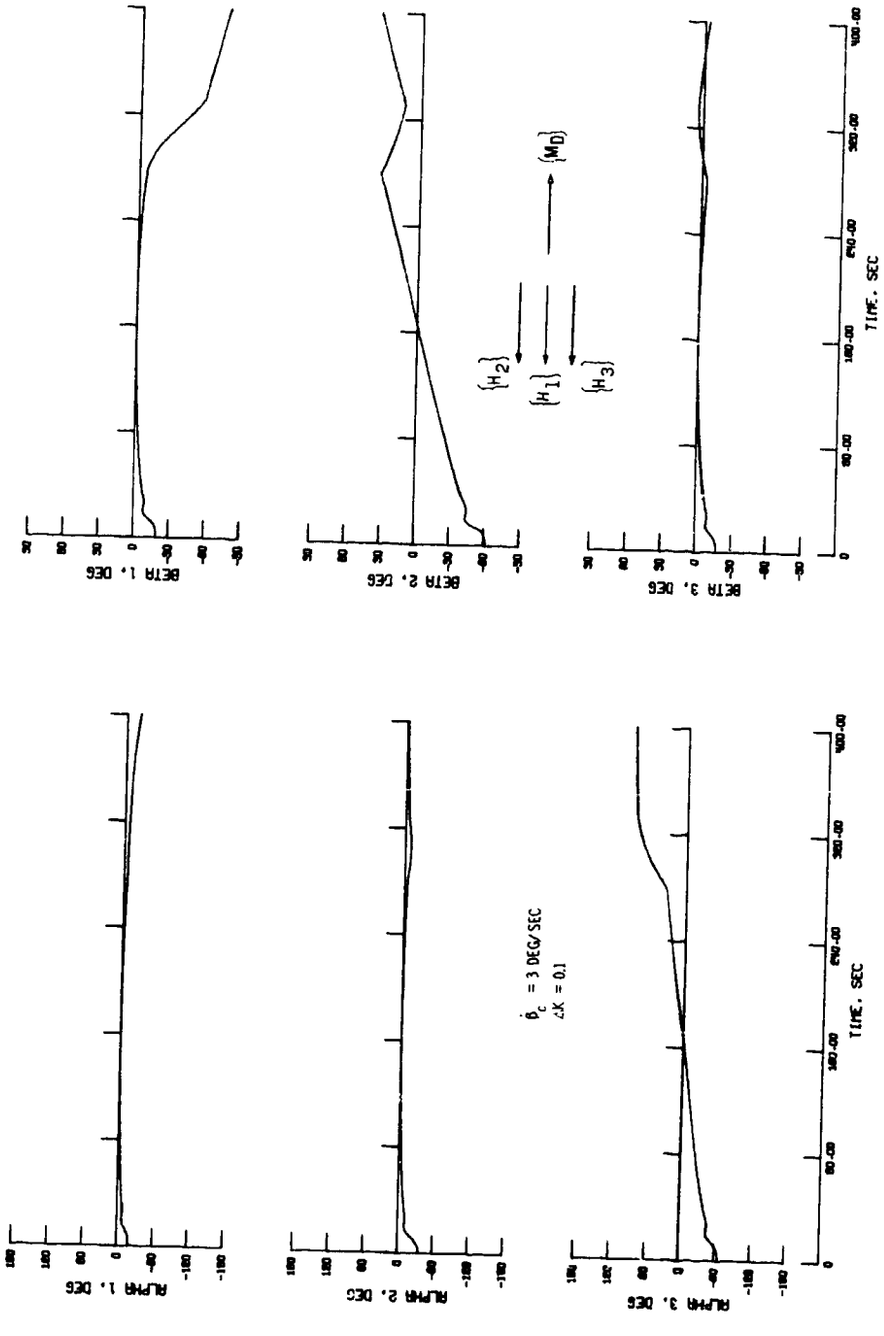

(b) CMG gimbal angles.

Figure 29.- Continued.

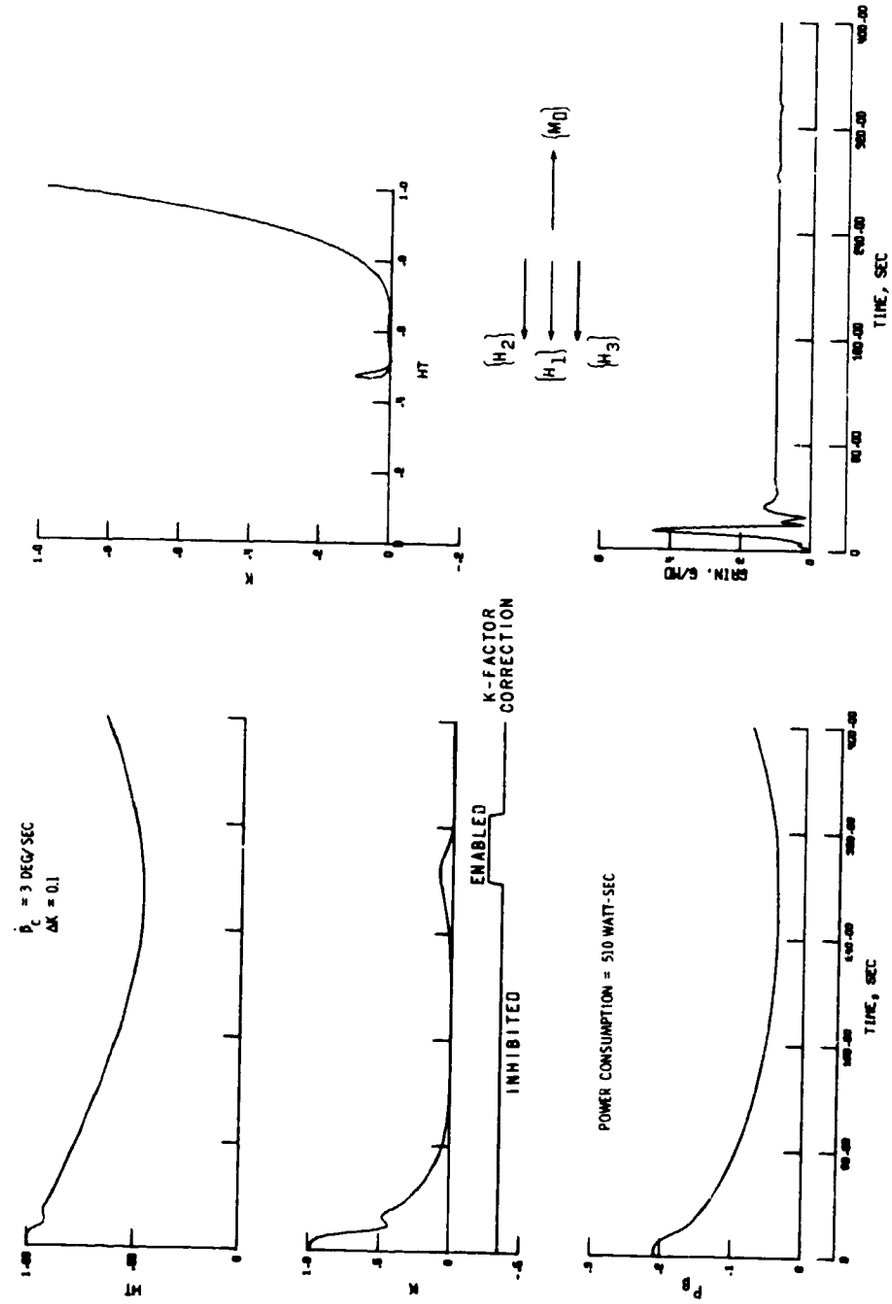

(c) Performance factors.

Figure 29.- Concluded

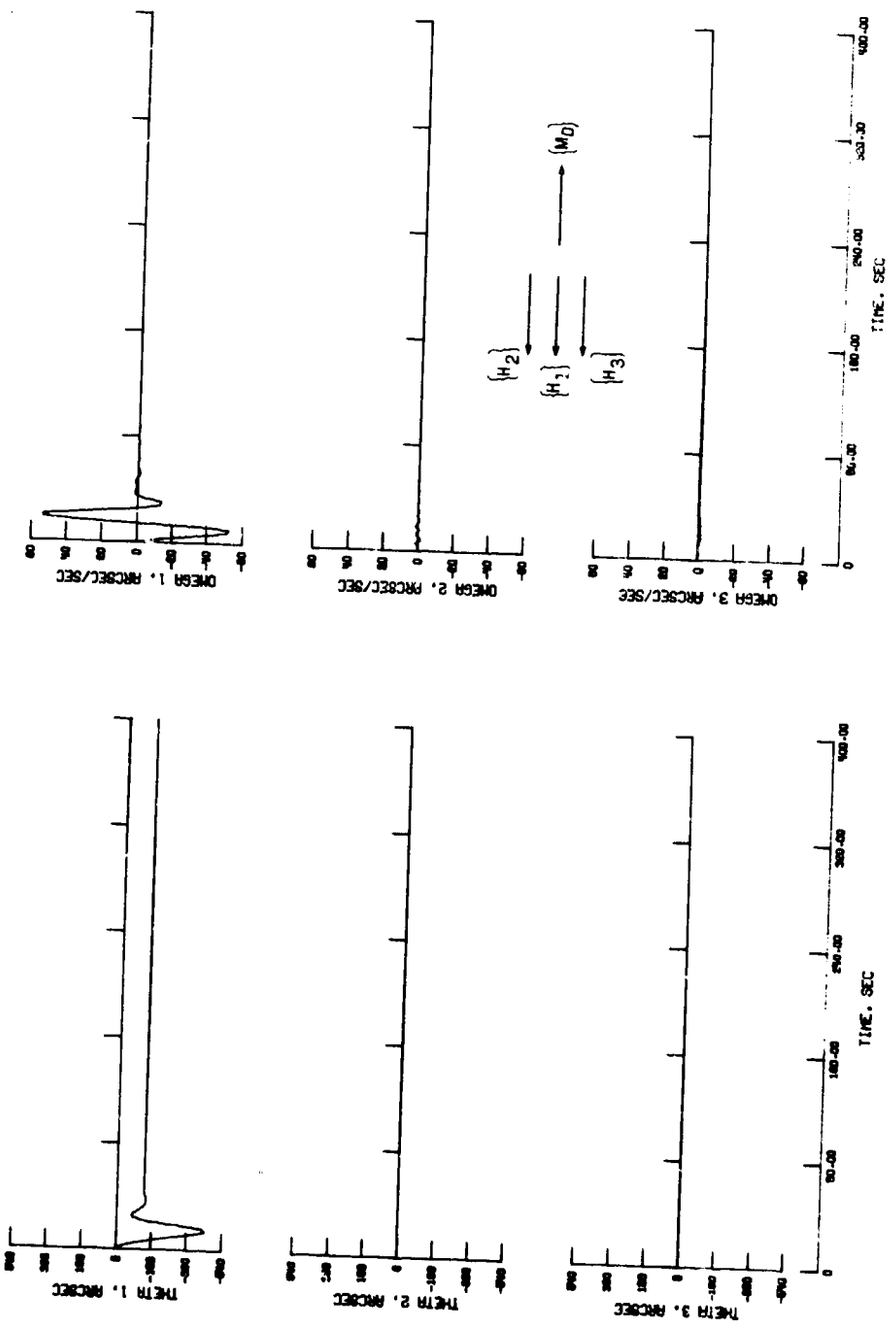

(a) Spacecraft errors.

Figure 30.- Isogonal exit from antisaturation orientation.

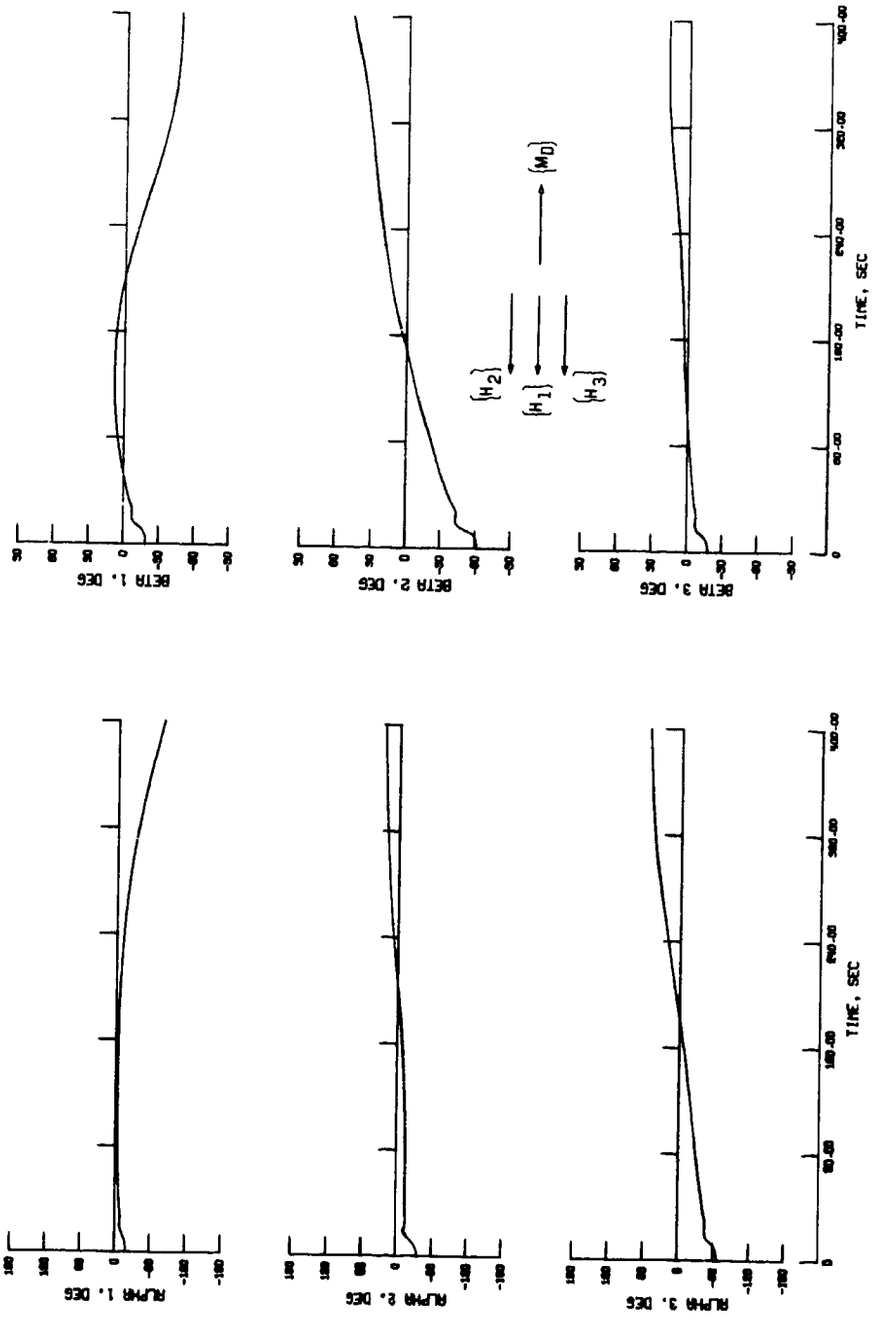

(b) CMG gimbal angles.

Figure 30.- Continued.

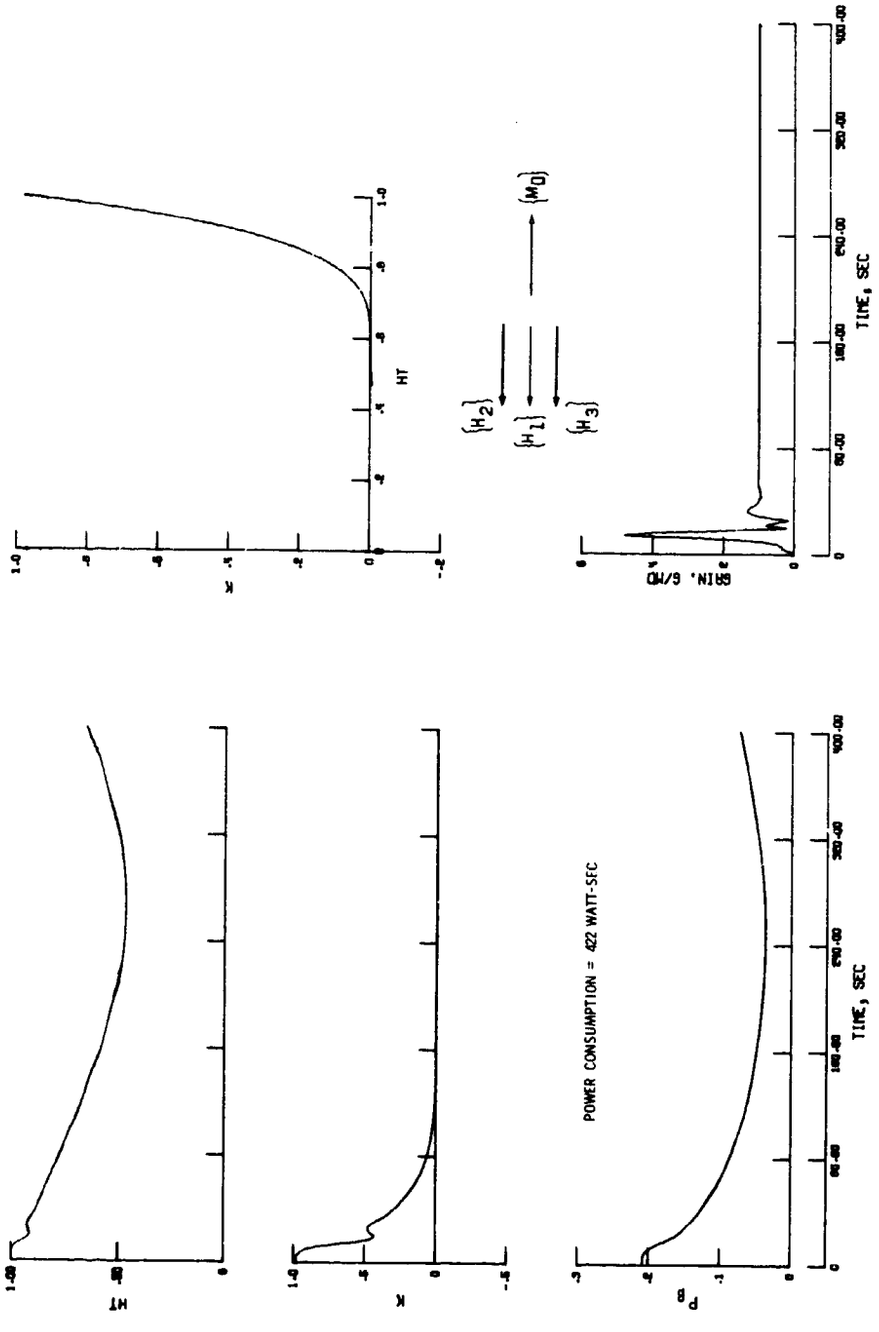

(c) Performance factors.

Figure 30.- Concluded.

CHAPTER VIII

CONCLUSIONS

At ATM design gains the K-factor correction technique described in this section effectively avoids adverse CMG orientations up to saturation and produces control for exit from the adverse orientations in the advent they are arbitrarily acquired. The correction thus improves the CMG system effective gain and, by reducing the CMG inner gimbal angles, requires less power than the H-vector control law alone. The K-factor correction can be readily implemented by analog or digital computer, and is an order of magnitude less complex than the current baseline isogonal correction. For the 20 ft-lb disturbance moment example computer simulations, the K-factor correction technique required considerably less CMG gimbal power than the isogonal correction, with the exception of exit from the antisaturation orientation, but had slightly larger inner gimbal angle excursions.

BIBLIOGRAPHY

1. Kurzhals, Peter R.; and Grantham, Carolyn: A System for Inertial Experiment Pointing and Attitude Control. NASA TR R-247, Aug. 1966.
2. Kennel, Hans F.: Individual Angular Momentum Vector Distribution and Rotation Laws for Three Double-Gimbaled Control Moment Gyros. NASA TM X-53696, Jan. 22, 1968.
3. Keckler, C. R.; Kyle, R. G.; Will, R. W.; and Wooley, C. T.: Real-Time Digital Computer-Hardware Simulation of an ATM Mission With CMG System Stabilization. Proposed NASA TM, 1969.
4. Chubb, William B.; and Epstein, Michael: Application of Control Moment Gyros in the Attitude Control of the Apollo Telescope Mount. Paper presented at the AIAA Guidance and Control Flight Dynamics Conference, Pasadena, California, 1968.

APPENDIX A

CONTROL SYSTEM EQUATIONS

Control Law Development

The control system for the ATM spacecraft uses a modified transpose steering matrix and CMG system momentum feedback (Ref. 4). The basic governing equations for this system are reformulated here to indicate the assumptions made in simulating ATM control with the antiparallel correction method.

Hardware components, such as the CMG units and the spacecraft rate and attitude sensors, are assumed to have a transfer function of unity and thus become ideal components during the computer evaluation of the antiparallel correction. Torque contributions due to gimbal inertia terms are also neglected. The CMG system control torque $\{G\}$ can thus be expressed in terms of the CMG momentum vector $\{H\}$ and the ATM spacecraft angular rate vector $\{\Omega\}$ by

$$\{G\} = -\{\dot{H}\} - [\Omega]\{H\} \tag{A1}$$

where

$$\{G\} \equiv \begin{Bmatrix} G_1 \\ G_2 \\ G_3 \end{Bmatrix}, \quad \{H\} \equiv \begin{Bmatrix} H_1 \\ H_2 \\ H_3 \end{Bmatrix}, \quad \{\Omega\} \equiv \begin{Bmatrix} \Omega_1 \\ \Omega_2 \\ \Omega_3 \end{Bmatrix} \tag{A2}$$

and the cross-product term $\langle\Omega\rangle$ is given by

$$[\Omega] = \begin{bmatrix} 0 & -\Omega_3 & \Omega_2 \\ \Omega_3 & 0 & -\Omega_1 \\ -\Omega_2 & \Omega_1 & 0 \end{bmatrix} \tag{A3}$$

In index notation, the ith component of the control torque form equation (A1) is

$$\begin{aligned} G_i = H((&\dot{\alpha}_i - \Omega_k)\sin\alpha_i \cos\beta_i + (\dot{\alpha}_k - \Omega_j)\cos\alpha_k \cos\beta_k \\ &+ (\dot{\beta}_i \cos\alpha_i + \Omega_j)\sin\beta_i - (\dot{\beta}_k \sin\alpha_k + \Omega_k)\sin\beta_k \\ &+ (\dot{\beta}_j + \Omega_j \sin\alpha_j + \Omega_k \cos\alpha_j)\cos\beta_j) \end{aligned} \tag{A4}$$

in its expanded form. Since the product of vehicle rates and CMG momenta is small, equation (A1) can be approximated by

$$\langle G\rangle \simeq -\langle\dot{H}\rangle \tag{A5}$$

for the purposes of control law analysis.

The CMG momentum vector in equation (A5) is

$$\langle H\rangle = H\begin{Bmatrix} \cos\beta_1 \cos\alpha_1 & -\cos\beta_3 \sin\alpha_3 & -\sin\beta_2 \\ \cos\beta_2 \cos\alpha_2 & -\cos\beta_1 \sin\alpha_1 & -\sin\beta_3 \\ \cos\beta_3 \cos\alpha_3 & -\cos\beta_2 \sin\alpha_2 & -\sin\beta_1 \end{Bmatrix} \tag{A6}$$

so that equation (A5) can be rewritten as

$$\langle G\rangle = -H[A]\langle\dot{\delta}\rangle \tag{A7}$$

where

$$[A] \equiv -\left[[A_1][A_2]\right] \tag{A8}$$

with

$$[A_1] = \begin{bmatrix} \sin\beta_1 \cos\alpha_1 & \cos\beta_2 & -\sin\beta_3 \sin\alpha_3 \\ -\sin\beta_1 \sin\alpha_1 & \sin\beta_2 \sin\alpha_2 & \cos\beta_3 \\ \cos\beta_1 & -\sin\beta_2 \sin\alpha_2 & \sin\beta_3 \cos\alpha_3 \end{bmatrix}$$

$$[A_2] = [A_3][A_4] = \begin{bmatrix} \sin\alpha_1 & 0 \\ \cos\alpha_1 & \sin\alpha_2 \\ 0 & \cos\alpha_2 \end{bmatrix} \begin{bmatrix} \cos\alpha_3 & \cos\beta_1 & 0 & 0 \\ 0 & 0 & \cos\beta_2 & 0 \\ \sin\alpha_3 & 0 & 0 & \cos\beta_3 \end{bmatrix}$$

and

$$\{\dot{\delta}\} \equiv \begin{Bmatrix} \dot{\beta}_1 \\ \dot{\beta}_2 \\ \dot{\beta}_3 \\ \dot{\alpha}_1 \\ \dot{\alpha}_2 \\ \dot{\alpha}_3 \end{Bmatrix} \tag{A9}$$

The gimbal rate vector $\dot{\delta}$ for the ATM system is commanded to be

$$\langle \dot{\delta} \rangle = K_{SL} \begin{bmatrix} [A_1]^T \\ [A_3]^T \end{bmatrix} \left(\langle H_C \rangle - \langle H \rangle \right) \tag{A10}$$

or in index notation

$$\begin{aligned} \dot{\alpha}_i &= K_{SL}((H_{Ci} - H_i)\sin \alpha_i + (H_{Cj} - H_j)\cos \alpha_i \\ \dot{\beta}_i &= K_{SL}((H_{Ci} - H_i)\cos \alpha_i \sin \beta_i - (H_{Cj} - H_j)\sin \alpha_i \sin \beta_i \\ &\quad - (H_{Ck} - H_k)\cos \beta_k) \end{aligned} \tag{A11}$$

with the result

$$\begin{aligned} \langle G \rangle &= -K_{SL} H \left[[A_1][A_1]^T + [A_3][A_4][A_3]^T \right] \left(\langle H_C \rangle - \langle H \rangle \right) \\ &\equiv -K_{SL} H [B] \left(\langle H_C \rangle - \langle H \rangle \right) \end{aligned} \tag{A12}$$

The two 3×3 matrices making up $[B]$ in equation (A12) are reasonably diagonal and permit the generation of continued control commands in the event of failure of a CMG unit. The gain factor K_{SL} is a constant.

The commanded momentum H_C in equations (A10) and (A12) is derived from desired control torques of the form

$$\langle M_C \rangle = \begin{Bmatrix} M_{C1} \\ M_{C2} \\ M_{C3} \end{Bmatrix} = \begin{Bmatrix} K_1\theta_1 + K_2\Omega_1 \\ K_3\theta_2 + K_4\Omega_2 \\ K_5\theta_3 + K_6\Omega_3 \end{Bmatrix} \tag{A13}$$

where $\{\Omega\}$ and $\{\theta\}$ are developed in Appendix B. The gains K_i are constant. A commanded moment is obtained from $\{MC\}$ by fourth-order filters, which eliminate high frequency input to the CMG system. The filtered commanded moment is thus

$$\left.\begin{aligned} M_{CF1} &= \frac{M_{C1}}{\left[1 + \frac{2\rho_1 s}{\omega_1} + \left(\frac{s}{\omega_1}\right)^2\right]^2} \\ M_{CF2} &= \frac{M_{C2}}{\left[1 + \frac{2\rho_2 s}{\omega_2} + \left(\frac{s}{\omega_2}\right)^2\right]^2} \\ M_{CF3} &= \frac{M_{C3}}{\left[1 + \frac{2\rho_3 s}{\omega_3} + \left(\frac{s}{\omega_3}\right)^2\right]^2} \end{aligned}\right\} \qquad \text{(A14)}$$

where s denotes the Laplace transform variable. The commanded momentum becomes

$$\{H_C\} \equiv \begin{Bmatrix} H_{C1} \\ H_{C2} \\ H_{C3} \end{Bmatrix} = \int \{M_{CF}\}\, dt \qquad \text{(A15)}$$

The magnitude of the commanded moment $\langle M_{CF} \rangle$ in equation (A15) is limited to ± 200 ft-lb because of the integrator limitations in the ATM control computer.

Equations (A5) and (A12) yield

$$\langle \dot{H} \rangle = K_{SL}H [B] \left(\langle H_C \rangle - \langle H \rangle \right) \tag{A16}$$

or

$$\langle \dot{H} \rangle + K_{SL}H [B] \langle H \rangle = K_{SL}H [B] \langle H_C \rangle \tag{A17}$$

For large values of $K_{SL}H$, the effective response of the system described by equation (A17) is given by

$$\langle H \rangle \rightarrow \langle H_C \rangle \tag{A18}$$

and

$$\langle G \rangle \rightarrow -\langle M_{CF} \rangle \tag{A19}$$

Since the CMG system momentum is fed back to the CMG gimbal torquers, any change in this momentum without a corresponding change in the commanded momentum must be compensated for by a redistribution of the CMG unit momentum vectors to maintain the condition of equation (A18). This inner-loop response of the ATM control law is extremely fast (with a time constant of $1/K_{SL}H$) and should be able to compensate for such a CMG system momentum change before the effects of the change are transmitted to the spacecraft.

Inner Gimbal Roll-Off Logic

Also incorporated into the control law logic was a roll-off scheme for the inner gimbals when they reached their $\pm 80^{\circ}$ stops. When an inner gimbal saturates as such, the corresponding outer gimbal is commanded to move in a direction as to back the inner gimbal off its stop to a specified limit (selected as $\beta_{iL} = \pm 75^{\circ}$) and at a specified outer gimbal rate (selected as $\alpha_{iC} = 3.5$ deg/sec).

Performance Factors

Several factors are used to permit assessment of the CMG system performance. The first performance factor is the theoretical gimbal power consumption P. The electrical power P_{Gi} for the ith gimbal torquer is approximately expressed by the relation

$$P_{Gi} = IK_B K_G \dot{\delta}_i + I^2 R \qquad \text{(A20)}$$

where the first term represents mechanical power and the second term electrical power losses. Here $\dot{\delta}_i$ is the gimbal rate, K_B reflects the back EMF constant, K_G is the gear ratio, and R is the winding resistance. The current I is given by

$$I = \frac{T_i}{K_T K_G} \qquad \text{(A21)}$$

and is a function of the gear ratio K_G, the stall torque constant K_T, and the effective gimbal torque command T_i. Substitution of equation (A21) into equation (A20) yields

$$P_{Gi} = \left(\frac{K_B}{K_T}\right) T_i \dot{\delta}_i + \left(\frac{R}{K_T^2 K_G^2}\right) T_i^2 \qquad \text{(A22)}$$

The effective control commands requiring power for the outer and inner gimbal become

$$\left.\begin{aligned} T_{\alpha_i} &= (H\dot{\beta}_i \cos \beta_i + T_F \operatorname{sgn} \dot{\alpha}_i) \\ T_{\beta_i} &= (H\dot{\alpha}_i \cos \beta_i + T_F \operatorname{sgn} \dot{\beta}_i) \end{aligned}\right\} \qquad \text{(A23)}$$

with

$$\left.\begin{aligned} T_{\alpha_i} &\equiv 0.0 \quad \text{if} \quad \operatorname{sgn} T_{\alpha_i} \neq \operatorname{sgn} \alpha_i \\ T_{\beta_i} &\equiv 0.0 \quad \text{if} \quad \operatorname{sgn} T_{\beta_i} \neq \operatorname{sgn} \beta_i \end{aligned}\right\} \qquad \text{(A24)}$$

where T_F is the gimbal friction torque magnitude and gimbal acceleration torques are neglected in equation (A23). When $T_i \dot{\delta}_i$ is negative, existing precessional torques are already producing the desired control moments and the effective torque command for that gimbal goes to zero.

Equations (A22) and (A23) are used to define the total CMG system gimbal power as

$$P_G = \sum_{i=1}^{3} \left(\left(\frac{K_B}{K_T}\right)(T_{\alpha i}\dot{\alpha}_i + T_{\beta i}\dot{\beta}_i) + \left(\frac{R}{K_T^2 K_G^2}\right)(T_{\alpha i}^2 + T_{\beta i}^2) \right) \qquad \text{(A25)}$$

and the power consumption becomes

$$P \equiv \int P_G dt, \text{ watt-sec} \tag{A26}$$

to complete the definition of the first performance factor.

The second performance factor GAIN is defined as the ratio of the control torque magnitude to the disturbance torque magnitude, so that

$$\text{GAIN} \equiv \frac{G}{M_D} \tag{A27}$$

This factor serves as a measure of the effective gain of the control system.

The third performance factor provides an indicator of the extent of saturation of the inner gimbals, and is defined as

$$P_\beta = 1 - \frac{1}{3} \sum_{i=1}^{3} \cos \beta_i \tag{A28}$$

APPENDIX B

SPACECRAFT EQUATIONS

Rigid-Body Contributions

The rigid-body rates for the ATM spacecraft are determined by integration of the Euler equations

$$\left\langle \dot{\Omega}_R \right\rangle = \left[I \right]^{-1} \left(\left\langle G \right\rangle + \left\langle M_D \right\rangle - \left[\Omega_R \right] \left[I \right] \left\langle \Omega_R \right\rangle \right) \tag{B1}$$

where $\left\langle G \right\rangle$ is the control torque defined by equation (A1), $\left\langle M_D \right\rangle$ is the applied disturbance moment, and the rigid spacecraft inertia and angular rate are defined as

$$\left[I \right] \equiv \begin{bmatrix} I_1 & 0 & 0 \\ 0 & I_2 & 0 \\ 0 & 0 & I_3 \end{bmatrix}, \quad \left\langle \Omega_R \right\rangle \equiv \begin{Bmatrix} \Omega_{R1} \\ \Omega_{R2} \\ \Omega_{R3} \end{Bmatrix} \tag{B2}$$

Products of inertia are neglected.

The rigid-body Euler rates become

$$\left\langle \dot{\theta}_R \right\rangle \equiv \begin{Bmatrix} \dot{\theta}_{R1} \\ \dot{\theta}_{R2} \\ \dot{\theta}_{R3} \end{Bmatrix} = \left[C \right] \left\langle \Omega_R \right\rangle \tag{B3}$$

where

$$[C] = \begin{bmatrix} 1 & \tan\theta_{R2}\sin\theta_{R1} & \tan\theta_{R2}\cos\theta_{R1} \\ 0 & \cos\theta_{R1} & -\sin\theta_{R1} \\ 0 & \sec\theta_{R2}\sin\theta_{R1} & \sec\theta_{R2}\cos\theta_{R1} \end{bmatrix} \tag{B4}$$

gives the transformation matrix between spacecraft and Euler rates.

Integration of equations (B1) and (B4) defines the rigid-body motion of the ATM spacecraft.

Flexible-Body Contributions

The flexible-body rates and attitudes are determined from dynamic and quasi-static modal representations of the ATM cluster. Seven modes are represented dynamically; all remaining modes are incorporated quasi-statically. The dynamic modes contribute both angular rate and Euler angle errors, while the quasi-static modes contribute only Euler angle errors.

The basic uncoupled modal differential equations for the dynamic modes are

$$\langle \ddot{q}_D \rangle + 2\xi \left[\underset{\sim}{\omega}_D \right] \langle \dot{q}_D \rangle + \left[\underset{\sim}{\omega}_D^2 \right] \langle q_D \rangle = [U_D] \langle E \rangle \tag{B5}$$

or in index notation (for $i = 1,2, \ldots, 7$)

$$\ddot{q}_{Di} + 2\xi\omega_{Di}\dot{q}_{Di} + \omega_{Di}^2 q_{Di} = \sum_{j=1}^{18} U_{Dij} E_j \tag{B6}$$

where q_{Di} is the modal displacement, ξ is the modal damping, and ω_{Di} is the modal frequency. The vector $\{E\}$ contains the 18 moment and force inputs (defined in Appendix C) corresponding to disturbances applied in the ATM/LM (E_1 to E_6), the CSM (E_7 to E_{12}), and the SIVB Workshop (E_{13} to E_{18}). The matrix $[U_D]$ is the 7×18 modal distribution matrix for the seven dynamic modes considered. The flexible rates and attitude errors for the dynamic modes become

$$\{\Omega_F\} = [\phi_D]\{\dot{q}_D\} \tag{B7}$$

and

$$\{\gamma_{FD}\} = [\phi_D]\{q_D\} \tag{B8}$$

or in index notation

$$\gamma_{FDi} = \sum_{j=1}^{6} \phi_{Dij}\dot{q}_i = \sum_{j=1}^{6} U_{Dji}q_i \tag{B9}$$

where $\dot{q}_D$ and q_D are determined by integrating equation (B5), and $[\phi_D]$ is the 3×7 modal participation matrix found by transposing the first three columns of $[U_D]$.

For all remaining modes, which are represented quasi-statically, the modal displacements become

$$\{q_S\} = \left[\omega_S^2\right]^{-1}[U_S]\{E\} \tag{B10}$$

by neglecting terms containing derivatives of the modal displacement in the modal differential equations, the resulting attitude errors are

$$\langle \gamma_{FS} \rangle = [\phi_S] \left[\omega_S^2 \right] [U_S] \langle E \rangle$$

$$\equiv [V] \langle E \rangle$$

The total flexible-body attitude errors correspond to

$$\langle \gamma_F \rangle = \langle \gamma_{FD} \rangle + \langle \gamma_{FS} \rangle \tag{B12}$$

from equations (B8) and (B11) and the flexible Euler angle errors are given by

$$\langle \theta_F \rangle = [C] \langle \gamma_F \rangle \tag{B13}$$

where $[C]$ is determined in equation (B4).

Evaluation of equations (B7) and (B13) defines the flexible-body motion of the ATM spacecraft.

Total Spacecraft Errors

The total spacecraft errors are found by adding the rigid-body and flexible-body contributions to the spacecraft motion. This gives

$$\langle \Omega \rangle = \langle \Omega_R \rangle + \langle \Omega_F \rangle \tag{B14}$$

using equations (B1) and (B7) for the rate errors and

$$\langle \theta \rangle = \langle \theta_R \rangle + \langle \theta_F \rangle \tag{B15}$$

using equations (B4) and (B13) for the Euler angle errors.

APPENDIX C

SIMULATION CONSTANTS

The program constants used in the ATM computer simulations are included in the following sections. For the ATM cluster the moments of inertia were chosen as:

$$I_x = 595131 \text{ slug-ft}^2$$
$$I_y = 3866985$$
$$I_z = 3753771$$

with zero products of inertia. The integration computing interval was 0.03125 sec for the equations of motion and the control law command signals. The ATM design gains were taken to be

$K_1 = 29500.$ ft-lb $K_2 = 162264.$ ft-lb-sec

$K_3 = 147512.$ $K_4 = 1305485.$

$K_5 = 368781.$ $K_6 = 1843906.$

with

$$K_{SL} = 0.00525 \text{ per ft-lb-sec}^2$$

In the control system equations the constant terms for the fourth order filters were

$$\rho_1 = \rho_2 = \rho_3 = 0.5$$

for the damping factor and

$$\omega_1 = 1.25 \text{ rad/sec}$$

$$\omega_2 = 1.25$$

$$\omega_3 = 1.90$$

for the filter frequencies.

The flexible spacecraft modal differential equations include the modal frequencies

$$\omega_{D1} = 0.9362$$

$$\omega_{D2} = 1.0116$$

$$\omega_{D3} = 2.6012$$

$$\omega_{D4} = 3.3929$$

$$\omega_{D5} = 4.0087$$

$$\omega_{D6} = 13.6534$$

$$\omega_{D7} = 15.8336$$

and the modal damping

$$\xi = 0.01$$

with the forcing function

$$\{E\} = \begin{Bmatrix} E_1 \\ E_2 \\ E_3 \\ \cdot \\ \cdot \\ \cdot \\ E_{18} \end{Bmatrix}$$

modified by the modal distribution matrix $[U]$ given in Table I.

The quasi-static contribution to the flexible spacecraft response requires the residual compliance matrix $[V]$ given in Table II. For the flexible spacecraft attitude solution the modal participation matrix $[\phi]$ is given in Table III.

In the gimbal power equations the following values were used for the ATM torque constants.

Gear ratio	$K_G = 56$
Back EMF	$K_B = 1.53$ volt/rad/sec
Stall torque	$K_T = 1.15$ ft-lb/amp
Winding resistance	$R = 6.9$ ohms
Friction torque	$T_F = 5.0$ ft-lbs

For the isogonal correction (Ref. 2) a distribution law gain of $K_D = 0.1$ and a rotation law gain of $K_R = -0.01$ were used for the ATM mission simulations.

TABLE II.- MODAL DISTRIBUTION MATRIX

$$[U]^T = \begin{bmatrix}
4.40E-4 & -4.27E-4 & 6.91E-3 & -2.21E-3 & -1.21E-4 & 2.21E-3 & -2.92E-3 \\
4.80E-6 & -8.40E-6 & -7.44E-5 & 1.50E-4 & -8.44E-3 & -8.88E-5 & -6.60E-5 \\
2.28E-5 & -2.28E-5 & 2.41E-4 & -6.72E-5 & -3.60E-6 & -1.89E-3 & -1.01E-2 \\
3.00E-5 & -6.00E-5 & -4.60E-4 & 6.90E-4 & -2.99E-2 & 7.00E-5 & 2.80E-4 \\
4.22E-3 & -4.41E-3 & 1.73E-3 & 4.64E-3 & 5.20E-4 & -2.15E-2 & 3.65E-2 \\
-9.00E-5 & -8.90E-4 & 7.90E-4 & -5.70E-4 & 6.07E-3 & -4.28E-3 & -1.54E-3 \\
7.28E-4 & -7.92E-4 & -6.20E-3 & 3.38E-3 & 2.44E-4 & 2.57E-4 & -3.52E-4 \\
4.80E-6 & -7.20E-6 & -3.72E-5 & 2.64E-5 & 6.01E-4 & -1.70E-4 & -6.48E-5 \\
2.16E-5 & -2.16E-5 & 1.96E-4 & -5.04E-5 & -4.80E-6 & 1.65E-3 & -1.88E-3 \\
-2.00E-5 & 4.00E-5 & 2.40E-4 & -4.80E-4 & 2.50E-2 & -6.20E-4 & 2.30E-4 \\
-1.55E-3 & 1.57E-3 & -9.62E-3 & 1.90E-3 & -2.00E-5 & -1.21E-2 & 2.25E-2 \\
-2.60E-4 & -6.10E-4 & 2.16E-3 & -1.57E-3 & -1.32E-2 & -1.29E-3 & -3.00E-5 \\
7.28E-4 & -7.90E-4 & -6.11E-3 & 3.37E-3 & 2.45E-4 & 1.13E-4 & -6.96E-5 \\
4.80E-6 & -8.40E-6 & -3.84E-5 & 3.12E-5 & 3.98E-4 & 4.80E-4 & 1.37E-4 \\
2.28E-5 & -2.40E-5 & 2.54E-4 & -7.08E-5 & -7.20E-6 & -3.25E-3 & 5.41E-3 \\
-2.00E-5 & 4.00E-5 & 2.40E-4 & -4.80E-4 & 2.50E-2 & -6.50E-4 & 2.70E-4 \\
-3.08E-3 & 3.11E-3 & -2.47E-2 & 5.98E-3 & 3.90E-4 & 5.47E-2 & -9.20E-2 \\
6.00E-5 & -1.14E-3 & -4.10E-4 & 4.00E-4 & 1.83E-2 & 9.55E-3 & 2.38E-3
\end{bmatrix}$$

TABLE III.- RESIDUAL COMPLIANCE MATRIX

$$[V]^T = \begin{bmatrix}
2.15E-09 & -2.06E-12 & 9.19E-11 \\
-2.06E-12 & 1.62E-09 & -4.6 E-11 \\
9.19E-11 & -4.6 E-11 & 7.09E-09 \\
6.09E-11 & -1.16E-08 & 1.44E-09 \\
-2.54E-08 & -2.4 E-12 & -1.33E-09 \\
1.10E-11 & -3.7 E-09 & 1.55E-10 \\
7.22E-10 & 9.71E-13 & 2.12E-11 \\
2.05E-11 & 2.41E-10 & 1.5 E-12 \\
-2.81E-10 & 1.38E-11 & 1.32E-11 \\
1.12E-12 & 3.35E-09 & 5.01E-12 \\
7.29E-09 & -2.31E-10 & -3.98E-10 \\
1.32E-10 & 3.47E-09 & -3.87E-11 \\
-2.56E-09 & -1.11E-11 & -6.73E-12 \\
-1.92E-11 & 6.13E-10 & -1.92E-11 \\
-3.27E-10 & -8.65E-13 & 6.49E-11 \\
1.08E-10 & 2.16E-09 & 6.89E-11 \\
3.53E-09 & -1.26E-10 & -2.93E-10 \\
-2.34E-10 & 6.47E-09 & -2.18E-10
\end{bmatrix}$$

TABLE IV.- MODAL PARTICIPATION MATRIX

$$[\phi] = \begin{bmatrix}
3.67E-05 & -3.56E-05 & 5.76E-04 & -1.841E-04 & -1.010E-05 & 1.836E-04 & -2.432E-04 \\
4.00E-07 & -7.00E-07 & -6.20E-06 & 1.250E-05 & -7.031E-04 & -7.400E-06 & -3.500E-06 \\
1.90E-06 & -1.90E-06 & 2.01E-05 & -3.600E-06 & -3.000E-07 & -1.573E-04 & -3.388E-04
\end{bmatrix}$$